

FINAL REPORT

Contract NAS5-30936

**REMOTE SENSING
TECHNOLOGY
RESEARCH AND
INSTRUMENTATION PLATFORM
DESIGN**

August 20, 1992

FWG ASSOCIATES, INC.
"Continuity with the Future"

(NASA-CR-190606) REMOTE SENSING
 TECHNOLOGY RESEARCH AND
 INSTRUMENTATION PLATFORM DESIGN
 Final Report (FWG Associates)
 202 p

N92-34145

Unclas

G3/45 0115088

**REMOTE SENSING TECHNOLOGY RESEARCH AND
INSTRUMENTATION PLATFORM DESIGN**

CONTRACT NAS5-30936

FINAL REPORT

AUGUST 20, 1992

PREPARED BY: FWG ASSOCIATES, INC.
217 LAKEWOOD DRIVE
TULLAHOMA, TN 37388

PREPARED FOR: NASA GODDARD SPACE FLIGHT CENTER
ATTN: CODE 289
GREENBELT, MD 20771

TABLE OF CONTENTS

	<u>Page</u>
INTRODUCTION	1
APPENDIX I PRESENTATION ON DESIGN CRITERIA AND INITIAL RECOMMENDATION	3
APPENDIX II AIRBORNE MEASUREMENT REQUIREMENTS FOR GENERAL CIRCULATION MODEL SUB-SCALE PARAMETERIZATION RESEARCH	38
1.0 Introduction	39
2.0 The Earth's Climatic System	40
3.0 GCM Description	43
4.0 GCM Research Needs	50
5.0 Energy Flux Mechanisms	57
6.0 Cloud Physics Studies	60
7.0 Conclusions	65
8.0 References	66
APPENDIX III INSTRUMENTATION PALLET DESIGN CONCEPTS AND AIRCRAFT DEFINITION FOR GENERAL CIRCULATION MODEL FLUX PARAMETERIZATION RESEARCH	68
1.0 Introduction	69
2.0 Pallet Concepts	69
3.0 Aircrafts	86
4.0 References	89
Appendix A - Derivation of Equations	91
Appendix B - Design Methodology and Procedures	100
Appendix C - Capabilities of the EGRETT II Aircraft	190
APPENDIX IV COVER SHEETS FROM SEPARATELY REPORTED WORK FOR DEFENSE INTELLIGENCE AGENCY; REDSTONE ARSENAL, AL	193

LIST OF FIGURES

	<u>Figure</u>	<u>Page</u>		
APPENDIX II	2.1	Schematic illustration of the Earth's climatic system, with some examples of the physical processes responsible for climate and climatic change (From Gates, 1979).	41	
	2.2	The average global radiation and heat balance of the atmosphere relative to 100 units of incoming solar radiation. (From U.S. National Academy of Sciences, 1975.)	42	
	3.1	Northern Hemisphere Rossby waves.	44	
	4.1	Schematic illustration of the processes commonly included in atmospheric general circulation models. The thickness of a particular arrow gives a qualitative indication of the importance of the interaction the arrow represents. (From Simmons and Bengtsson, 1988.)	56	
	6.1	Conceptual flight paths for convective column study.	61	
	6.2	Conceptual flight paths for cirrus cloud study.	63	
	6.3	Conceptual flight paths for radiant transport study.	64	
	APPENDIX III	2.1	Modular turbulent flux sensor concept.	77
		C.1	EGRETT II characteristics (provided by E-Systems).	191

LIST OF TABLES

<u>Table</u>	<u>Page</u>
APPENDIX III	
2.1 Variables Requiring Airborne Measurement in Support of Flux Parameterization Models	70
2.2 Instrumentation List for Airborne Mass Momentum and Energy Flux Measurements (Assumption of an aircraft with under-wing mounting is inherent.)	71
2.3 Related References to Wind Measurements With Aircraft	73
2.4 Integrated Atmospheric Radiation Measurement Program	80
2.5 Objectives of Proposed Atmospheric Radiation Instrumentation (Table 2.4) as Stated by Langford, et al. (1990)	83
3.1 Types of Aircraft Surveyed	87
3.2 Results of Aircraft Survey (Summarized from Johnson and Cooper (1989))	88
A.1 Variables Requiring Measurement In Order To Compute Wind Velocity Components	97
C.1 Payload, Weight, Altitude, Time, Range, and Cost of Certain Aircraft	192
C.2 General Performance Capabilities, EGRETT II	192

INTRODUCTION

This report documents a study by FWG Associates, Inc., in support of NASA Contract # NAS5-30936 to Goddard Space Flight Center. This report documents the Task 3 requirements of the Basic Contract and Task 1 of Option 1 to that contract. The objective of these tasks were to specify the airborne instrumentation and the optimum airplane to best support the advancement of parameterization research for General Circulation Models (GCM). The report consists of four major appendices. Appendix I is an indepth review presentation which fully outlines the overall NASA requirements of the contract effort. Appendix II documents a review of the physical principles involved in state-of-the-art GCM models. Measurement requirements to advance parameterization models of these physical principles were identified from the review. These requirements establish the selection criteria for the instrumentation specification and airplane recommendation which is documented in Appendix III. Results of the other tasks carried out under NASA Contract NAS5-30936 have been reported under separate cover to the Defense Intelligence Agency, Redstone Arsenal, AL 35898-5500. Cover sheets from these three reports are given in Appendix IV.

FWG prepared an indepth review (Appendix I) of the procedures used in the selection of the criteria for the instrumentation and the aircraft. The intent was to schedule a review meeting with NASA to establish NASA's inputs and approval of the design and budget to proceed with the hardware development. The review was never accomplished so that instrumentation design presented herein will require a number of iterations relative to the user inputs prior to final design and hardware construction. NASA could never schedule a time for this indepth review. Copies were sent to the contract COTR for in-house review.

In the review, however, the mission of the instrumented aircraft has been defined and the aircraft recommendation has been narrowed to two options. The instrumentation and data acquisition system, to be installed on the aircraft, has also been identified. The final choice of instrumentation will be influenced by the aircraft selection to some degree and a final consensus of the measurement requirements by the user.

The aircraft recommended is either the EGRETT II or the remotely piloted Aurora Perseus B. Both these aircraft have high altitude capability and are thus suited for the cloud parameterization studies identified as a major need for advancing GCM models. Specification of instruments and a preliminary airborne pallet designed to support the instruments is given in Appendix III. The main thrust of the report deals with turbulent flux modeling in which FWG's strengths lie. However, the report also considers instrumentation for cloud physics and radiation flux studies. In this area reference is frequently made to a feasibility study by Aurora Flight Science Corporation supported under a Battelle Pacific Northwest Laboratories contract. This system appears to represent an advanced approach in this area.

Both Appendix II and III are considered stand-alone reports containing their own appendices as needed.

APPENDIX I

**PRESENTATION ON DESIGN CRITERIA AND
INITIAL RECOMMENDATION**

**CRITERIA SPECIFICATION
AND PRELIMINARY
INSTRUMENTATION DESIGN
AND AIRCRAFT
RECOMMENDATION
PRESENTATION**

NAS5-30936

FWG Associates, Inc.
July, 1991

PROJECT OBJECTIVES

- Primary goal is improvement of general circulation model capabilities
- Identify potential GCM improvements
- Identify data for addressing improvements
- Design and build an instrumented pallet
- Select an airplane for study support

OVERVIEW

- Discuss general circulation models
- Identify potential GCM improvements
- Outline research for improvements
- Define supportive measurements for research
- Define instrumentation for measurements
- Define airplane specifications and make recommendations

GENERAL CIRCULATION MODELS (GCM)

- GCM is a long term climate forecasting tool
- Finite element models predict large scale atmospheric motion from first principles
- Sub-element processes predicted from large scale phenomena by parameterization

GCMs CONSERVATION LAWS

Momentum:

$$\frac{d\vec{v}_H}{dt} = -fkx\vec{v}_H - \nabla_H p + \vec{F}_H$$

- Horizontal flow driven by Coriolis, pressure, and friction forces

Energy:

$$\frac{dT}{dt} = \frac{1}{\rho c_p} \frac{dp}{dt} + \frac{\dot{Q}}{c_p}$$

- Temperature driven by expansion and external sources

Moisture:

$$\frac{\partial q}{\partial T} = E - C$$

- Moisture content changes with evaporation and condensation

GCM SUPPLEMENTAL EQUATIONS

Mass:

$$\frac{\partial w}{\partial p} + \nabla \times \rho \nabla_H = 0$$

- Vertical velocity related to large scale convergence

Hydrostatic Equation:

$$\frac{\partial p}{\partial z} = -g\rho$$

- Pressure is related to air mass

Ideal gas law:

$$p = \rho RT$$

- Pressure is proportional to temperature and density

GCM PARAMETERIZATIONS

- Surfaces fluxes (energy, moisture, momentum) are related to bulk properties

$$F_{\alpha} \propto u_* \Delta\alpha$$

- Cloud interaction with radiation related to bulk water (liquid and vapor) content
- Convection predicted from large scale lifting and stability
- Complex radiant exchange simplified to broad band models

POTENTIAL PARAMETERIZATION IMPROVEMENTS

- Hydrological effects on radiant exchange
- Convection and compensating subsidence
- Clear sky radiation data for model validation

RADIANT EXCHANGE

- Concentrate on cirrus clouds
- Measure effects of cirrus on radiant divergence
- Characterize crystal sizes and number densities

CONVECTION

- Concentrate on cumulus/convective columns
- Measure moisture/heat flux surrounding column
- Determine net transport from boundary layer to upper altitudes

RADIATION DATA

- Clear sky data needed for model validation
- Flux data needed at all levels
- Top of tropopause data particularly scarce

MEASUREMENTS SUMMARY AND DOMAIN

- Energy flux (sensible and latent heat)
- Moisture flux
- Radiant flux
- Particle sizing
- Boundary layer → Top of tropopause

ENERGY FLUX

$$\rho c_p \left(\overline{w} \frac{\partial \overline{T}}{\partial z} + \frac{\partial}{\partial z} (T'w') \right) = \nabla \cdot \vec{R} + S$$

- Driven by mean and turbulent advection, radiant divergence, evaporation/condensation sources
- Wind velocity, temperature, humidity and broad band radiation measurements needed

MOISTURE FLUX

$$\bar{w} \frac{\partial \bar{q}}{\partial \bar{z}} + \frac{\partial}{\partial z} (\overline{q'w'}) = Q$$

- Driven by mean and turbulent advection, evaporation/condensation sources
- Wind velocity, humidity measurements are needed

RADIANT FLUX

- Short wave ($<4 \mu$) flux from solar sources and reflections needed
- Long wave ($> 4 \mu$, $<40 \mu$) from surface and atmospheric emissions

PARTICLE SIZING

- Number densities and sizes needed for high altitude cirrus
- Smallest sizes (1-100 μ) have greatest impact on radiant flux

MEASUREMENTS SUMMARY

- Wind velocity
- Temperature
- Humidity
- Pressure
- Long and short wave radiant flux
- Particle sizes and counts

STATE VARIABLES

TEMPERATURE

- Measurement complicated by velocity
kinetic energy \Leftrightarrow temperature
flow \Leftrightarrow convective cooling
- Steady state thermometer has high
temperature recovery factor (Rosemount)
- Fast response thermometer has high
frequency response (NANMAC)

STATE VARIABLES

HUMIDITY

- Steady state cooled mirror has long term stability (Eastern)
- Lyman-alpha (AIR) has high frequency response

STATE VARIABLES

AMBIENT PRESSURE

- Measurement complicated by velocity pressure \leftrightarrow momentum
- Pressure measurement is position sensitive
- Proper placement and calibration required for true measurement

AIRBORNE WIND VELOCITY OVERVIEW

- Wind is calculated as the vector difference of relative air velocity and airplane inertial velocity
- Gust probe is used to measure relative air velocity
- Inertial attitude (from an INS) is used to "rotate" the airplane coordinates to earth coordinates
- Inertial velocity (from an INS) is subtracted from relative air velocity resulting in earth-frame wind velocity

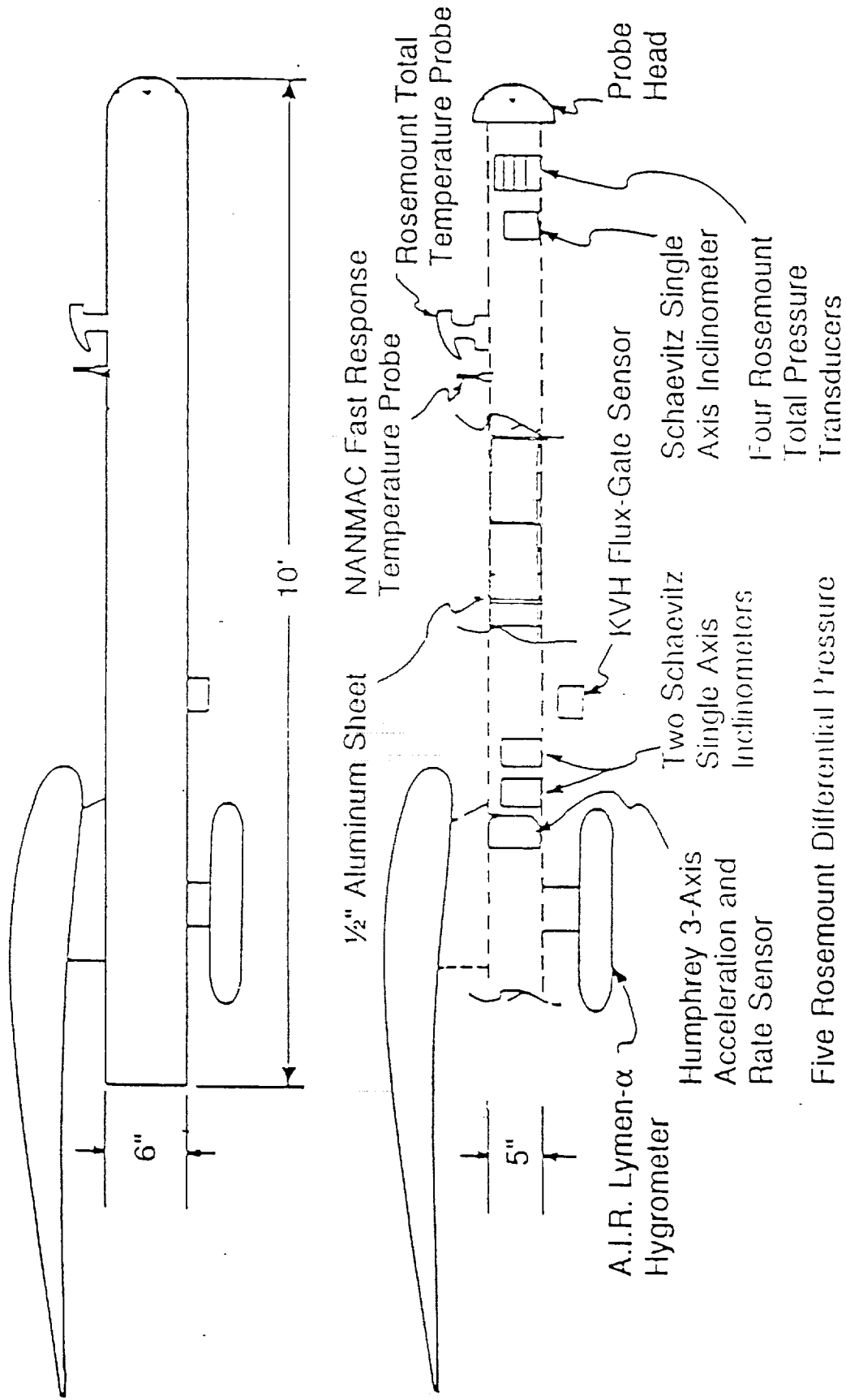
AIRBORNE WIND VELOCITY GUST PROBE

- Airspeed and flow angles define air velocity
- Airspeed calculated from impact pressure, ambient pressure, and temperature
- Flow angles calculated from probe differential pressures

AIRBORNE WIND VELOCITY INS

- Inertial navigation system (INS) traditionally provides attitude (elevation, bank, heading) and velocity (north, east, vertical)
- Recent approach replaces INS with GPS system and inertial measurement transducers
- Will use combination of GPS, IMU, inclinometers, and magnetic flux sensor

INSTRUMENT POD



RADIANT FLUX

- Requires measurement of gross flux (upwelling and downwelling)
- Requires separation of solar and terrestrial components

PARTICLE SIZING

- Smallest particles affect radiation (1-100 μ)
- PMS forward scattering spectrometer probes

DATA ACQUISITION SYSTEM

- DAS controller
- Analog input
- GPS interface
- PMS interface
- Large capacity tape storage

REMOTE SOUNDING

- Lidar can potentially be used for cloud height, humidity profiles, and flux measurements
- Requires development of both instrument and data acquisition system

AIRPLANE REQUIREMENTS

- Payload capacity of ~ 100 kg+
- Altitude capability ideally ~ 18 km
- Low airspeed ~ 100 m/s
- Initial and operational costs

CONVENTIONAL AIRPLANES

- Gulfstream IV
 - Has good payload, duration, altitude capability
 - Highly recommended by NCAR study
- Egrett II
 - Has good payload, duration, altitude capability
 - Extremely low airspeed at high altitudes
 - Inexpensive compared to gulfstream IV

REMOTELY PILOTED VEHICLES (RPV)

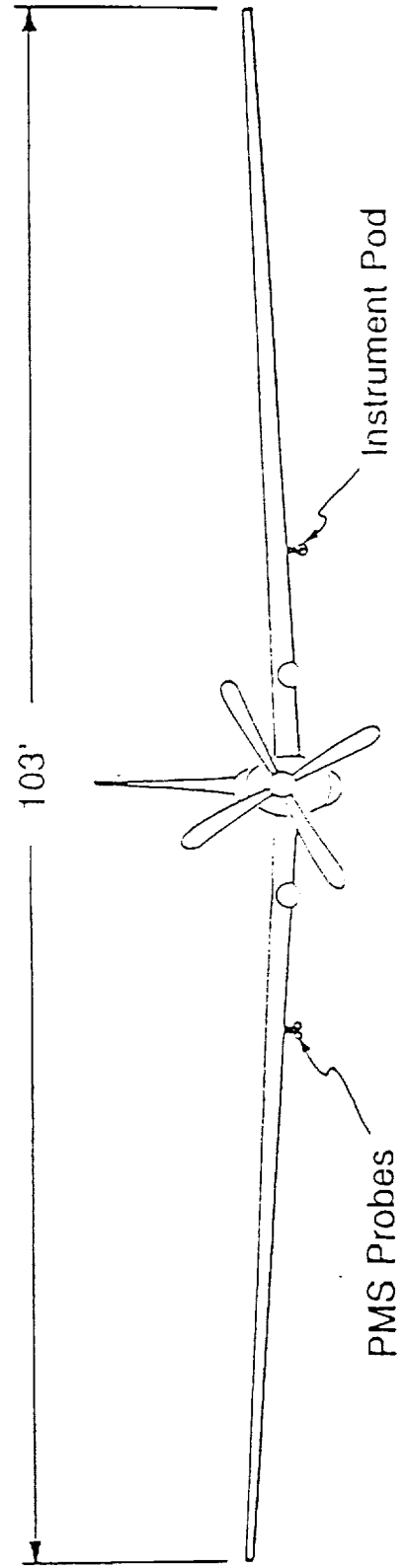
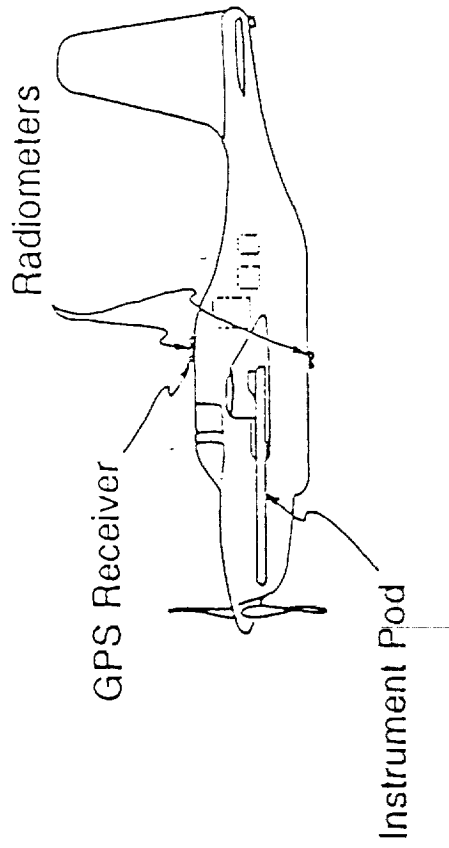
- Boeing Condor
 - Has good payload, duration, altitude capability
 - Potentially expensive acquisition
 - Pursued by NOAA

- Aurora Perseus B
 - Has good duration, altitude capability
 - Low acquisition and operating costs
 - Marginal payload capacity
 - Potential for dedicated studies

EGRETT II

Wingspan	30 m
Aspect ratio	20:1
True cruise airspeed	80 m/s @ 14 km
Maximum rate of climb	8 m/s
Maximum payload	900 kg
Endurance	6-9 hrs
Service ceiling	14 km +

EGRETT II



CONCLUSIONS

- Dedication to hydrological cycle study needed
- Radiative exchange relations to hydrological cycle
- High altitude capability needed (EGRETT II)
- Development of lidar instrument

APPENDIX II

**AIRBORNE MEASUREMENT REQUIREMENTS FOR
GENERAL CIRCULATION MODEL SUB-SCALE
PARAMETERIZATION RESEARCH**

1.0 INTRODUCTION

A General Circulation Model (GCM) is a numerical model, typically requiring the services of a super-computer, which solves the partial differential equations describing the motion of the atmosphere. Implicit in the prediction of atmospheric motion is the solution of the equations describing the transport of momentum, energy and moisture within and at the boundaries of the atmosphere. Energy is transported as sensible heat, latent heat of vaporization and fusion, and radiation. Moisture is transported as vapor, liquid, and solid. Because of the nature of these transport processes, particularly as influenced by turbulence and in the case of thermal radiation, as influenced by reflection and scattering, parameterization or empirical models are used within the GCM to describe the physical process.

The parameterization of energy and moisture transport is typically the cause of the greatest discrepancy between predictions made by different current models; given the same initial conditions and forcing functions. Additionally, problems with transport parameterization can be attributed to both cumuloform (convective) and high altitude stratiform (cirrus) clouds. Cumuloform clouds are the mechanism by which both moisture, and sensible and latent heat are convected from the planetary boundary layer (PBL) to the free atmosphere. Moisture that does not precipitate to the surface or subside in the region surrounding the cloud can feed the formation of high altitude stratiform, or cirrus clouds. Cirrus clouds, although physically thin compared to their towering cumulus brethren, are optically thick. Thus, cirrus clouds significantly influence the exchange of radiation between space and the atmosphere. In Section 3.0, recent research regarding inter-model comparisons and the influence of clouds is discussed. The discussion emphasized measurements required from an airborne instrument pallet in support of parameterization modeling research. These include measurements for moisture, latent heat, sensible heat, radiant heat, and momentum flux calculations, and measurements for describing

the compositions of cirrus clouds. Measurement of cirrus cloud particles include water droplets and ice crystal size distributions and concentrations. Airborne measurements under, over, around, and in clouds are required.

The conclusion of this study, calling primarily for the study of clouds, is supported by reported results of recent major research programs. In these programs both airplanes and other measurement platforms were used to support research in defining the mechanisms which govern the birth, death, and influence of clouds and in defining the mechanism of radiative transport. The long range goal of this study is to customize the present understanding of airborne instrumentation to support GCM parameterization models and to recommend instruments and a pallet design for future research programs. As second goal is to analyze the capability of several airplanes, commercially available and those presently operated by NASA and other government agencies for use in experimental parameterization studies. Many capabilities are duplicated to a large degree, but deficiencies in the existing fleet of research aircraft were apparent. For example, a large gap in altitude capability can be seen in the existing fleet. This gap is from approximately 9 to 15 km above sea level as is clearly recognized in a recent study by Johnson and Cooper (1989). An airborne instrument pallet design and suggested aircraft with performance characteristics to bridge this gap are recommended in FWG Contract Report (1992).

2.0 THE EARTH'S CLIMATIC SYSTEM

The climate system consists of the atmosphere (comprising the Earth's gaseous envelope and its aerosols), the hydrosphere (comprising the liquid water distributed on or beneath the Earth's surface), the cryosphere (comprising the snow and ice on and beneath the surface), the surface lithosphere (comprising the rock, soil and sediment of the Earth's surface), and the biosphere (comprising the Earth's plant and animal life, and, by extension, man himself). These components have quite different physical characteristics. They are linked together such that

changes in one part generally affect the behavior of other parts, thus setting in motion a chain of events which may either reinforce or cancel the original changes. These various physical processes of the Earth's climate system are illustrated schematically in Figure 2.1.

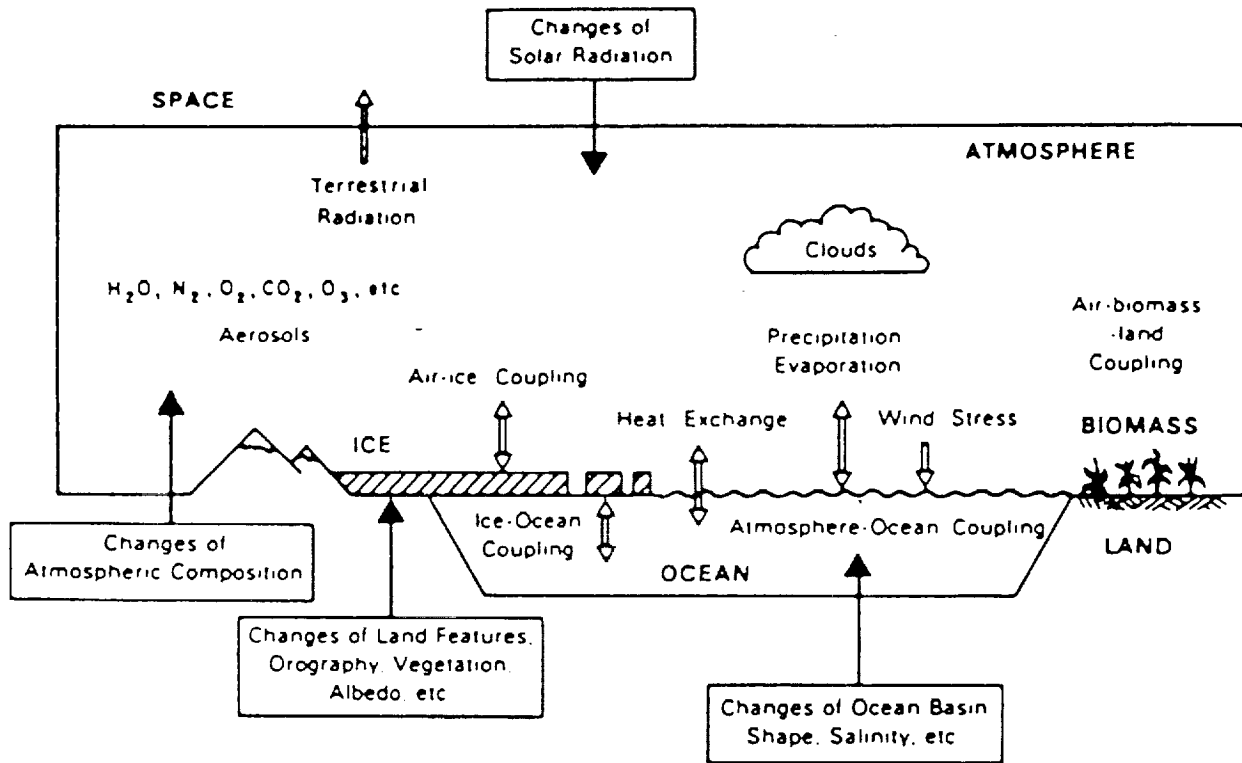


Figure 2.1 Schematic illustration of the Earth's climatic system, with some examples of the physical processes responsible for climate and climatic change (From Gates, 1979).

The fundamental process driving the Earth's climatic system is heating of the Earth's atmosphere by incoming shortwave solar radiation and the cooling by long-wave radiation to space. The heating is strongest at tropical latitudes, while cooling predominates at the polar latitudes of at least the winter hemisphere (Vonder Haar and Suomi (1971)). The bulk of the net

incoming solar radiation is absorbed not by the atmosphere but by the underlying surface. Evaporations of moisture and the heating of the Earth's surface lead, however, to much of this energy being transferred to the atmosphere as latent heat and, to a lesser extent, sensible heat. Thus the dominant direct heating of the atmosphere is found to be the latent heat release associated with deep tropical convergence. Figure 2.2 summarized the global radiation and heat balance of the climate system. The balance is maintained by a large number of feedback processes involving the transfer of radiation between the atmosphere, clouds, and the Earth's surface.

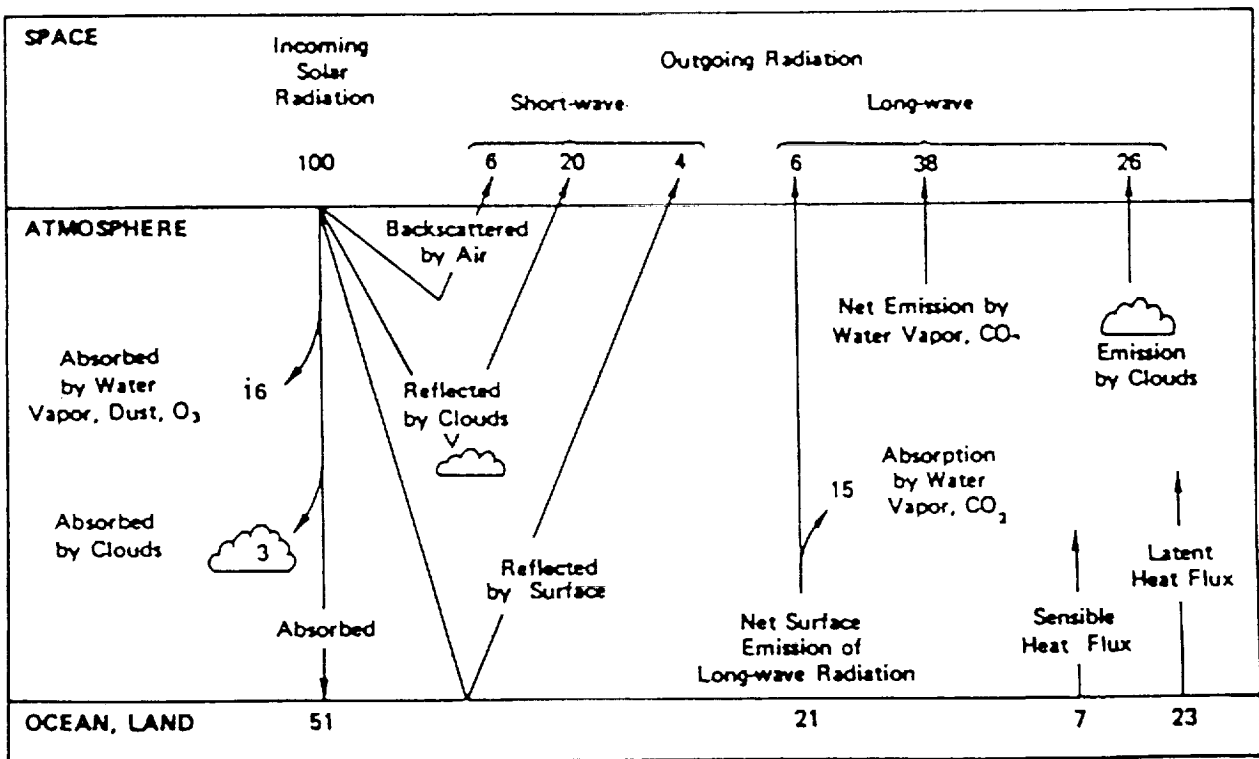
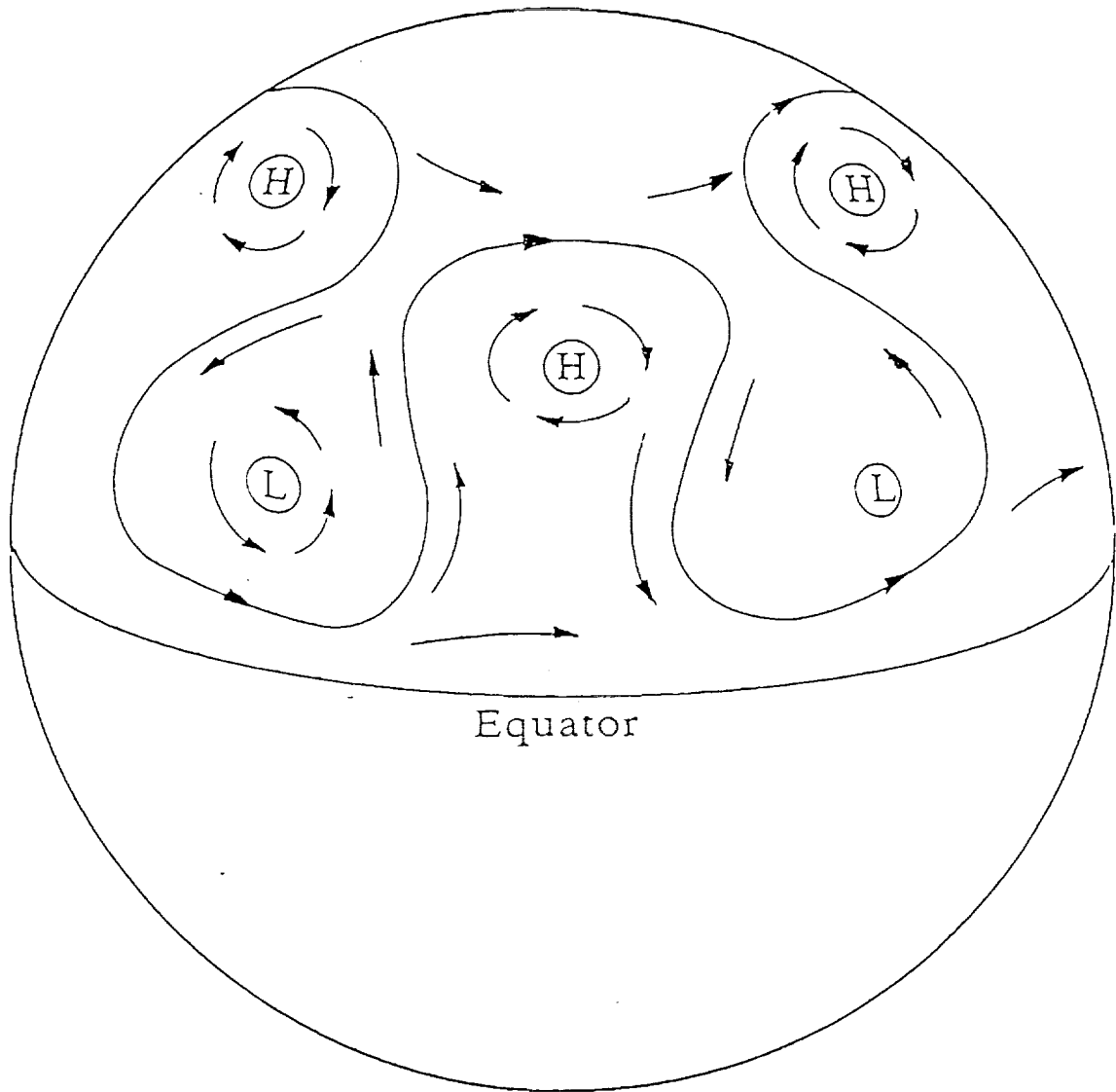


Figure 2.2 The average global radiation and heat balance of the atmosphere relative to 100 units of incoming solar radiation. (From U.S. National Academy of Sciences, 1975.)

3.0 GCM DESCRIPTION

General circulation models are numerical simulations of the dynamics of the interactions between sun, land, sea, and atmosphere. The forcing from any of these elements in driving the atmosphere can be prescribed as a boundary condition or calculated, depending on the temporal and spatial extent of the model and the complexity of the model. A simulation which uses the entire planet as the domain is commonly referred to as a global circulation model. These models are either finite difference models, with horizontal mesh sizes of several degrees latitude and longitude and with vertical layers several kilometers thick, or spectral models. The wind velocity vector field and the temperature and moisture scalar fields are controlled by the conservation of momentum, moisture, and energy. The following description of the mechanics of GCMs comes largely from Gates (1985), with modifications in nomenclature consistent with Panofsky and Dutton (1984). The language used is in the context of global circulation models, although the text is more often than not applicable to smaller scale models.

Time dependent partial differential equations developed from physical principles of heat, mass and momentum transfer are solved simultaneously for the description of atmospheric motion and the distribution of moisture and energy in the atmosphere. Large scale atmospheric motion is often described in terms of variations from geostrophic winds. Geostrophic winds result from a balance between pressure and Coriolis forces. The uneven solar heating of the atmosphere between the equatorial and polar regions creates pressure gradients which drive winds poleward. An apparent force, or Coriolis force, induced by the rotation of the Earth, drives a north or south wind eastward. Friction between the atmosphere and the Earth drives winds eastward. The balance of these forces results in a circulation pattern comprised of Rossby waves (Donn (1975)), centered around alternating high and low pressure centers, depicted in Figure 3.1.



Equator

- Ⓛ = Low Pressure Center
- Ⓜ = High Pressure Center
- = Wind Direction

Figure 3.1 Northern Hemisphere Rossby waves.

The differential equation for the conservation of momentum is derived by application of these forces to a differential volume element of air as:

$$\frac{D\vec{V}}{Dt} = -\frac{1}{\rho} \nabla p - g\vec{k} - 2\vec{\Omega} \times \vec{V} + \frac{1}{\rho} \nabla \cdot \mu \nabla \vec{V} \quad (3.1)$$

This equation is integrated for the solution of the horizontal wind velocity field, \vec{V} , where ρ is air mass density, p is ambient pressure, g is the acceleration due to gravity, \vec{k} is the unit vector in the direction of gravity, $\vec{\Omega}$ is the vector representation of the rotation of the Earth, μ is the viscosity of air, and t is time.

The term on the left-hand-side of Equation (3.1) is the total derivative of the vector velocity \vec{V} and represents the change of \vec{V} with time and with divergence in the convective transport. The first and fourth terms on the right-hand-side of Equation (3.1) represent the surface forces on a differential volume due to pressure gradients and frictional forces, respectively. The second and third terms of the right-hand-side of Equation (3.1) represent the body forces on the differential volume from gravity and Coriolis effects, respectively.

Pressure gradients, on large scales, and buoyancy gradients on smaller scales, are the result of the uneven distribution of thermal energy through the atmosphere. The sources and transport of thermal energy are modeled in much the same way as those of momentum. The differential equation for the conservation of energy is:

$$C_v \rho \frac{DT}{Dt} + p \nabla \cdot \vec{V} = -\nabla \cdot \vec{R} + \nabla \cdot k_H \nabla T + S_H + \mu |\nabla \vec{V}|^2 \quad (3.2)$$

where C_v is the constant volume specific heat of the air/moisture mixture, T is temperature, \vec{R} is the vector representing radiant flux, k_H is the thermal conductivity of air, and S_H is a latent heat source/sink term.

The first term in the left-hand-side of Equation (3.2) is the total derivative of the scalar temperature T . The second term is a compression or expansion work term. An example of this work term is the effect of a vertical exchange of air, where a rising parcel of air expands and is cooled as it does work on the surrounding environment. Conversely, a sinking parcel of air is compressed and receives work energy from the surrounding environment. This action heats the sinking parcel of air. On the right-hand-side of Equation (3.2), the first term represents the divergence of radiation flux, the second term represents the heat transfer from thermal conduction, and the third term represents the net release of heat due to the evaporation and condensation of moisture. The last term represents work done on a differential volume due to friction forces.

The explicit treatment of atmospheric moisture is also crucial to modeling the circulation of the atmosphere. Moisture, through evaporation, is the mechanism by which latent heat is transported from the surface of the Earth. The condensation of moisture at higher altitudes releases latent heat, maintaining the buoyancy of clouds and heating the upper atmosphere. The differential equation representing the conservation of moisture is:

$$\frac{Dq}{Dt} + q \nabla \cdot \vec{V} = S_q + \nabla \cdot k_q \nabla q \quad (3.3)$$

where q is specific humidity, S_q is a source/sink of humidity, and k_q is the mass diffusivity of water vapor in air.

The first term on the left-hand-side of Equation (3.3) is the total derivative of specific humidity and the second term represents the loss of specific humidity from a differential volume due to flow dilation. The first term on the right-hand-side of Equation (3.3) is the net gain of specific humidity from evaporation and condensation, and the last term represents the diffusion of water vapor by concentration gradients.

The final differential equation is the conservation of mass:

$$\frac{D\rho}{Dt} + \rho \nabla \cdot \vec{V} = 0 \quad (3.4)$$

Constitutive equations consist of the ideal gas equation of state,

$$p = \rho RT \quad (3.5)$$

where R is the ideal gas constant for air.

Thus, seven equations are available for the solution of the three wind velocity components, and the pressure, density, temperature, and moisture.

In the solution of Equations (3.1) through (3.5), some approximations are made for calculation simplification. In solving for horizontal winds, the gravitational term is ignored in Equation (3.1) by assuming negligible vertical winds in comparison to horizontal winds. Frictional work is considered small in the energy Equation (3.2), and is ignored. Molecular dissipation, represented by thermal conduction in Equation (3.2) and mass diffusion Equation (3.3), is also considered small compared to transport by convection and turbulent mixing, and is ignored.

Parameterization Methods

The grid size, which is large compared to crucial micro-meteorological events, requires bulk treatment of momentum, moisture, heat, and radiation transport. The sub-scale processes which are not solved explicitly include surface-friction effects on the horizontal wind, the complex interaction of the long-wave radiation field between the Earth and clouds, and the transport of moisture and energy through convective clouds. Surface drag is modeled as proportional to the characteristic surface roughness and to the square of the wind speed at the surface. For example, the effect of surface drag is modeled in the University of California at Los Angeles (UCLA) GCM as the flux of momentum from the surface layer (Suarez and Arakawa (1983)):

$$F_{V_s} = \eta C_u^2 \vec{V}_M | \vec{V}_M | \quad (3.6)$$

where F_{V_s} is surface momentum flux, C_u is an empirical surface transfer coefficient, \vec{V}_M is the vertical mean velocity for the PBL, and η denotes surface conditions.

Similarly, the flux of energy and water vapor from the surface layer are modeled as:

$$F_{\theta_s} = \eta u_* C_\theta (\theta_s - \theta_M) \quad (3.7)$$

and

$$F_{r_s} = \eta u_* C_\theta \beta (r^*(T_g) - r_M) \quad (3.8)$$

respectively. F_θ and F_r are the fluxes of thermal energy and water vapor mixing ratio, respectively. u_* is the friction velocity, defined by the surface stress and density, $\left(\sqrt{F_{V_s} / \rho} \right)_s$. C_θ is an empirical surface transfer coefficient, $r^*(T_g)$ is the temperature dependent saturation

water vapor mixing ratio, r is the water vapor mixing ratio, and β is the fraction of available surface water, Θ is potential temperature, subscript g denotes the ground value, and subscript M denotes the vertical mean for the PBL.

The empirical surface transfer coefficients are correlated to stability through the bulk Richardson number. The same approach as used in the UCLA GCM model is used in the Goddard Institute for Space Studies (GISS) GCM (Hansen, et al. (1983)).

Convection of moisture and latent heat (and subsequent precipitation) is modeled as flow induced by unstable temperature lapse rates, although other methods are used (as discussed by Del Genio and Yao (1988)). Vertical mass flow is predicted by buoyancy gradients between stacked elements in a model. Further discussion of convective parameterization schemes will be given in Section 4.0.

The net long wave radiation flux through the different levels of the atmosphere are calculated as functions of the temperature-dependent surface flux, the ambient temperature, pressure, and humidity, carbon dioxide and water concentration, and the fractional cloud cover. The method of calculating short wave flux is simpler because of the relative transparency of the atmosphere to solar radiation (with the exception of ozone and ultraviolet light). The complex interaction between reflecting and absorbing surfaces and gases is modeled. The most detailed, and probably the most accurate method of calculated air constituent dependent radiant flux is the line-by-line (LBL) method, by which each absorption band of a given constituent in the atmosphere is considered in transmittance and emittance calculations. Because of the complexity of this calculation and subsequent computation time, the LBL method is not used directly in GCM codes. However, simplifications of the LBL method, namely narrow band models (NBM) and wide band models (WBM), are used. Description of the LBL, NBM, and WBM models are given in Luther and Ellingson (1985) and will be discussed further in Section 4.0. Short-wave

models are simpler due to the transparency of the atmosphere (with the exception of clouds and ozone) to solar radiation. Slingo (1989) gives a simple model for calculating the transmittance of short-wave flux through clouds as a function of depth and liquid water content.

4.0 GCM RESEARCH NEEDS

The widely recognized weaknesses of GCMs are in the sub-scale parameterizations of turbulence convective transport and cloud feedback. Presently, a wide-scale application of GCMs is the study of increasing amounts of carbon dioxide in the atmosphere, and the associated "greenhouse effect". The increase in carbon dioxide will not only directly cause an increase in the temperature of the atmosphere, but the predicted change in cloud cover and patterns will create a positive feedback to the carbon dioxide-induced warming (Wetherald and Manabe (1988)). Del Genio and Yao (1988) give some insight into the difficulties of modeling convection with the varying results of different parameterizations with the Goddard Institute for Space Studies (GISS) GCM. Cess, et al. (1990) demonstrated the radiative cloud feedback modeling difficulties by comparing predictions made from different GCMs given the same boundary conditions. Finally, Gates (1985) gives priorities for GCM improvement, which includes better parameterization of sub-grid processes, such as the effect of non-precipitating stratiform and cirrus clouds on radiation flux and greater validation of model predictions with observations.

Luther and Ellingson (1985) discuss the effect of past and projected increases in the atmospheric concentration of carbon dioxide. An increase in the amount of carbon dioxide in the atmosphere is the primary forcing function of the greenhouse effect, or the projected increase in the temperature of the atmosphere. Carbon dioxide is transparent to short wave solar radiation incident on the earth's atmosphere, but opaque to the long wave radiance of the relatively cool atmosphere. Thus, an increase in the concentration of carbon dioxide in the atmosphere will

cause a decrease in the radiance of long wave energy, at a constant atmospheric and surface temperature, while leaving short wave transmission unchanged. The net effect, however, is a compensating increase in surface and atmospheric temperatures to balance the atmospheric radiation budget. This atmospheric and surface warming will also increase the amount of water in the atmosphere, which acts much in the same way as carbon dioxide in the transmission and absorption of short and long wavelength radiation. The significance of the research of Luther and Ellingson (1985) to the goals of this project is to emphasize the importance of accurate cloud modeling; this emphasis is also apparent in the research of others discussed below.

Wetherald and Manabe (1988) modeled an atmosphere with fixed cloud cover and an atmosphere with a calculated cloud cover, both with a doubling of the concentration of carbon dioxide in the atmosphere. In both simulations, the doubling of carbon dioxide affecting an increase in average global surface temperature and a decrease in the average stratospheric temperature. Furthermore, the increase of surface temperature in the model with a calculated cloud cover was 25 percent greater than the surface temperature increase in the model with a prescribed cloud cover. Decreases in high altitude moist static stability from the increase in surface temperature causes moisture to rise to the upper troposphere and tropopause in the tropics, and the transmission of solar radiation subsequently is increased due to a net loss of albedo. In the middle latitudes, a similar shift in cloud covers occurs, although not to the same extent as in the tropics. In the high latitudes, the more stable atmosphere traps moisture close to the ground and results in an increase of low altitude cloud cover. The middle and high altitude increases in cloud cover, affects a net increase in surface albedo and subsequent decrease in solar radiation. The middle and high altitude cloud-induced cooling, however, is not sufficient to offset the increase in solar radiation in the tropics. Thus, a change in clouds patterns induced by warmer global temperatures was predicted to further increase the average global temperature.

Del Genio and Yao (1988) experimented with different convective parameterizations to demonstrate the sensitivity of GCM predictions to the validity of the convective model. A control run was made with the GISS GCM, simulating a perpetual January climate, with convection prescribed as a mass movement upwards between stacked elements coinciding with the occurrence of buoyant instability. The predictions made by the control run were compared to four separate simulations in which the convective parameterization was varied. These were:

- (1) the use of large scale lifting for cumulus mass flux,

$$M_c = \rho_B W_B \quad (4.1)$$

where M_c is the cumulus mass flux and W is the large scale vertical velocity. The subscript B denotes conditions at cloud base,

- (2) the combination of large scale lifting with surface flux influence,

$$M_c = \rho_B \left(W_B + \frac{F_{q_s}}{\Delta q} \right) \quad (4.2)$$

where Δq is the moisture discontinuity across the cloud base,

- (3) the addition of mass flux from a fluctuating boundary layer height,

$$M_c = \rho_B W_B + \frac{F_{q_s}}{\Delta q} - \rho_B \frac{\partial Z_{LCL}}{\partial t} \quad (4.3)$$

where Z_{LCL} is the lifting condensation level, and

- (4) the inclusion of explicit downdraft calculations.

Two results of this experiment were (1) that one simple cumulus flux parameterization may not be appropriate for all situations, and (2) that the appropriate explicit modeling of the downdraft, compensating the cumulus updraft, may have significant positive results in the accuracy of model predictions. The use of calculated large scale lifting to model cumulus mass flux helped to improve the comparison between some model predictions and observation, and the use of surface flux effects had mixed results. The surface flux effects on convection from the boundary layer were positive over land but over-predicted precipitation over oceans. The explicit modeling cumulus mass flux due to the rise and collapse of boundary layer height had little effect on the predictions of the model. The modeling of downdraft fluxes, however, had effects considered worth further study. The effects were considered qualitatively realistic but the simple parameterization was in need of "fine tuning". The deep convective columns with downdrafts were predicted to dry the boundary layer, similarly to the predictions of dry subsidence modeling. Downdrafts coinciding with shallow convection, however, were predicted to restore moisture to the boundary layer. This produced humidity profiles more consistent with observation. It was concluded that studies of precipitation climatologies were needed, complementing the data set of International Satellite Cloud Climate Project (ISCCP) and others, to better understand the convective process, particularly the nature of downdraft in and around the convective column.

The studies of Cess, et al. (1990) further illustrate the affect of cloud feedback to atmospheric warming and a shortfall of current GCMs. Nineteen different GCMs were subjected to an experiment in which the global average simulated sea surface temperature, rather than the atmospheric concentration of carbon dioxide, was forced through a 4 K° temperature change. Although expression was made for a more realistic forcing function, such as an atmospheric carbon dioxide concentration increase, modulation of sea surface temperatures was advantageous in terms of computation time and inter-model comparisons. The qualitative results were

consistent with those of Wetherald and Manabe (1988) (discussed above) in that the changes in cloud cover resulting from atmospheric warming further increased the warming. However, the magnitude of the increase in the predicted average temperature varied considerably between the different models. These differences were attributed to the treatment of clouds in the different models, e.g., cloud formation and optical properties. The radiation exchange in the areas of clear (cloud free) sky compared well between the different models.

Ellingson, et al. (1991) describe parameterizations used for modeling long wave (terrestrial) radiation propagation in the atmosphere. The importance of accurate long-wave flux modeling is demonstrated by the influence of the atmosphere on the upwelling radiation back into space; it is estimated that 90 percent of the long wave flux at the top of the troposphere originates from the atmosphere rather than the ground. Radiation modeling comes in three levels of complexity, only the simplest of which is used in GCMs. The most complex, and most consistent model, is based on the LBL (line-by-line) method as mentioned in Section 3.0. The LBL method calculates spectral transmittance in a finite element by considering each pressure and temperature dependent absorption band of each atmospheric constituent in the element. The monochromatic transmittance of the air in an element is calculated by:

$$\tau_v = \exp \left\{ - \int_{\delta z} K_v \rho_a \frac{dz'}{\mu} \right\} \quad (4.4)$$

where τ_v is the monochromatic transmissivity, δz is the transmittance path length, K_v is the monochromatic absorption coefficient, ρ_a is the density of one absorbing gas, and μ is the Zenith angle cosine.

The monochromatic absorption coefficient is calculated by:

$$k_\nu = \sum_j S_j f_j \quad (4.5)$$

where S_j is the integrated line intensity at the j th frequency, and f_j is a line shape factor dependent on pressure, temperature, and frequency. Sparrow and Cess (1978) define the integrated band absorption in terms of wavelength as:

$$S = \int_{\Delta\lambda} \frac{K\lambda}{p} d\left(\frac{1}{\lambda}\right) \quad (4.6)$$

where $\Delta\lambda$ is the wavelength interval containing the absorption band. The shape factor is an empirical fit of the shape of the measured absorption band.

Various LBL model predictions of radiative properties compare consistently, lending credence to the accuracy of the model. Unfortunately, the tremendous computation time required by LBL models precludes their direct use in GCMs. Simplified versions of LBL model, narrow band models and wide band models are used instead. The LBL models are used to validate the prediction of the simpler models.

Both Ellingson, et al. (1991) and Luther and Ellingson (1985) discuss the need for validation data for LBL models. The data used for the development of the LBL models (such as HITRAN; Rothman, et al. (1987)) is derived in the laboratory; model validation by comparison with atmospheric observations is often hindered by the absence of a complete data set. The data most significant to clear sky fluxes are the profiles of water vapor, carbon dioxide, ozone, and aerosols. Of these, the determination of water vapor distribution is the most important. Cloudy sky flux modeling is further complicated by the difficulty in obtaining data in a field of

sufficiently homogeneous cloud distribution conducive to finite element description.

It is thus concluded that the greatest potential for the advancement of GCMs lies in the better understanding of the (1) creation and dispersion of cirrus clouds and the affect of cirrus clouds on the Earth's radiation budget, (2) the transport of moisture and latent heat from the planetary boundary layer to the free atmosphere through convective clouds, and (3) the validation of radiation codes by comparison of data to predicted constituent dependent radiant fluxes. Since model performance and observational and theoretical knowledge are far from perfect in many instances, parameterization tends to vary substantially from model to model, at least in questions of detail. The general extent of interactions involved in GCMs is summarized and illustrated in Figure 4.1.

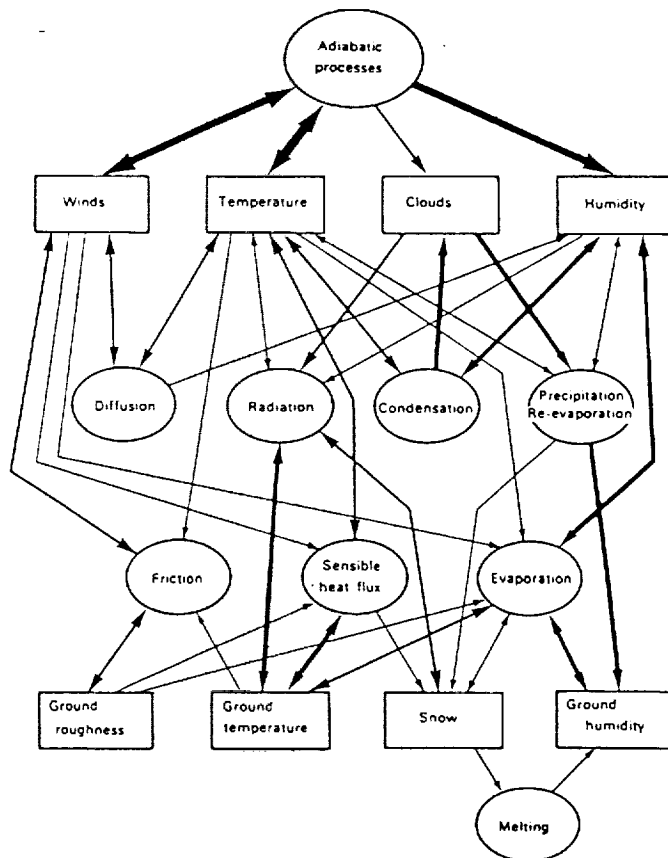


Figure 4.1 Schematic illustration of the processes commonly included in atmospheric general circulation models. The thickness of a particular arrow gives a qualitative indication of the importance of the interaction the arrow represents. (From Simmons and Bengtsson, 1988.)

5.0 ENERGY FLUX MECHANISMS

Energy exchange in the atmosphere occurs due to sensible and latent heat transfer by convective turbulent mixing and due to radiative absorption and emission. The study of atmospheric energy transport must also include the study of cloud physics, which significantly governs the transport of atmospheric energy. The air currents which transport the thermal energy originate from radiant heating by the sun, which warms both land and sea by day and from radiant cooling at night due to transfer of energy to the cold sky which cools the earth. Thus, a periodic cycle is born, by which the sun heats the earth, and the heat is lost, ultimately by radiation to the upper atmosphere.

The different forms of thermal energy of interest to the climatologist, excluding radiant energy, propagate with the atmosphere as a medium. As a result, the determination of atmospheric motion is required for a complete model of the atmospheric energy flux. The motion of the atmosphere can be considered as consisting of a mean and of a fluctuating flow, representing the convection of energy due to the mean motion and the diffusion of energy by the turbulent eddies. The energy in the flow can also be divided into two components, the first being the sensible heat of the moving air, realized in vertical gradients in potential temperature, and the second being the latent heat in the water vapor contained in the air. Water vapor rises from warm low altitudes to condense in clouds, releasing the heat of vaporization, which drives the buoyancy of the cloud or which may be released as radiant heat from the cloud summit. The measurements and calculation required for the determination of these fluxes are discussed herein.

The transport of radiant heat is also a complex process. Short wave solar radiation is scattered and absorbed by clouds and the Earth's surface and the seas. The long wave terrestrial radiation is scattered, emitted, and absorbed by comparatively cool bodies, the Earth's surface, the seas, the clouds, and the atmosphere. The absorption and emittance of long wave radiation

by the atmosphere is highly sensitive to the composition of the air.

The flux of sensible and latent heat is dependent on the motion of the atmosphere; vertical mean and fluctuating motions are correlated to the mean and fluctuating horizontal velocity, temperature, and humidity, for the calculation of momentum, velocity, and temperature fluxes, respectively. The separation of mean and fluctuating flux components is done by means of Reynolds decomposition of the conservation equations (momentum, energy, and mass) discussed earlier.

A simplified version of the momentum conservation equation, after decomposing velocity into mean and fluctuating parts, is:

$$\bar{u} \frac{\partial \bar{u}}{\partial x} + \bar{w} \frac{\partial \bar{u}}{\partial z} + \frac{\partial}{\partial z} (\overline{u'w'}) = -\frac{1}{\rho} \frac{d\bar{p}}{dx} \quad (5.1)$$

where velocity is broken into horizontal and vertical components, u and w , the overbar denotes a mean component, and the prime denotes a superimposed fluctuating component. This simplification is for illustrative purposes and ignores the Coriolis, buoyancy, and frictional effects in Equation (3.1).

The additional flux advection terms in the momentum conservation Equation (5.1) compared to Equation (3.1) are due to the decomposition of the momentum flux divergence into mean and fluctuating components by means of ensemble averaging. The fluctuating exchange of fluid, with no net fluid exchange, particularly in the boundary layer, is often the more significant means of transport for momentum. As can be seen from Equation (5.1), the determination of vertical momentum fluxes will require measurements of time dependent horizontal and vertical wind speeds which can be decomposed into mean and fluctuating

components. The fluctuating components can then be correlated to provide terms like $\overline{u'w'}$ from which a physical understanding and parameterization models can be developed. To make these measurements from an aircraft, will require pressure, temperature, and flow angle measurements relative to the airplane.

The conservation of energy and moisture equations can be decomposed likewise into the simplified forms:

$$\rho C_v \left[\bar{u} \frac{\partial \bar{T}}{\partial x} + \bar{w} \frac{\partial \bar{T}}{\partial z} + \frac{\partial}{\partial z} (\overline{T'w'}) \right] = \nabla \cdot \vec{R} + C \quad (5.2)$$

and

$$\bar{u} \frac{\partial \bar{q}}{\partial x} + \bar{w} \frac{\partial \bar{q}}{\partial z} + \frac{\partial}{\partial z} (\overline{q'w'}) = S \quad (5.3)$$

As with momentum, the fluctuating exchange or turbulent mixing of air is often the more significant means of energy and moisture transport. These parameters will require the time dependent measurement of temperature and humidity from the airplane in order to determine turbulent fluxes of energy and mass represented by such terms as $\overline{T'w'}$ and $\overline{q'w'}$, respectively.

Clear sky and cloudy sky radiative modeling support will require knowledge of both radiative divergence and atmospheric constituents affecting divergence. This will require a combination of spectral radiometers and measurement of water vapor, carbon dioxide, and ozone concentrations, at a variety of altitudes through the troposphere. The spectral measurements will include a reference band unaffected by the atmosphere, by which a virtual black body temperature and Plank function for the long wave flux can be established, and for the absorption bands of the listed constituents affecting the long wave flux.

6.0 CLOUD PHYSICS STUDIES

The cloud studies promoted herein are intended to advance the parameterizations used to predict the interaction of clouds with the transport of energy through the atmosphere. Energy transport affected by clouds includes (1) convective transport, from the boundary layer to the free atmosphere, (2) the compensating flow from the free atmosphere back to the boundary layer, and (3) radiative transport, by the interdiction of stratiform clouds, particularly cirrus, in the exchange of both solar and terrestrial radiation between space and the Earth/atmosphere system. The measurements needed for convective studies have already been discussed; the parameters needed are wind velocity, temperature, and humidity. Radiative transport will require radiation flux measurements and a physical description of clouds affecting that flux. A description of clouds will be comprised of vertical extent, horizontal extent, particle sizes, particle number densities, and emissivity and transmissivity for both solar and terrestrial radiation.

The airborne instrumentation system design must consider convection related measurements pertaining to determination of moisture and heat transport upwards through a convective column and of the nature of the compensating flow downwards. Determination of the transport of moisture and heat from the boundary layer by airplane flights is envisioned to consist of flights on the surface of a hypothetical control volume containing the cumulus column of interest. The net flux into the volume, at cloud base, would be measured, as well as the net flux from the cloud by measurements at the cloud top and sides. Penetration into the cloud will be desirable, although turbulence, precipitation, and ice accretion on the airplane may preclude such maneuvers. The subsidence of air surrounding the cumulus column will also be studied for determination of the moisture in flow compensating the cumulus updraft. Such a mission is illustrated in Figure 6.1. Any studies of this nature will require measurements of momentum, heat, and moisture flux as previously discussed.

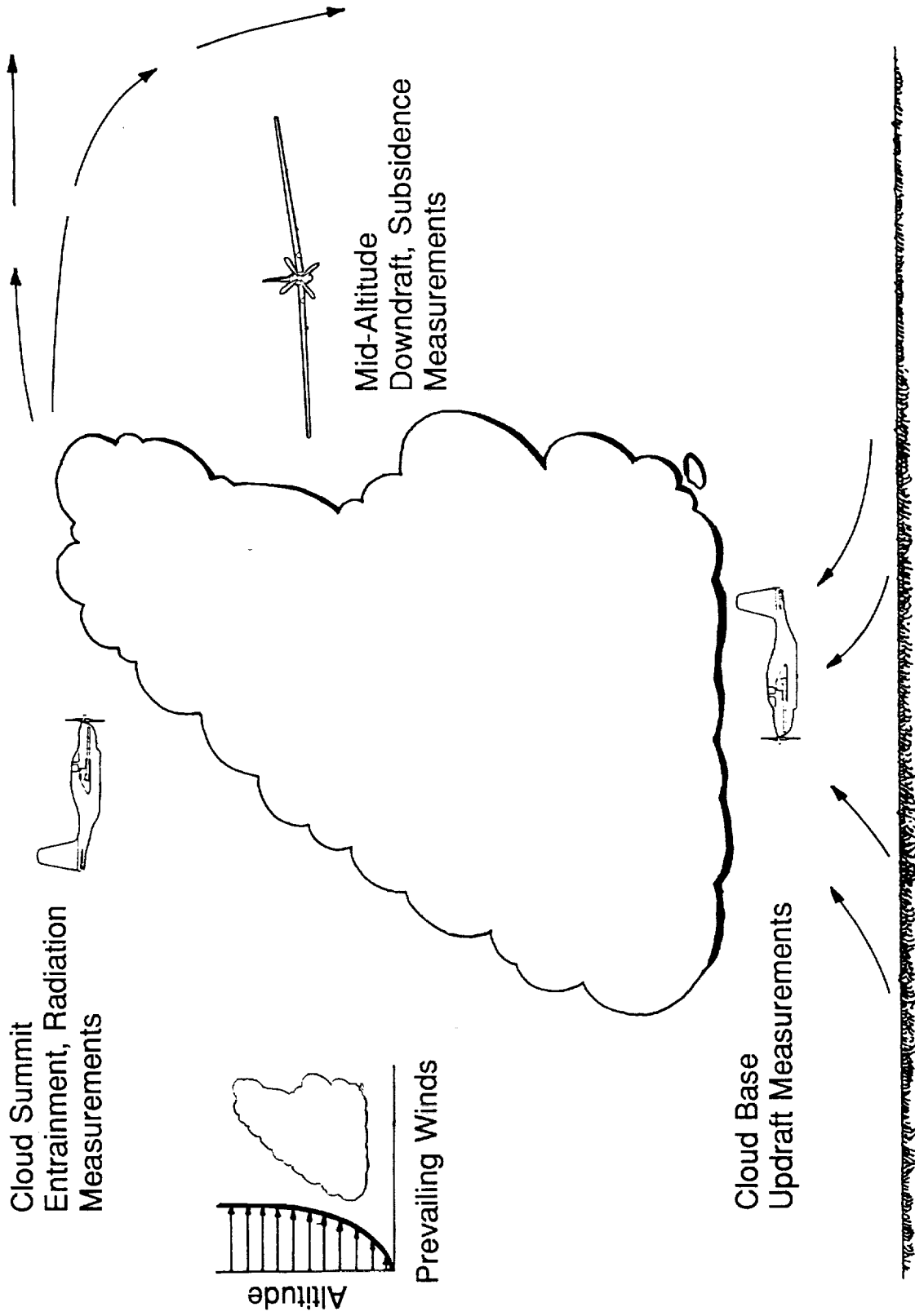


Figure 6.1 Conceptual flight paths for convective column study.

Radiative transport can be determined in much the same way that convective transport can be determined; the primary difference lies in the measurement of radiative flux into and out of stratiform clouds instead of convective heat and moisture into and out of cumulus clouds. A typical mission, as envisioned, is illustrated in Figure 6.2. It will involve the measurement of gross radiation flux beneath and above a cirrus cloud. Radiometers, above and below the airplane, will be required for such measurements. As a minimum, broad band radiometers, enabling the differentiation between solar and terrestrial radiant flux are required. The cloud should also be penetrated for determination of the particles comprising the cloud, in size and number density. State-of-the-art technology with particle sizing requires probes using laser scattering for particle measurement and counting. Particle mapping might also be done remotely by lidar. The radiation balance of the cloud, combined with a description of the cloud material, will advance the parameterization of cloud optical properties by predicted moisture content, pressure, and temperature (Figure 6.3).

Above Cloud Flux,
Lidar Measurements



Cloud Penetration
Particle Measurements



Below Cloud
Flux Measurements



Figure 6.2 Conceptual flight paths for cirrus cloud study.

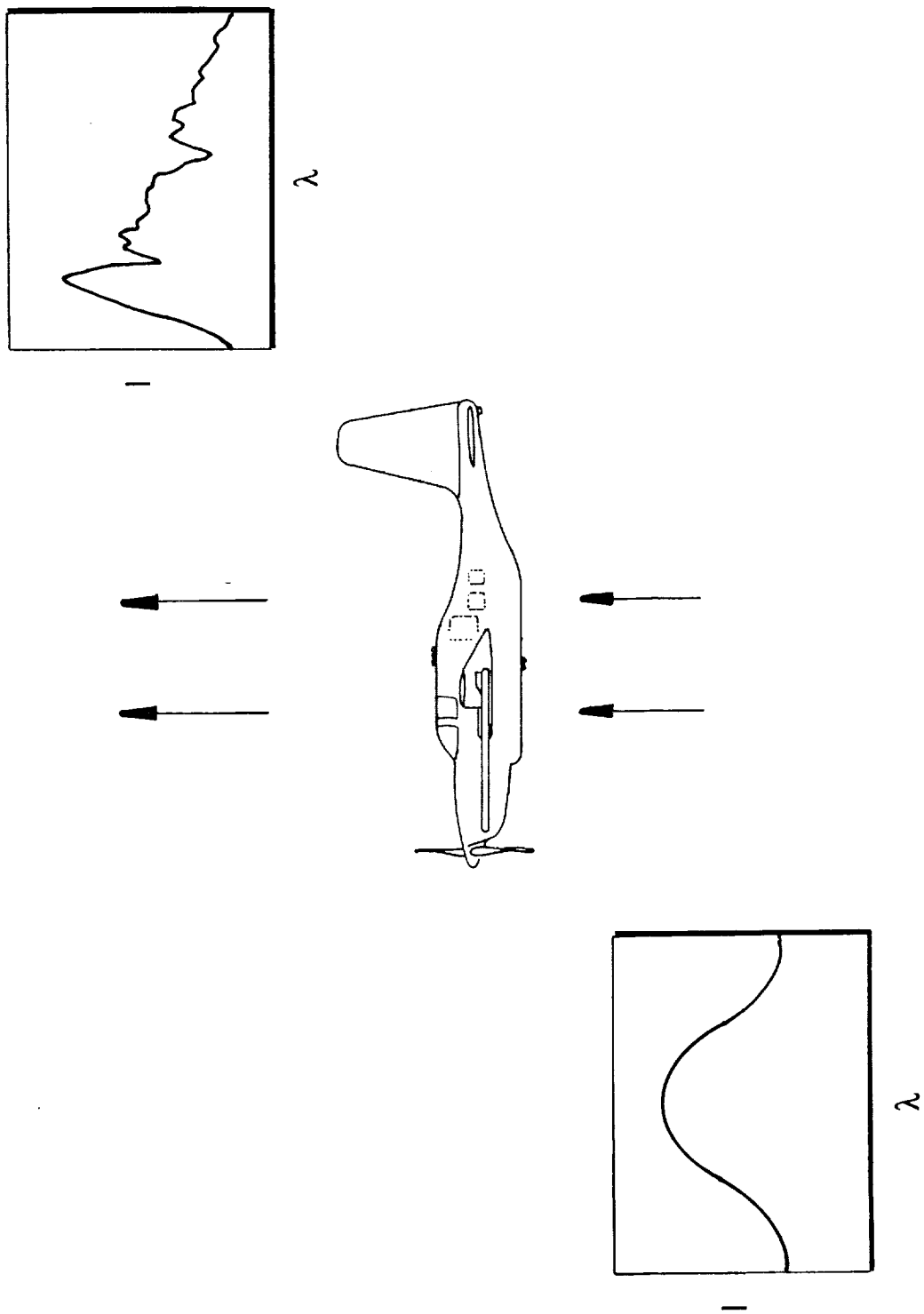


Figure 6.3 Conceptual flight paths for radiant transport study.

7.0 CONCLUSIONS

The most significant potential for advancements in the performance of GCMs lies in a better understanding of the hydrological cycle and in improvements in the modeling of radiative transfer within an atmosphere of spatial and temporal varying optical properties. The measurements which are best supported by an airplane in realizing the goals of more accurate numerical climate modeling will determine the flux of energy and moisture from the top of the boundary layer to the top of the troposphere and will provide increased understanding of some of the factors affecting these fluxes. In short, the instrumented pallet recommended as most needed by the GCM community is one which primarily supports studies of clouds, both cumuliform and high altitude stratiform and which secondarily supports collection of data for the validation of numerical codes used for radiative flux predictions.

The pallet will be comprised, in part, of the instrumentation necessary for the measurement of momentum, energy, and moisture turbulent flux. This is considered a baseline for aircraft involved with atmospheric research. Turbulent flux determination requires temporal and spatial measurements of wind velocity, temperature and humidity below, above and around convective columns and cirrus clouds. The pallet will, in turn, have the capability of supporting studies of cloud microphysics which influence latent heat and radiation transport.

The measurements necessary for support of radiative transfer models are spectral radiation and concentrations of particular atmospheric constituents. These constituents, which most significantly influence the transfer of both short and long wave radiation, are water vapor, carbon dioxide, and ozone. Other constituents, of lesser importance but worth consideration, are methane and nitrous oxide.

The scope of these measurements will define the requirements of the supporting airplane. The measurement of the fluxes of momentum, energy, and moisture, are most easily performed

at low airspeeds since increasing airspeed directly affects the confidence in these measurements. Thus, as is desirable with any airplane performing in-situ measurements of state variables, a low airspeed aircraft is a requirement. The most important specification for this airplane, however, is the service ceiling. Ideally, the airplane has the capability of penetrating the lower stratosphere for cirrus cloud studies; a compromise is a tropopause capability, which will encompass the great majority of the domain intended for study of cloud physics and spectral radiative flux.

8.0 REFERENCES

- Cess, R.D., et al. (1990): "Intercomparison and Interpretation of Climate Feedback Processes in 19 Atmospheric General Circulation Models", Journal of Geophysical Research, 95, 16601-16615.
- Del Genio, A.D., and M.S. Yao (1988): "Sensitivity of a Global Climate Model to the Specifications of Convective Updraft and Downdraft Mass Fluxes", Journal of the Atmospheric Sciences, 45:2641-2668.
- Donn, W.L. (1975): Meteorology, Fourth edition, McGraw-Hill:New York.
- Ellingson, R.G., J. Ellis, and S. Fels (1991): "The Intercomparison of Radiation Codes Used in Climate Models: Long Wave Results", Journal of Geophysical Research, 96:8929-8953.
- FWG Associates, Inc. (1992): Appendix II of NASA Contract NAS5-30936, Final Contract Report.
- Gates, W.L. (1979): "The Physical Basic of Climate", Proceedings of the World Climate Conference, WMO, Geneva, pp. 112-131.
- Gates, W.L. (1985): "Modeling as a Means of Studying the Climate System" Projecting the Climatic Effects of Increasing Carbon Dioxide, DOE/ER-0237.
- Hansen, J., G. Russell, D Rind, P. Stone, A. Lacis, S. Lebedeff, R. Ruedy, and L. Travis (1983): "Efficient Three-Dimensional Global Models for Climate Studies: Models I and II", Mon. Weather Rev., 111, 609-662.
- Johnson, W.B. and W.A. Cooper (1989): "The Second NCAR Research Aircraft Fleet Workshop", Meeting Review for NCAR/TN-332+PROC, Boulder, CO.
- Luther, F.M., and R.G. Ellingson (1985): "Carbon Dioxide and the Radiation Budget", Projecting the Climatic Effects of Increasing Carbon Dioxide, DOE/ER-0237.

- Panofsky, H.A., and J.A. Dutton (1984): Atmospheric Turbulence, John Wiley & Sons: New York.
- Rothman, L.S., R.R. Gamache, A. Goldman, L.R. Brown, R.A. Toth, H.M. Pickett, R.L. Poynter, J.-M. Flaud, C. Camy-Peyret, A. Barbe, N. Husson, C.P. Rinsland, and M.A.H. Smith (1987): "The HITRAN DataBase", 1986 Edition, Appl. Opt., Vol. 26, No. 19, 4058-4097.
- Simmons, A.J. and L. Bengtsson (1988): "Atmospheric General Circulation Models: Their Design and Use for Climate Studies", The Global Climate, Cambridge University Press, pp. 37-62.
- Slingo, A. (1989): "A GCM Parameterization for the Shortwave Radiative Properties of Water Clouds", Journal of the Atmospheric Sciences, 46:1419-1427.
- Sparrow, E.M. and R.D. Cess (1978): Radiation Heat Transfer, Revised Edition, Brooks/Cole Publishing Co., Belmont, CA.
- Suarez, M.J. and A. Arakawa (1983): "The Parameterization of the Planetary Boundary Layer in the UCLA General Circulation Model: Formulation and Results", Monthly Weather Review, Vol. 111, pp. 2224.
- U.S. National Academy of Sciences (1975): Understanding Climatic Change, Washington, DC, pp. 239.
- Vonder Haar, T.H., and V.E. Suomi (1971): "Measurements of the Earth's Radiation Budget From Satellites During a Five-Year Period. Part 1. Extended Time and Space Means", J. Atmos. Sci., 28, 305-314.
- Wetherald, R.T., and S. Manabe (1988): "Cloud Feedback Processes in a General Circulation Model", Journal of the Atmospheric Sciences, 45:1397-1415.

APPENDIX III

**INSTRUMENTATION PALLET DESIGN CONCEPTS
AND AIRCRAFT DEFINITION FOR
GENERAL CIRCULATION MODEL
FLUX PARAMETERIZATION RESEARCH**

1.0 INTRODUCTION

The objective of this report is to specify the instrumentation for an airborne pallet and to recommend an airplane with which it can be deployed in support of advancing mass, momentum and energy flux parameterization studies for General Circulation Models (GCM).

2.0 PALLET CONCEPTS

Two preliminary concepts have been developed of an airborne instrumentation pallet designed for atmospheric measurements in support of flux parameterization studies for general circulation models. The concepts emphasize primarily the determination of energy and mass flux, in the atmospheric boundary layer, in and around cumuliform clouds, and in and around high altitude cirrus clouds. Consideration, however, is also given to determination of high altitude cloud microstructures which effect the Earth's long- and short-wave radiation flux budget.

The atmospheric parameters considered of primary importance and which can be effectively measured from an airborne platform, are listed in Table 2.1. The parameter list represents the consensus of high priority needs as expressed by a sample of the GCM community (Paige (1991)) and from a literature review (FWG Contract Report (1992)). The measurements necessary to determine these parameters, with recommended candidate transducers for the airborne pallet design, are listed in Table 2.2.

The instrumentation component can be essentially divided into two groups. Those required to measure wind velocity, temperature and moisture fluctuations which produce the turbulent fluxes such as momentum flux ($\overline{u'w'}$, $\overline{u'v'}$, $\overline{v'w'}$), heat flux ($\overline{T'u'}$, $\overline{T'w'}$, $\overline{T'v'}$), and moisture flux ($\overline{q'u'}$, $\overline{q'w'}$, $\overline{q'v'}$); and those required to measure thermal radiation flux and liquid or solid mass flux.

Table 2.1 Variables Requiring Airborne Measurement in Support of Flux Parameterization Models

<p>Momentum and Sensible Heat Flux</p>	<p>Ambient Pressure</p> <p>Ambient Temperature</p> <p>Density</p> <p>Wind Velocity</p>
<p>Mass and Latent Heat Flux</p>	<p>Humidity</p> <p>Dew Point Temperature</p> <p>Particle Size Distribution</p> <p>Particle Concentration</p>
<p>Radiation Heat Flux</p>	<p>Short- and Long-wave Radiant Flux</p> <p>Cloud Reflectivity</p> <p>Cloud Transmissivity</p> <p>Cloud Emittance</p>

Table 2.2 Instrumentation List for Airborne Mass Momentum and Energy Flux Measurements
 (Assumption of an aircraft with under-wing mounting is inherent.)

PARAMETER	MEASUREMENT	RANGE		UNITS	QTY.	MANUFACTURER /MODEL
		LOW	HIGH			
State Variables	<u>Fast Response:</u> Ambient Temperature	-100	30	Deg C	1	Rosemount 102
	Ambient Pressure	100	1000	mbar	1	NAN MAC/Right Angle Rosemount 1201 and 1221
	Dew Point Temperature	-75	30	Deg C	1	General Eastern: 1011B A.I.R.: AIR-LA-1AC
Wind Velocity	<u>Fast Response:</u> Total Pressure	100	1000	mbar	2	Rosemount 1201 F2AF
	Dynamic Pressure	0	20	mbar	2	Rosemount 1221 F2AF
	Total Temperature	-100	30	Deg C	1	Rosemount 102
	Angle-of-Attack Differential Pressure	-10	10	mbar	2	Rosemount 1221 F2VL
	Angle-of-Sideslip Differential Pressure	-10	10	mbar	1	Rosemount 1221 F2VL
	<u>Slow Response:</u> Heading	360		Degrees	1	KVH Flux-Gate
	Bank	-15	15	Degrees	3	Schaevitz Forced Inclinometers
	Elevation	-15	15	Degrees	2	GPS Receiver and Preamplifier
	North Velocity	100		m/s		
	East Velocity	100		m/s		
	Vertical Velocity	10		m/s		
Cloud Physics	<u>Fast Response:</u> Heading					Humphrey Three-axis Accelerometer and Angular Rate Sensor
	Bank					
	Elevation					
	North Velocity					
	East Velocity					
	Vertical Velocity					
	Particle Size	10	100	microns		PMS OAP-2D-GA2
Thermal Radiation	Particle Count	Approx. 10 ³		cm ⁻³		
	Short and Long Wavelength	0.3 3	3 30	microns microns	2 2	Epp. Pyranomtr PSP, 8-48 Epp. Pyrogeomtr PIR

Turbulent Flux

The calculation of turbulent flux of momentum, energy and moisture, in the atmosphere, from measurements made from an airplane with six degrees of motional freedom, requires instruments from which the velocity of the moving air mass with respect to the earth can be extracted. The velocity of a moving air mass with respect to earth, is obtained by vectorially subtracting aircraft velocity with respect to the air mass from aircraft velocity with respect to earth. These velocities are referred to as airspeed and ground speed, respectively. Since airspeed is measured in a body-axis (airplane fixed) reference system, it is necessary to transform the airspeed vector into the inertial (earth fixed) frame of reference. FWG has derived the detailed governing equations required to make this transformation in a number of related studies. A derivation of these equations is given in Appendix A (see also: Frost, et al. (1987); Crooks, et al. (1967); Houbolt, et al. (1964); Lenschow (1972); Axford (1968); and Crawford, et al. (1990)).

The instruments specified in Table 2.2 are selected to provide measurements of all the variables required to solve the equations given in Appendix A. FWG has also carried out numerous analyses of sources of inaccuracy in data reduction procedures and identified instrumentation errors which influence the accuracy of the computed wind velocities. A recent overview of measuring winds with instrumented aircraft carried out for NASA/MSFC under Contract NAS8-37893 is provided in Appendix B for the convenience of the reader. This report provides a detailed description of instrumentation and principles of wind measurements, uncertainty analysis and methods of data communication. The selection of the instruments and data communication system recommended in Table 2.2 are based on the methods described in Appendix B and on FWG's extensive experience with turbulence measurements from aircraft and other systems (see pertinent documentation listed in Table 2.3).

Table 2.3 Related References to Wind Measurements With Aircraft

- | | |
|--|--|
| <p>1. Frost, W., H. P. Chang, and E. A. Ringnes. "Analyses and Assessments of Spanwise Gust Gradient Data from NASA B-57B Aircraft," Final report under Contract NAS1-17989 for NASA Langley Research Center, February 1987.</p> | <p>5a. Turkel, B. S., and W. Frost. "Computer Program for Determining Three-Components of Atmospheric Wind from Flight Instruments," Prepared for DOT/FAA/NAFEC, Atlantic City, N.J., April 1979.</p> |
| <p>2. Camp, D. W., W. Campbell, W. Frost, H. Murrow, and W. Painter. "NASA's B-57B Gust Gradient Program," <u>Journal of Aircraft</u>, 21(3):175-182, March 1984.</p> | <p>5b. Frost, W. "Comments on the Wind Shear Flight Measurement Program," Consulting report, FAA/NAFEC, Atlantic City, N.J., May 1976.</p> |
| <p>2a. Frost, W., "Measuring STS Winds with Instrumented Aircraft," Presentation at NASA/Dryden on Contract NAS8-37377, May 1987.</p> | <p>5c. Campbell, W., D. W. Camp, and W. Frost. "An Analysis of Spanwise Gust Gradient Data," AMS Ninth Conference on Aerospace and Aeronautical Meteorology, June 6-9, 1983.</p> |
| <p>2b. Frost, W., E.F. Arman, K. Hill, and D. Skow. "Analysis of Data from STS/Aircraft Wind Measurement Program," Presentation at NASA/Dryden on Contract NAS8-37377, May 1988.</p> | <p>6. Huang, K.H., W. Frost, and E.A. Ringnes. "Comparison of Wind and Turbulence Measurements from Doppler Lidar and Instrumented Aircraft," Final report under Contract NAS8-36188, May 1985.</p> |
| <p>2c. Frost, W., H.P. Chang, and K. Hill. "Measurement of Space Shuttle Launch Winds with an Instrumented Aircraft," presented at AIAA 26th Aerospace Sciences Meeting, Jan. 11-14, 1988, Reno, Nev.</p> | <p>7. Chang, H.P., D.W. Camp, and W. Frost. "Analysis of Aircraft Data Measured Near Microbursts," Interim report under Contract NAS5-29302 for NASA Goddard Space Flight Center, December 1986.</p> |
| <p>3. Camp, D. W., W. Campbell, C. Dow, M. Phillips, R. Gregory, and W. Frost. "Visualization of Gust Gradients and Aircraft Response as Measured by the NASA B-57B Aircraft," AIAA 22nd Aerospace Sciences Meeting, Jan. 9-12, 1984, Reno, Nev.</p> | <p>8. Chang, H.P., and W. Frost. "NASA B-57 Orographic Data Reduction and Analysis Relative to PBL Parameterization Models," Final report under Contract NAS5-28558 for NASA Goddard Space Flight Center, February 1986.</p> |
| <p>4. Frost, W., M. C. Lin, H. P. Chang, and E. A. Ringnes. "Analysis of Data From NASA B-57B Gust Gradient Program," Final Report under NASA Contracts NAS8-36177 and NAS8-35347, NASA Marshall Space Flight Center, Huntsville, Alabama, Sept. 1985.</p> | <p>9. Frost, W. "Remote Versus In-Situ Turbulence Measurements," <u>Proceedings of the Workshop on Atmospheric Turbulence Relative to Aviation, Missile, and Space Programs</u>, pp. 61-84, NASA Conference Publication 2468, pp. 53-71, April 1987.</p> |
| <p>5. Frost, W., and S. Arman. "Two-Point Spatial Turbulence Spectra for Aerospace Analysis Applications," presented at AIAA 27th Aerospace Science Meeting, January 1989, Reno, Nev.</p> | <p>10. Paige, T.S., A.E. Nelius, P.J. Murphy, and W. Frost. "Instrumented Rocket Wind Profiler," NASA Contract NAS8-38465 Final Report, August 24, 1990.</p> |

Table 2.3 (Continued)

- | | | | |
|-----|---|-----|---|
| 11. | Frost, W., R.E. Turner, K. Hill, and D. Skow. "Error Analysis of Winds Measured with an Instrumented Aircraft," presented at the Third International Conference on the Aviation Weather Systems, Southern United States, Jan. 1989. | 16. | Frost, W. "Flight in Low-Level Wind Shear," NASA CR 3678, March 1983. |
| 12. | Eraslan, A., and W. Frost. "Atmospheric Data Analysis Measured by Aircraft", NASA Goddard Contract NAS5-29302 Final Report, October 31, 1990. | 17. | Ringnes, E. A., and W. Frost. "Analysis of Aerodynamic Coefficients Using Gust Gradient Data: Spanwise Turbulence Effects on Airplane Performance," Final report for NASA/MSFC under Contract NAS8-36186, December 1984. |
| 13. | Bowles, R., and W. Frost (eds.). <u>Wind Shear/Turbulence Inputs to Flight Simulation and Systems Certification</u> , NASA CP 2474, Proceedings of workshop at NASA/Langley, May 30-June 1, 1984. | 18. | Frost, W., and A. M. Shahabi. "A Field Study of Wind Over a Simulated Block Building," NASA CR 2804, March 1977. |
| 14. | Chang, H. P., and W. Frost. "NASA B-57 Orographic Data Reduction and Analysis Relative to PBL Parameterization Models," Final report under Contract NAS5-28558 for Goddard Space Flight Center, February 1986. | 19. | Frost, W., G. H. Fichtl, J. R. Connell, and M. L. Hutto. "Mean Horizontal Wind Profiles Measured in the Atmospheric Boundary Layer About a Simulated Block Building," <u>Boundary-Layer Meteorology</u> , 11:135-145, 1977. |
| 15. | Frost, W., and R. L. Bowles. "Wind Shear Terms in the Equations of Aircraft Motion," <u>Journal of Aircraft</u> , 21(11):866-872, Nov. 1984. | 20. | Frost, W., and M. C. Lin. "Statistical Analysis of Turbulence Data from the NASA Marshall Space Flight Center Atmospheric Boundary Layer Tower Array Facility," NASA CR 3737, Nov. 1983. |
| | | 21. | Frost, W., and K. H. Huang. "Doppler Lidar Signal and Turbulence Study," Final report under NAS8-35185 for NASA/MSFC, Dec. 1983. |

The pallet design concept is thus based on a foundation established with flux measurement systems from previous and existing aircraft studies. The traditional approach for airborne measurement of turbulence employs an Inertial Navigation System (INS). Though well proven, the INS approach is very expensive. It requires significant space and power, limiting application to large platforms and further increasing cost. Its large size precludes co-location with the air motion sensors that are usually mounted on a boom. Thus, relative motion between the INS and

the air motion sensors is significant, introducing additional terms into the governing equations (Appendix A) which require additional measurements, which must be very accurate.

Recently however, Crawford, et al. (1990) developed the theory and instrumentation and demonstrated a low cost "generic" Mobile Flux Platform (MFP) to measure atmospheric turbulent structure and trace-gas air-surface exchange. The Atmospheric Turbulence and Diffusion MFP was made possible by recent technological advances in both low cost miniature sensors and computer technology.

The system proposed by Crawford, et al. (1990) is simplified by co-location of sensors, an approach recently made possible by technological advances in low-cost miniature acceleration and pressure sensors. Although orientation with respect to earth coordinates is not measured, overall accuracy is enhanced by directly measuring the linear translation components of the sensor-head motion. At each time step (40 Hz) the velocity vectors are computationally translated from platform to earth coordinates, obviating the need for a physically oriented measurement platform.

Platform velocity is determined by measuring the three acceleration components and integrating. Since the coordinate system orientation of the mobile platform is continually changing relative to the earth, each acceleration measurement is computationally rotated to earth coordinates before integrating with an efficient coordinate rotation algorithm. Since integration compounds any error over time, a low-frequency (0.67 Hz) position measurement is blended with the accelerometer data during integration. This technique retains fast response while suppressing the error growth.

The instrumentation specified in Table 2.2 is based on the design concept of Crawford, et al. (1990) and thus calls for "fast" and "slow" response instruments. The gust probe, state variable measurements, and inertial reference unit are handled as separate subsystems positioned

carefully on the airframe. The preliminary design proposes a modular unit, compatible with the suggested airframes, in which the critical hardware will be mounted in a bolt-on pod. The concept of such a pallet is shown in Figure 2.1. The gust probe, fast response temperature sensor, fast response humidity sensor, and inertial reference unit are packaged within the same rigid structure. Other hardware, such as radiometers, particle sizers, and steady-state temperature and humidity sensors, can readily be located elsewhere on the aircraft without detriment to the accuracy of the measured turbulent flux data.

The instrument pallet design has been biased towards the acquisition of an EGRETT II aircraft, recommended in Section 3.0 as the instrument pallet deployment vehicle. In Section 3.0 results of a survey of potential airplanes for use in the parameterization program is discussed and a recommendation as to the optimum aircraft for the GCM parameterization studies is provided.

The proposed modular instrument pallet would be mounted as a pod under the wing of an EGRETT II. The pod, which would resemble a missile, and be aerodynamically designed to minimize drag will house the fast response instruments necessary for the inertial dependent measurements (to be used for correlation and cross-correlation calculations supporting turbulent flux studies) and instruments for which the mounting alignment is critical. These instruments include the IMU, inclinometers, flux gate sensor, and probe head. Other instruments, such as the radiometers and particle measuring units, can be located elsewhere.

The initial design of the pod calls for a truss frame with a non-supporting skin. Analysis based on the weight of the pod, static deflection, and vibrational characteristics of the truss frame suggest this design is preferable to a thick walled tube with no internal supports. Confirmation of the design is pending a decision by NASA to proceed with hardware procurement and construction. Ease of fabrication and maintenance has also been considered in the recommended selection between the two potential design approaches.

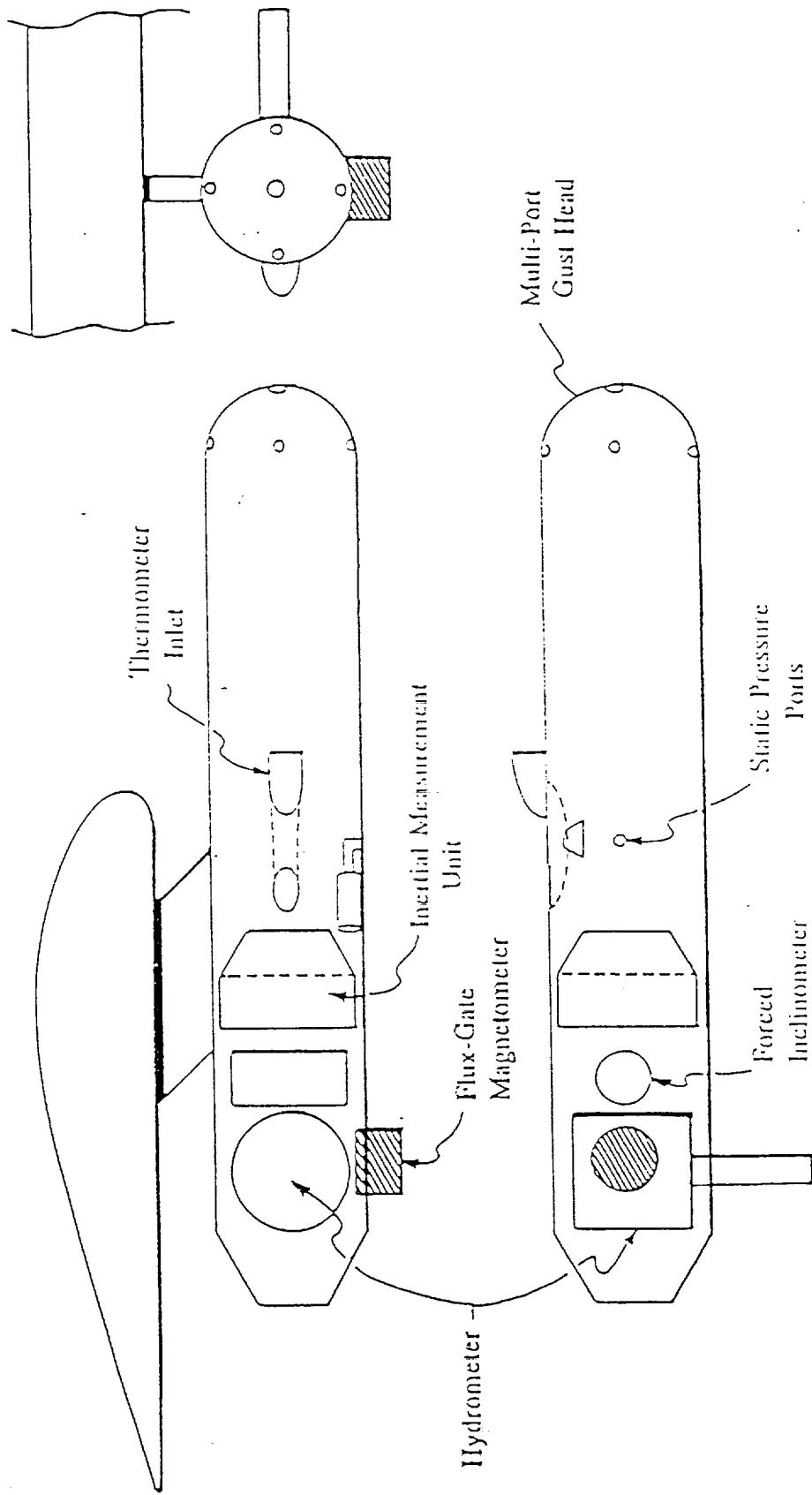


Figure 2.1 Modular turbulent flux sensor concept.

Inertial Measurement

Typically, an INS system is required for measuring the inertial velocity of the aircraft. However, based on the study by Crawford (1990), it is recommended that the inertial navigation system (INS) be deleted from the system and a low cost inertial measurement unit (IMU), forced inclinometers, and a flux-gate compass be employed in its place. The concept behind this choice of instruments, which will be used to determine the inertial velocity, attitude, and heading of the aircraft, is fully described by Crawford (1990).

Slow response, but highly stable, inclinometers and flux gate sensor are used to determine the attitude and heading of the aircraft. The differentiation of the position of the aircraft, as determined by the global positioning satellites (GPS), will provide the slow response, but very accurate, inertial velocity of the aircraft. An inexpensive IMU will be used for high frequency changes in the velocity, attitude, and heading of the aircraft. Because the IMU will be used as a fast response instrument, the effects of long term drift typical of INS systems will be nonexistent. Additionally, this combination is significantly less expensive than an INS and is suitable for the airborne modular instrumentation system under development.

The fundamental concept of inertial navigation is the existence of an inertial reference frame in which Newton's second law holds. By measuring accelerations in three independent directions, vehicle motion in this reference system can be described. Velocity is found by integrating acceleration by one integration and position by a second integration. In an INS, a reference frame with one component along the gravity vector and the two others in a plane normal to the gravity vector is maintained. This is accomplished by three gyroscopic elements. The gyroscopes are positioned on the stable table which is gimballed to the aircraft such that it is free to rotate about the three axis (roll, pitch, and yaw). Any angular disturbances are sensed by the gyros and proportional signals sent to three torque motors that keep the stable table in the

same inertial plane independent of aircraft motion. The three accelerometers also located on the stable table describe the time history of aircraft movement along the three axis in an inertial reference frame.

A major source of error in an INS with a gimballed stable table is the Schuler pendulum effect. An initial alignment error or a system imperfection will set in motion an oscillation of the stable table equivalent to an earth radius pendulum. The resulting misalignment of the stable table causes the two horizontal accelerometers to pick up a component of the gravitational acceleration thus introducing the error. This error is carried through the integrations and will translate into velocity and position errors, as well. The nature of this oscillation is such that the Schuler errors are small initially but will grow with time and periodically change polarity.

Earth rotation errors may be a significant source for inertial navigation errors depending on the time span of aircraft missions. Also, because of the relation upon latitude, earth rotation errors are greatest in the polar regions of the earth. Pertaining to the specified area of operation these errors may be of significance. By removing the source of these errors through the GPS system, the accuracy of the wind velocity calculations is expected to be significantly improved. Also, the cost of the system is significantly reduced.

Cloud and Radiation Physics

It is envisioned that the aircraft missions, as determined in FWG Contract Report (1992), will concentrate on studies of high altitude clouds, particularly high troposphere and tropopause cirrus, and convective cumulus and on radiation flux and its interaction with clouds. This requires the measurement of cloud particle sizes and radiation flux, as well as momentum, heat, and moisture flux. Langford, et al. (1990) recently examined the scientific questions to be addressed in defining instruments for an airborne cloud and radiation testbed. Although the design was tailored to the unique capabilities of the unmanned aircraft, the study is

comprehensive of the major needs for all aircraft. Their study focused on four missions:

- Measuring net radiation at the top of the troposphere
- Conducting radiometric measurements between cloud layers
- Cirrus cloud microphysics
- Warm cloud microphysics

Table 2.4 taken from Langford, et al. (1990) summarizes a canonical instrument array believed appropriate to accomplish essentially all of the major measurements required to support these missions.

Table 2.4 Integrated Atmospheric Radiation Measurement Program

Proposed by Prof. J.G. Anderson, Harvard University, as reported by Langford, et al. (1990)

OBJECTIVE	INSTRUMENT DESIGNATION
IR Radiance IR Radiance Difference (Upwelling, downwelling) IR Radiance Directionality IR Radiance Divergence	Dual Channel Interferometer Sounder Spectral resolution: 1 cm^{-1} Spectral range: $600\text{-}2800 \text{ cm}^{-1}$ Weight: 20 kg Instrument description: Bias between upwelling/downwelling channel removed by 180° rotation, dual black body in-flight calibration
IR Broadband Flux IR Broadband Flux Difference IR Broadband Flux Divergence	Pyrogeometer Spectral range: $3\text{-}50 \mu$ Weight upwelling channel: 2 kg Weight downwelling channel: 2 kg Instrument description: Bias between upwelling/downwelling removed by 180° rotation Subunits commercially available: EKO MS-200

Table 2.4 (Continued)

OBJECTIVE	INSTRUMENT DESIGNATION
Visible Radiance, Radiance Directionality, and Radiance Divergence	Dual Channel Ebert 1/4 meter Spectrometer with Diode Array Detection Spectral resolution: 1.5 nm Spectral range: 300-700 nm Weight: 10 kg Instrument description: Fiber optic coupled upward/downward radiance directionality observing heads, 180° rotation to eliminate offset
Visible Flux, Flux Difference (Upwelling/downwelling) Flux Divergence	Dual Channel (upwelling/downwelling) Pyranometer Spectral range: 0.3-3 μ Weight: 1 kg per channel Instrument description: Detector heads Available commercially: K & Z CM 11
UV Radiance, Radiance Difference (Upwelling/downwelling) Radiance Directionality Radiance Divergence	Dual Channel Ebert 1/4 meter Spectrometer with Diode Array Detection Spectral range: 250-400 nm Spectral resolution: 1 nm Weight: 10 kg Instrument description: Fiber optic coupled upward/downward radiance directionality observing heads, 180° rotation to eliminate offset
UV Flux, Flux Difference (Upwelling/downwelling) Flux Divergence	Dual Channel Fiber-Optic Coupled UV Integrating Radiometer Spectral range: 250-400 nm Weight: 2 kg
H ₂ O Vapor Cloud Liquid Water H ₂ O Ice	Lyman-α Fast Flow Fragment Fluorescence: $\text{H}_2\text{O} + h\nu \rightarrow \text{OH}^* + \text{H}$ $\downarrow 309 \text{ nm}$ OH with simultaneous Lyman-α absorption heated inlet for ice and liquid phase
Ozone	In Situ UV Absorption
CO ₂	In Situ IR Absorption
CCN Aerosols 0.1-3 μ	PMS ASASP-X

Table 2.4 (Continued)

OBJECTIVE	INSTRUMENT DESIGNATION
Cloud drop and large aerosol concentration and size distribution 2-50 μ size	PMS FSSP
Two-dimensional images of ice crystals	PMS-2DP
Pressure, Temperature Relative Humidity	
Data Systems, Instrument Control Telemetry, Data Storage	386-based, space-qualified flight systems developed for ER-2 and unmanned aircraft

The advantages of the integrated instrumentation/unmanned aircraft approach as summarized by Langford, et al. (1990) is presented in Table 2.5.

The properties of clouds that govern the latent, as well as the radiant energy flux and mass flux include not only the bulk structure of the cloud, but also their microphysical characteristics including the liquid water content, droplet size distribution, and ice particle concentration and size distribution. The size of water droplets and ice particles has been measured by many researchers dating back as far as 1972 (Heymsfield and Knollenberg (1972)). However, in past studies, the instrumentation used has not been able to sample small particles and thus has led to underestimates of particle densities and over estimates of mean particle size. Heymsfield and Platt (1984) estimated that 50 percent of extinction in cirrus is due to particles less than 20 microns in diameter which have not been measured with instruments used to date.

Table 2.5 Objectives of Proposed Atmospheric Radiation Instrumentation (Table 2.4) as Stated by Langford, et al. (1990)

- **OBJECTIVE 1: Radiance and Flux Observations**

These observations depend on the instruments themselves, rather than on the details of their installation in the unmanned aircraft or on the trajectory flown by the unmanned aircraft. Each wavelength interval (UV, VIS, IR) will provide both spectrally resolved data, as well as absolute radiance and flux measurements, as described in the instrument section. An advantage of the dual channel approach is the redundant cross-calibration it affords between each spectrometer/interferometer and the pyranometer/pyrogeometer combinations.

- **OBJECTIVE 2: Radiance and Flux Divergence**

Dramatic improvements in the determination of this quantity is realized with the integrated design of the instrument and fuselage. Suppose ϕ_i represents the observed radiance for flux, and let the hemisphere represent a single channel of the detector such that in configuration (a) channel 1 would be observing the downwelling radiation and channel 2 would be observing the upwelling radiation:



in configuration (b) the channels would be rotated by 180°:



The flux difference would then be observed first in configuration (a) and then in configuration (b) so that the downwelling flux, ϕ_{\downarrow} , would first be determined in configuration (a) by channel 1, yielding $\phi_{1\downarrow}$ and ϕ upwelling, ϕ_{\uparrow} , by channel 2, yielding $\phi_{2\uparrow}$. Configuration (b) would generate $\phi_{2\downarrow}$ and $\phi_{1\uparrow}$. But since ϕ_{\downarrow} and ϕ_{\uparrow} are both real quantities independent of the observing channel,

Table 2.5 (Continued)

$$\phi_{1\downarrow} - \phi_{2\downarrow} = \epsilon_1$$

is the offset between the channels for downwelling, and

$$\phi_{1\uparrow} - \phi_{2\uparrow} = \epsilon_2$$

is the offset for the upwelling channel. First, a consistency check can be applied to the difference, $\epsilon_1 - \epsilon_2$, to determine its cause. But second, this approach allows a very precise determination of

$$\phi_{\downarrow} - \phi_{\uparrow} = \text{Flux or Radiance Difference}$$

because the instrumental offset can be precisely eliminated at high frequency during each flight measurement phase.

- OBJECTIVE 3: Radiance or Flux Divergence

Determination of the $\vec{\nabla} \cdot \vec{\Phi}$ is the ultimate goal of radiation measurements in the atmosphere and a quantity for which previous observations were insufficiently precise to determine at a level of interest to theoretical analysis. The barriers to such observations are removed using the unmanned aircraft in conjunction with the dual channel optical instruments. The strategy of Langford, et al. (1990) is to use two aircraft flying trajectories initially together to inter-calibrate the dual channel instruments (UV, VIS.IR) then diverging to determine the radiance gained or lost in columnar increments, and then reconverging to cross-calibrate at the end of the measurement sequence.

Ice particle samplers follow two approaches - those based on impact coupled with some mechanism of imaging. Advanced systems under testing promise 7 μm size detection with 1 μm resolution (Heymsfield and Hagen (1989)). Other samplers use optical array techniques. These units are commercially available and detect 10-600 μm size particles (Heymsfield and Baumgardner (1985)). However, at high aircraft speeds, the minimum detectable size is on the order of 100 μm . Moreover, crystal habit is detectable only to ice sizes greater than 125 μm with current optical systems.

The liquid water content of ice particles can be obtained by integrating the particle size spectrum when knowledge of the crystal shape and density is available. At cirrus cloud formation temperatures, ice crystal habits typically include hexagonal plates, columns, single bullets, and bullet rosettes in order of occurrence at increasing temperatures. Aggregates of crystals are common at the warmer end of the temperature spectrum (i.e. 25 - 45 degrees C) with average sizes ranging from 0.5 - 1.0 mm. In some cases at slightly cooler temperatures, ice particles have been observed to be as large as 2.0 mm (Langford, et al. (1990)). The density of ice in cirrus particles is typically in the range of 0.6 - 0.9 g cm^{-3} (Heymsfield and Knollenberg (1972)).

FWG has recommended that for the interim, particle size information be obtained in the range of 10-100 μm with a PMS Model OAP-2D-GA2. The PMS Model OAP-2D-GA2 probe with the ice phase detection option can be set-up with any magnification from unity up to 20 \times which allows the user to select any sizing resolution from 10 to 100 microns per element. The probe can operate at slice rates up to 5 MHZ which allows reported resolution down to 20 microns per element at 100 meters per second particle velocity. Mechanical and optical constraints limit the selectable sizing resolution of the two configurations of the probe as follows:

Microns Per Array Element

<u>Configuration</u>	<u>MIN</u>	<u>MAX</u>
Cloud Droplet	10	100
Precipitation	50	150

For interim radiation measurements the Epp Pyranometer PSP8-48 and Epp Pyrogeometer PIR instruments are suggested. However, it is further recommended that for radiation and cloud physic measurements that the comprehensive work of Langford, et al. (1990) be closely followed. The feasibility of their system was established under Battelle Pacific Northwest Contract 126351-A-R2 and appears to represent an advanced system concept which will meet the measurement needs of NASA's future parameterization modeling studies.

3.0 AIRCRAFTS

FWG Associates, Inc. considered the pros and cons of several different aircrafts as to optimal characteristics for deployment of the flux measurement system. These are listed in Table 3.1. The considerations were based heavily on a report by Johnson and Cooper (1989) who reported results in a survey of atmospheric and oceanic scientists and of research managers representing all or most of the scientific areas of NASA. Table 3.2 gives a reduced version of the results and recommendations from Johnson and Cooper's (1989).

FWG, however, chose to focus attention on two, state-of-the-art aircraft which were not considered in the Johnson and Cooper (1989) survey. These two options are based on an analysis of the foreseeable missions of the instrumented aircraft required for the NASA GCM flux parameterization measurement programs, along with cost and operational considerations.

Table 3.1 Types of Aircraft Surveyed

Gulfstream I
Gulfstream II
Gulfstream III
Gulfstream IV
Sabreliner
Canadair Challenger 601-3A
Electra
King Air
Queen Air
F-111
T-28
Falcon 900
F-106
Grumman A-6
Lockheed S-3A
Convair F-106B
DC-9
DC-10
DC-8
ER-2
P-3
Boeing 737
EGRETT II
Aurora Perseus B (unmanned)

Table 3.2 Results of Aircraft Survey (Summarized from Johnson and Cooper (1989))

What is your choice selection limited to?

G-I Turboprop	1
Mid-Sized Jet	35
Storm-Penetration Aircraft	2

What is your choice selection limited to?

G-I Turboprop	1
King Air	2
Electra	1
Small Jet	0
Mid-Sized Jet	27
DC-9	5
Storm-Penetration Aircraft	0

Which mid-sized jet would you select?

G-II Class	0
G-III Class	0
G-IV Class	31

What is your second choice aircraft?

King Air Class	2
Turboprop (large)	1
Turboprop (middle)	2
Medium-large Jet	7
Storm-Penetration	16

The first option is a manned aircraft with a payload, range and altitude, comparable to that of the Gulfstream IV which is the favorite of Cooper, et al. (1989). FWG's investigation, however, indicates that an E-systems EGRETT II aircraft has an acquisition and operating cost significantly less than that of the Gulfstream IV (the Gulfstream IV has an acquisition and operating cost of, respectively, \$25M and \$1,100/hr, whereas the EGRETT II has an acquisition cost of \$10M and an operating cost of \$330/hr). The EGRETT II does sacrifice, however, the inherent capability of the Gulfstream IV to carry passengers. Details of the EGRETT II are given in Appendix C. The second option is an unmanned aircraft which is limited to a much smaller payload than the EGRETT II, but has a greater altitude, range and duration capability. The unmanned aircraft considered is the Aurora Perseus B.

Neither the EGRETT II nor the Perseus B is currently under production. However, an early version of the EGRETT II has flown in support of the International Cirrus Experiment (ICE) over northern Europe (Raschke, et al. (1989)) and a Perseus proof-of-concept is expected to fly in late spring of this year.

4.0 REFERENCES

- Axford, D.N. (1968): "On the Accuracy of Wind Measurements Using an Inertial Platform in an Aircraft, and an Example of a Measurement of the Vertical Mesostructure of the Atmosphere", J. of Applied Met., 7:645-666.
- Crawford, T.L., R.T. McMillen, and R.J. Dobosy (1990): "Development of a 'Generic' Mobile Flux Platform with Demonstration on a Small Airplane", NOAA Technical Memorandum ERL ARL-184, July.
- Crooks, W.M., F.M. Hoblit, D.T. Prophet, et al. (1967): "Project Hicat an Investigation of High Altitude Clear Air Turbulence", Technical Report AFFDL-TR-67-123, Vol. I, Wright-Patterson Air Force Base, OH, November.
- Etkin, B. (1972): Dynamics of Atmospheric Flight. New York: John Wiley & Sons, Inc.
- Frost, W., H.P. Chang, and E.A. Ringnes (1987): "Analyses and Assessments of Spanwise Gust Gradient Data from NASA B-57B Aircraft", Final report under Contract NAS1-17989 for NASA Langley Research Center, February.

FWG Associates, Inc. (1992): Appendix III of NASA Contract NAS5-30936, Final Contract Report.

Heymsfield, A.J. and R.G. Knollenberg (1972): "Properties of Cirrus Generating Cells", J. Atmos. Sci., 29:1358-1366.

Heymsfield, A.J. and C.M.R. Platt (1984): "A Parameterization of the Particle Size Spectrum of Ice Clouds in Terms of Ambient Temperature and the Ice Water Content", J. Atmos. Sci., 41:846-855.

Houbolt, J.C., R. Steiner, and K.G. Pratt (1964): "Dynamic Response of Airplanes to Atmospheric Turbulence Including Flight Data on Input and Response", NASA TR R-199.

Johnson, W.B. and W.A. Cooper (1989): "Meeting Review - The Second NCAR Research Aircraft Fleet Workshop", NCAR/TN-332+PROC, May.

Langford, J.S., J.G. Anderson, and J. Wyss (1990): "Unmanned Science Research Aircraft for the Atmospheric Radiation Measurement Program: A Feasibility Study", Battelle Northwest Laboratories Contract 126351-A-R2, Aurora Flight Sciences Corp., Alexandria, VA.

Lenschow, D.H. (1972): "The Measurement of Air Velocity and Temperature Using the NCAR Buffalo Aircraft Measuring System", NCAR-TN/EDD-74.

Paige, T.S. (1991): Personal telephone communications.

Raschke, E., D. Hennings, R. Sefzig, and M. Quante (Ed.) (1989): "ICE - International Cirrus Experiment, 1989 Field Phase Plan).

Rhyne, R.H. (1976): "Accuracy of Aircraft Velocities Obtained from Inertial Navigation Systems for Application to Airborne Wind Measurements", NASA TM-81826.

APPENDIX A

DERIVATION OF EQUATIONS

The velocity of a moving air mass (or the wind) with respect to earth, is obtained by vectorially subtracting aircraft velocity with respect to the air mass from aircraft velocity with respect to earth. Since airspeed is measured in a body-axis (airplane fixed reference system), it is necessary to rotate the airspeed vector into the inertial (earth fixed) frame of reference. The governing equations are listed below. For a more detailed derivation of these equations see Frost, et al. (1987); Crooks, et al. (1967); Houbolt, et al. (1964); Lenschow (1972); and Axford (1968).

The wind velocity vector components at some position \vec{r} measured from the c.g. of a rigid aircraft are designated W_N , W_E and W_Z . These are measured in the coordinate system with the x-axis pointing north, the y-axis point east, and the vertical axis pointing along the local vertical (gravity vector; positive downward). The coordinate system is called the true north coordinate system and is taken as the inertial system in this analysis (however, see Rhyne (1976)).* The W_N , W_E and W_Z components point north, east, and vertical, respectively, and are given by:

$$\begin{pmatrix} U+W_N \\ V+W_E \\ W+W_Z \end{pmatrix} = \begin{pmatrix} V_N \\ V_E \\ V_Z \end{pmatrix} + \begin{pmatrix} U_R \\ V_R \\ W_R \end{pmatrix} \quad (A-1)$$

where it is assumed that effects due to the earth's rotation are small.

* Grid north is true north at the platform alignment location, but as the platform moves east or west from its initial alignment point, its north-south axis is not torqued to point at true north but remains parallel to a vertical plane through the meridian at which it was aligned. (The north-south and east-west axes are torqued to be perpendicular to the local vertical at all times, however.) For all practical purposes, the inertial-platform axis system can be assumed to be aligned with true north, considering the latitudes of operation and the east-west distances flown.

The symbols, U, V, and W designate the components of the aircraft velocity vector relative to the air mass measured in the true north coordinate system; V_N , V_E and V_Z are the inertial velocity vector components of the c.g. of the aircraft; and U_R , V_R and W_R are the rotational velocity components of the position \vec{r} relative to the c.g. (or INS) of the aircraft due to rotation of the frame of reference fixed on the airplane, i.e., the body coordinate system.

The velocity of a point $\vec{r} = l_x \vec{i} + l_y \vec{j} + l_z \vec{k}$ measured in the airplane frame of reference (i.e., body coordinates) which is rotating relative to the fixed frame of reference (i.e., inertial frame taken as the true north coordinate system in this study) is given by $\vec{\Omega} \times \vec{r}$, where $\vec{\Omega}$ is the angular velocity of the airplane frame of reference relative to the inertial frame of reference. The velocity components of the position \vec{r} in body coordinates, U'_R , V'_R , and W'_R (rotational velocity) expressed in terms of the Euler angles (Ψ , θ , ϕ) are:

$$\begin{pmatrix} U'_R \\ V'_R \\ W'_R \end{pmatrix} = \begin{pmatrix} l_z(\dot{\theta} \cos \phi + \dot{\Psi} \sin \phi \cos \theta) + l_y(\dot{\theta} \sin \phi - \dot{\Psi} \cos \phi \cos \theta) \\ -[l_x(\dot{\phi} - \dot{\Psi} \sin \theta) + l_z(\dot{\theta} \sin \phi - \dot{\Psi} \cos \phi \cos \theta)] \\ l_y(\dot{\phi} - \dot{\Psi} \sin \theta) - l_x(\dot{\theta} \cos \phi + \dot{\Psi} \sin \phi \cos \theta) \end{pmatrix} \quad (A-2)$$

These rotational velocity components, U'_R , V'_R , and W'_R (in the body coordinate system) are transformed into the velocity components, U_R , V_R , and W_R in the inertial coordinate system by:

$$\begin{pmatrix} U_R \\ V_R \\ W_R \end{pmatrix} = L_{IB} \begin{pmatrix} U'_R \\ V'_R \\ W'_R \end{pmatrix} \quad (\text{A-3})$$

where, the matrix L_{IB} transforms the velocity components in the body coordinate system to the inertial coordinate system. This transform matrix has the following form: roll angle (ϕ), yaw angle (Ψ), and pitch angle (θ).

$$L_{IB} = \begin{pmatrix} \cos\theta\cos\Psi & \sin\phi\sin\theta\cos\Psi & \cos\phi\sin\theta\cos\Psi \\ & -\cos\phi\sin\Psi & +\sin\phi\sin\Psi \\ \cos\theta\sin\Psi & \sin\phi\sin\theta\sin\Psi & \cos\phi\sin\theta\sin\Psi \\ & +\cos\phi\cos\Psi & -\sin\phi\cos\Psi \\ -\sin\theta & \sin\theta\cos\theta & \cos\phi\cos\theta \end{pmatrix} \quad (\text{A-4})$$

The values of U , V , and W in Equation (A-1), which are the true airspeed components in the inertial coordinate system, are not measured directly in the flight experiments. Rather, the true airspeed of the aircraft, \bar{V} , is measured in a coordinate system aligned along the relative airspeed vector. The velocity components U' , V' , and W' (i.e., measured in body coordinates) are related to the true airspeed, \bar{V} , by the relationship:

$$\begin{pmatrix} U' \\ V' \\ W' \end{pmatrix} = L_{BW} \begin{pmatrix} \bar{V} \\ 0 \\ 0 \end{pmatrix} \quad (\text{A-5})$$

where

$$L_{BW} = \begin{pmatrix} \cos\alpha\cos\beta & -\cos\alpha\sin\beta & -\sin\alpha \\ \sin\beta & \cos\beta & 0 \\ \sin\alpha\cos\beta & -\sin\alpha\sin\beta & \cos\alpha \end{pmatrix} \quad (\text{A-6})$$

and α and β are the angle of attack ($\alpha = \tan^{-1} W'/U'$) and sideslip angle ($\beta = \sin^{-1} V'/\bar{V}$), respectively. L_{BW} transforms the velocity components measured in a frame of reference for which x-axis is located along the relative velocity vector (Etkin (1972)) (calls this the "wind" coordinate system) to the body coordinate system.

The above assumes that the actual magnitude of the relative velocity or true airspeed is measured and not some fractional component such as can occur with a pitot tube. The aircraft velocity components U , V , and W in the inertial coordinate system are:

$$\begin{pmatrix} U \\ V \\ W \end{pmatrix} = L_{IB} \begin{pmatrix} U' \\ V' \\ W' \end{pmatrix} \quad (\text{A-7})$$

Substituting Equations A-3 and A-7 into Equation A-1, the wind velocity measured in the inertial coordinate system is thus given by:

$$\begin{pmatrix} W_N \\ W_E \\ W_Z \end{pmatrix} = \begin{pmatrix} V_N \\ V_E \\ V_Z \end{pmatrix} + L_{IB} \begin{pmatrix} U'_R - U' \\ V'_R - V' \\ W'_R - W' \end{pmatrix} \quad (\text{A-8})$$

In fully expanded form, the nonlinear system of equations for computing the wind velocity vector components in an inertial frame of reference is:

$$\begin{aligned}
W_N &= -\bar{V}[\cos \alpha \cos \beta \cos \Psi \cos \theta + \sin \beta(-\sin \Psi \cos \phi + \cos \Psi \sin \theta \sin \phi) \\
&\quad + \sin \alpha \cos \beta(\cos \Psi \sin \theta \cos \phi + \sin \Psi \sin \phi)] + V_N \\
&\quad - l_x(\dot{\Psi} \sin \Psi \cos \theta - \dot{\theta} \cos \Psi \sin \theta) \\
&\quad + l_y[\dot{\theta} \sin \phi \cos \theta \cos \Psi + \dot{\phi}(\sin \phi \sin \Psi + \cos \phi \sin \theta \cos \Psi) \\
&\quad - \dot{\Psi}(\cos \phi \cos \Psi + \sin \theta \sin \phi \sin \Psi)] \\
&\quad + l_z[\dot{\theta} \cos \phi \cos \theta \cos \Psi + \dot{\phi}(\cos \phi \sin \Psi - \sin \phi \sin \theta \cos \Psi) \\
&\quad + \dot{\Psi}(\sin \phi \cos \Psi - \sin \theta \cos \theta \sin \Psi)] \\
W_E &= -\bar{V}[\cos \alpha \cos \beta \sin \Psi \cos \theta + \sin \beta(\cos \Psi \cos \phi + \sin \Psi \sin \theta \sin \phi) \\
&\quad + \sin \alpha \cos \beta(\sin \Psi \sin \theta \cos \phi - \cos \Psi \sin \phi)] + V_E \\
&\quad - l_x(\dot{\theta} \sin \theta \sin \Psi - \dot{\Psi} \cos \phi \cos \theta) \\
&\quad + l_y[\dot{\theta} \sin \phi \cos \theta \sin \Psi + \dot{\phi}(-\sin \phi \cos \Psi + \cos \phi \sin \theta \sin \Psi) \\
&\quad - \dot{\Psi}(\cos \phi \sin \Psi - \sin \theta \sin \phi \cos \Psi)] \\
&\quad + l_z[\dot{\theta} \cos \phi \cos \theta \sin \Psi - \dot{\phi}(\cos \phi \cos \Psi + \sin \phi \sin \theta \sin \Psi) \\
&\quad + \dot{\Psi}(\sin \phi \sin \Psi + \sin \theta \cos \phi \cos \Psi)] \\
W_Z &= -\bar{V}[-\cos \alpha \cos \beta \sin \theta + \sin \beta \cos \theta \sin \phi + \sin \alpha \cos \beta \cos \theta \cos \phi] \\
&\quad + V_Z + l_x \dot{\theta} \cos \theta - l_y[\dot{\theta} \sin \phi \sin \theta - \dot{\phi} \cos \phi \cos \theta] \\
&\quad - l_z[\dot{\theta} \cos \phi \sin \theta + \dot{\phi} \sin \phi \cos \theta]
\end{aligned}$$

The variables which must be measured in order to compute wind velocity vector components from these equations are listed in Table A.1 and l_x , l_y , l_z are distances in meters from the INS measuring element to the probe measuring station (assuming the α , β and \bar{V} sensors are mounted on a probe) along the three body axes, respectively.

Table A.1 Variables Requiring Measurement In Order To Compute Wind Velocity Components

CHANNEL	SYMBOL	DESCRIPTION
1	τ	time (sec)
2	α	angle of attack (rad)
3	β	sideslip angle (rad)
4	ϕ	roll angle (rad)
5	θ	pitch angle (rad)
6	ψ	heading angle (rad)
7	$\dot{\phi}$	roll rate (rad/sec)
8	$\dot{\theta}$	pitch rate (rad/sec)
9	$\dot{\psi}$	yaw rate (rad/sec)
10	P	static pressure (Kpa)
11	T	temperature (Kelvin)
12	LAT	latitude (deg)
13	LONG	longitude (deg)
14	V_N	north-south airplane inertial velocity (m/sec)
15	V_E	east-west airplane inertial velocity (m/sec)
16	V_Z	vertical airplane inertial velocity (m/sec)
17	∇	true airspeed (m/sec)

Crawford, et al. (1990) have located the airspeed sensors around the INS system (actually the accelerometers). This significantly simplifies the equations because the l_x , l_y and l_z terms vanish. Thus:

$$W_N = -\bar{V} [\cos\alpha \cos\beta \cos\psi \cos\theta + \sin\beta (-\sin\psi \cos\phi + \cos\psi \sin\theta \sin\phi) + \sin\alpha \cos\beta (\cos\psi \sin\theta \cos\phi + \sin\psi \sin\phi)] + V_N$$

$$W_E = -\bar{V} [\cos\alpha \cos\beta \sin\psi \cos\theta + \sin\beta (\cos\psi \cos\phi + \sin\psi \sin\theta \sin\phi) + \sin\alpha \cos\beta (\sin\psi \sin\theta \cos\phi - \cos\psi \sin\phi)] + V_E$$

$$W_z = -\bar{V} [-\cos\alpha \cos\beta \sin\theta + \sin\beta \cos\theta \sin\phi + \sin\alpha \cos\beta \cos\theta \cos\phi] + V_z$$

The above equations assume that inertial velocities V_N , V_E and V_z are available from the INS output. Crawford, et al. (1990) does not use an INS or stabilized platform and integrates accelerometer outputs. The wind velocity becomes:

$$\vec{W} = L_{IB} \vec{V} + \vec{V}_e + \int_0^t \dot{V}_e dt'$$

where

$$\vec{W} = W_N \vec{i} + W_E \vec{j} + W_z \vec{k}$$

$$\vec{V}_e = V_N \vec{i} + V_E \vec{j} + V_z \vec{k}$$

and is obtained from the relationship:

$$\vec{V}_e = L_{IB} \vec{b} + \vec{g}$$

The term \vec{b} is the output of the accelerometers.

The advantages of Crawford, et al. (1990) approach is explained in the main text.

APPENDIX B

DESIGN METHODOLOGY AND PROCEDURES

This appendix contains the report "Guide to Measurement of Winds with Instrumented Aircraft". It describes, in detail, the basic methodologies used in selecting instruments and data communication systems present in the main text of this report.

The report is appended for the convenience of the reader since it is not readily available in the open literature and, in principle, has served as the design handbook for the airborne unit developed under this NAS5-30936 contract effort.

Submitted by:

Walter Frost
Terry S. Paige
Andrew E. Nelius
FWG Associates, Inc.
217 Lakewood Drive
Tullahoma, TN 37388

Submitted to:

NASA Marshall Space Flight Center
Marshall Space Flight Center, AL 35802

ENCLOSED FOR THE CONVENIENCE OF THE READER

FINAL REPORT
Contract NAS8-37893

GUIDE TO MEASUREMENT
OF WINDS WITH
INSTRUMENTED AIRCRAFT

March 25, 1991

Approved:

A handwritten signature in cursive script, appearing to read "Walter Frost", written over a horizontal line.

Dr. Walter Frost, President

TABLE OF CONTENTS

<u>Section</u>	<u>Page</u>
NOMENCLATURE	iii
LIST OF FIGURES	iv
LIST OF TABLES	v
1.0 INTRODUCTION	1
2.0 INSTRUMENTATION AND PRINCIPLES OF WIND MEASUREMENT	9
2.1 Relative Airspeed	14
2.2 Inertial Measurements	23
3.0 UNCERTAINTY ANALYSIS	28
3.1 Design Uncertainties	28
3.2 Operational and Dynamic Uncertainties	33
3.2.1 Sources of Inaccuracy in Data Reduction	33
3.2.2 Inertial Velocity and Position Errors	33
3.2.3 Flow Vane Errors	41
3.2.4 Influence of Error Corrections	44
4.0 DATA COMMUNICATION	49
4.1 Data Transmission	49
4.2 Data Acquisition	54
5.0 SUMMARY	57
6.0 REFERENCES	58
APPENDIX A Wind Vector Calculations from an Airborne Platform	66
A.1 Body-Fixed Frame	66
A.2 Vehicle-Centered Vertical Frame	73
A.3 Earth-Surface Frame	73

TABLE OF CONTENTS, continued

<u>Section</u>	<u>Page</u>
APPENDIX B Error Analysis for Instrumentation Requirements for Wind Velocity Calculation from Measurements Made from an Airborne Platform	75

NOMENCLATURE

\bar{a}	Vehicle acceleration
a_x	Acceleration component in the x direction
a_y	Acceleration component in the y direction
a_z	Acceleration component in the z direction
F	An arbitrary function
k	Flow angle sensitivity factor
L_{BV}	Vehicle-centered to body-fixed frame vector transformation matrix
l_x	Displacement component of the gust probe in the x direction
l_y	Displacement component of the gust probe in the y direction
l_z	Displacement component of the gust probe in the z direction
M	Mach number
p	Roll rate
p	Static pressure
p_o	Total pressure
q	Dynamic pressure
r	Yaw rate
R	Ideal gas constant for air
T_o	Total temperature
t	Time
t_o	Initial time
V_a	Airspeed
\vec{V}_a	Relative airspeed velocity
\vec{V}_e	Vehicle inertial velocity
\vec{W}	Wind velocity
α	Angle-of-attack
β	Angle-of-sideslip
κ	Ratio of specific heats
$\Delta()$	Uncertainty of the parameter in ()
τ	Integration dummy variable
ξ_i	A set of independent variables
ϕ	Bank angle
ψ	Heading
θ	Elevation angle
θ	Displacement angle

LIST OF FIGURES

<u>Figure</u>	<u>Page</u>
2.1 Physical quantities required for airspeed measurement.	15
2.2 Angle-of-attack and sideslip angle type sensors.	16
3.1 Calculated airspeed uncertainty as a function of pressure and temperature measurement uncertainties.	29
3.2 Relative airspeed velocity uncertainty as a function of airspeed and flow angle uncertainties.	30
3.3 Wind velocity uncertainty as a function of relative airspeed velocity uncertainty, inertial velocity uncertainty, euler angle uncertainty, and airspeed.	32
3.4 Event marker location of B-57 on box pattern flights.	36
3.5 In-flight Schuler position error.	37
3.6 In-flight Schuler position error.	39
3.7 In-flight Schuler inertial speed error.	40
3.8 Error in east inertial speed.	42
3.9 Error in north inertial speed.	43
3.10 Horizontal wind vectors without corrections.	45
3.11 Horizontal wind vectors with sideslip-angle corrections.	46
3.12 Horizontal wind vectors after airspeed, sideslip-angle and inertial velocity and position corrections.	48
4.1 Data path aboard aircraft.	51
4.2 Minimum sampling frequency for 11-channel system.	52
A.1 Free vanes on an airdata probe for flow angle measurements (Sakamoto, 1976).	69
A.2 ER-2 radome with angle-of-attack and sideslip angle pressure ports (Scott, et al., 1989).	70
A.3 Typical flow angle error from free vanes (Sakamoto, 1976).	72

LIST OF TABLES

<u>Table</u>	<u>Page</u>
2.1 Variables required for wind computations.	11
3.1 Example measurement uncertainties.	31
4.1 Telemetry comparison.	54

1.0 INTRODUCTION

Instrumented aircraft have been used for measuring atmospheric winds and turbulence for a number of years. In general, these measurements have been for straight and level flight where limited range instrumentation can be used to measure the parameters of interest and linearized equations can be used to reduce the data. Recently, however, there has been considerable interest in measuring winds along steep flight paths, for example, with respect to STS wind profile measurements in support of day-of-launch activities. The purpose of this report is to review aircraft measurements techniques. Review of past and present applications of instrument aircraft to atmospheric observations is presented. Questions to be answered relative to measuring mean wind profiles as contrasted to turbulence measurements are then addressed. Finally, requirements of instrumentation and accuracy, data acquisition, data reduction, and theoretical and certainty analysis are considered.

Review of Past and Present Applications of Instrumented Aircraft to Atmospheric Observations

The past and present use of instrumented aircraft has been primarily to measure clear air turbulence and winds and turbulence associated with convective storms or gust fronts. The limitations of these aircraft experiments were primarily straight level flight with limited range sensors, limited environmental exposure, simplification of the trigonometric functions of the aircraft attitude and linearized wind equations. A review of the scope and objectives of a variety of aircraft measurement programs as reported in the literature follows.

Telford, Wagner, and Vaziri (1977) point out that the measurement of air motion has now advanced to the stage where routine measurements of the three components of the velocity of the air can be made from aircraft to an accuracy

of about 0.3 m/s. They further note that techniques have advanced, from using a simple accelerometer at the center of gravity of the aircraft to give an indication of the updrafts causing the aircraft gust load, to the present inertial platform base systems now in use. Prior to this report, Telford and Wagner (1974) described the measurements of horizontal motion near clouds from aircraft. They described the measurement of air motion for flight in and around small cumulus clouds using a high quality inertial platform and an integrated data handling system. McBean and MacPherson (1976) discuss measurements of the fluctuations of wind, temperature, and humidity using an instrumented aircraft at altitudes from 30 to 300 meters above Lake Ontario. A NAET-33 turbulence research aircraft (a single engine military trainer) was used for the experiment. As instrumented, this aircraft was capable of measuring the three orthogonal components of the true gust velocity and the related fluxes of heat, momentum, and water vapor. Other in flight measurements allowed computation of atmospheric pressure, temperature, humidity, and Doppler wind speed and direction, as well as the altitude, speed, and orientation of the aircraft. A description of the aircraft, its instrumentation, and the data analysis program are available in MacPherson (1973).

Extensive clear air turbulence measurements have been carried out with an instrumented NASA B-57B aircraft. These measurements were part of the NASA Langley Research Center's MAT (Measurement of Atmospheric Turbulence) program. Measurements were carried out to altitudes ranging as high as 15 km. The particular emphasis of this program was to extend power spectral measurements of atmospheric turbulences to wavelengths of at least 9,000 m under several different meteorological conditions. The flight instrumentation system for acquisition of the atmospheric turbulence data is given by Meissner (1976). Some of the measurement results are presented in two volumes. The first volume (Davis, Champine

and Ehernberger (1979)) presents the flight planning, operations, and turbulence forecasting aspects. The second volume (Waco (1979)) presents 27 maps of flights of particular meteorological interest with narrative summaries and with synoptic maps and rawinsonde sounding data.

Winebarger (1986) employed a highly instrumented F-106B Delta Dart airplane to make thunderstorm penetrations in the storm hazards program. Details on the F-106B airplane and the criteria used in choosing the airplane for the mission can be found in Fisher, Keyser, Gerald, Deal, Perry, Thomas, and Pitts (1980) and Fisher, Keyser, Gerald, and Deal (1982). The F-106B is equipped with a number of data systems to measure the environmental and electro- magnetic characteristics of thunderstorms during penetration.

The Royal Aircraft establishment, Woodfield and Vaughn (1983), has employed an HS-125 to conduct both windshear and vortex wake studies for many years. In addition to basic instrumentation to measure turbulence in three axis at frequencies up to 20 Hz, the RAE HS-125 was uniquely instrumented with a laser airspeed system (LATAS), which detects windshear several hundred meters ahead of the aircraft and a Marconi AD660 Doppler Velocity Sensor which could be used as the basis of a ground speed/airspeed display.

Rider, Thomson, and Verinder (1971) fitted a Mirage A-376 with a modified nose cone to carry a differential pressure gust probe. The probe was extensively tested in a transonic wind tunnel and the results were confirmed by comprehensive flight test programs. The instrumented Mirage fighter aircraft carried out three flights in an area of severe and low level turbulence. True gust velocities were computed for 540 seconds of recorded data and power spectral energy distributions were determined which confirm various levels of turbulence.

Crooks, Hoblit, and Prophet (1967) describe high altitude clear air turbulence

(HICAT) flight investigations. A digital instrumentation system for the measurement of CAT in the wavelength range from about 100 ft to 60,000 ft was utilized. The program effort required the measurement of CAT velocity components at altitudes of 45,000 to 75,000 ft in seven geographical areas. Instrumentation carried aboard the HICAT aircraft, and Air Force U2 consisted of a PCM system, an inertial navigation system, aerodynamic and aircraft response sensors (including a fixed vane gust probe), an oscillograph record, and a digital magnetic tape recorder. The program objective was to determine the statistical characteristics of high altitude CAT so as to improve structural design criteria. Time histories and power spectra are provided in Volume I of the report while meteorological data and flight track maps are included in Volume II.

Frost, Chang, and Ringnes (1987) present the analysis of turbulence measured across the airfoil of a Cambera B-57 aircraft. The aircraft was instrumented with probes for measuring winds at both wing tips and at the nose. Statistical properties of the turbulence are reported. These consist of the standard deviations of turbulence measured by each individual probe, standard deviations and probability distributions of difference in turbulence measured between probes, and auto and two-point spatial correlations in spectra.

Ganzer, Joppa, and van der Wees (1977) used a similarly equipped aircraft to measure turbulence. A Beechcraft D-18S, a low wing all-metal semi-mono-coque, aircraft was used. The aircraft was instrumented to measure and record the variables necessary for the calculation of the turbulence velocity in longitudinal, lateral, and vertical directions at the wing tips of the aircraft. A detailed description of the instrumentation and calibration is presented in the report.

Kraus, Hacker, and Hartmann (1990) carried out research flights in the Coorong coastal area of South Australia to investigate sea breeze fronts. The flights yielded

data sets of the structure of the fronts in the cross frontal direction with a spatial resolution of approximately three meters. The study is focused on the budgets of sensible and latent heat in the vicinity of the front and on frontogenesis/frontolysis processes which are closely related to budget considerations. A light, well instrumented aircraft developed by the Finders Institute for Atmospheric and Marine Sciences (FIAMS) was used. The aircraft, a GROB G109B, along with its instrumentation and capabilities are described in detail by Hacker and Schwerdtfeger (1988). Air temperature was measured using a fast PT100 sensor, humidity was measured with an A.I.R., Inc. Lyman- α hydrometer and a Meteolab dewpoint mirror. The three dimensional wind vector was sensed by a system consisting of a five-hole probe, a Rockwell-Collins AHS-85 altitude and heading reference system and a Trimble TANS GPS navigation system (satellite based Global Positioning Systems). The horizontal wind vector was determined from an algorithm which utilized high resolution integrated inertial data from the AHRS with the stable low resolution data from the GPS navigation system. The accuracies of the instrumentation were reported as approximately $0.02 K^{\circ}$ for temperature and 0.02 g/kg for humidity. For the wind vector, the reported accuracies were 0.9 m/s for the horizontal wind and a few centimeters per second for the vertical wind.

Lenschow, Li, Zhu, and Stankov (1987) present measurements of the stable stratified nocturnal boundaries layer obtained with the Queen Air NCAR aircraft during the severe environmental storms in a mesoscale experiment (SESAME). The cases presented were obtained over rolling terrain in central Oklahoma, with a mean slope of about 0.003. The results are reported to be in general agreement with previous modeling and observational studies for the mean and turbulence structure of the nocturnal boundary layer. An exception was that the eddy diffusivity of heat and consequently the flux Richardson numbers are less than expected.

Stromberg, Mill, Choularton, and Gallagher (1989) made airborne measurements of stably stratified airflow over the Pennines using an instrumented glider. The parameters measured in flight were air temperature, airspeed, vertical acceleration, and vertical velocity. Airspeed and pressure altitude were measured using sensitive pressure transducers and resolution was reported as better than one millibar for altitude and approximately one meter per second for airspeed. Vertical velocity of the air was measured using the sail plane variometer system. In this system, the inherent sink rate at a particular speed was automatically subtracted from the total signal to give the vertical velocity of the air itself. The resolution was better than 1 meter per second and accuracy to within plus or minus 0.1 meter per second.

Lenschow and Johnson (1968) made concurrent airplane and balloon measurements of atmospheric boundary layers structure over a forest. Mean wind profiles up to a height of 2,000 m and supporting surface layer measurements were observed. The airplane measurements of vertical and horizontal velocity were obtained from a pressure differential gust probe mounted on a boom on the nose of a twin engine Cessina 310 airplane. Further description of the airplane is provided in Dutton and Lenschow (1962) and Lenschow (1965). The system removes airplane motions from the air vertical velocity measurements by measuring the pitch angle and vertical acceleration of the airplane. The technique is limited to wavelengths of less than 1.3 km for airspeeds of 70 m/s primarily because of drift in the gyro used to measure pitch angle. The velocity fluctuations were filtered with an RC high-pass filter with a time constant of 3.0 seconds which results in a half power wavelength of 1.3 km. Temperature was measured with a thermal couple mounted on the boom less than 50 cm behind the gust probe sensors. The time constant of the thermal couple is about 1 second.

8

Benjamin (1989) reports an objective analysis scheme for meteorological variables on constant potential temperature surfaces. The analysis uses the form of multivariant statistical interpretation and is designed to retain mesoscale detail in various observations including rawinsonde, surface, aircraft, satellite, and wind profiler data while combining them with a forecast background field. Commercial aircraft observations of temperature and wind were used. Aircraft reports of icing were converted into approximate observations of 100% relative humidity.

Parish and Bromwich (1989) report instrumented aircraft observations of the katabatic wind region near Terra Nova Bay. Two aircraft missions were flown to sample the boundary layer dynamics associated with the intense katabatic winds. An LC-130 instrumented aircraft developed for meteorological research was utilized. The data system is described in Renard and Foster (1978) and an itemization of the onboard instrumentation is given in Gosink (1982). The LC-130 is equipped to record a total of 18 data channels of meteorological and navigational parameters at 1 second intervals on high density magnetic tapes.

Gage and Nastrom (1986) present a theoretical interpretation of the wave number spectra of winds and temperature obtained from an analysis of data from over 6,900 flights during the global atmospheric sampling program (GASP). Data were collected automatically on specially instrumented Boeing 747 aircraft in routine commercial service, with most measurements made in the altitude range between 9 and 14 km. For most flights the flight interval is 75 km and the length scale sampled range to about 5,000 km. The 6,900 flights in the GASP data base were made during all seasons and covered a wide variety of latitudes and longitudes.

The proceeding summarizes types of aircraft measurement programs which have been carried out using a range of aircraft from highly instrumented aircraft, to gliders to commercial aircraft of "opportunity". The principle of extracting

7

winds from the measurements, however, is basically the same. This principle is described in the next section. Essentially, it is a matter of measuring the aircraft inertial velocity vector and the velocity vector of the air relative to the aircraft. The difference is the wind velocity vector. The parameters which need to be measured and a variety of the instrument types used are described in the next section.

2.0 INSTRUMENTATION AND PRINCIPLES OF WIND MEASUREMENT

The principle and governing equations relative to the measurement of winds from an aircraft are well documented (for example see Axford (1968); Lenschow (1986); Frost, Chang, and Ringnes (1987)). The basic physical principle is embodied in the vector relationship

$$\vec{W} = \vec{V}_e - \vec{V}_a \quad (2.1)$$

where \vec{W} is the wind vector, \vec{V}_e is the aircraft inertial velocity vector and \vec{V}_a , is the relative airspeed vector. The aircraft therefore must be equipped with instruments that measure ground speed (i.e., inertial) and the speed of the air relative to the aircraft. Expressing the vectors \vec{V}_e and \vec{V}_a in an appropriate coordinate system to provide windspeeds in the earth's coordinate system requires that the 6 degree-of-freedom motion of the aircraft be measured. The system of equations required to reduce the aircraft measurements into components of windspeed are thus complex. They have been fully derived, however, and are reported in the previously mentioned references (Frost, Chang and Ringnes (1987) is an example). This derivation is partially reproduced in Appendix A.

The fully expanded form of the system of equations for computing the wind velocity vector components in the earth's frame of reference is:

$$\begin{aligned} W_N = & -\bar{V}[\cos \alpha \cos \beta \cos \Psi \cos \theta + \sin \beta(-\sin \Psi \cos \phi + \cos \Psi \sin \theta \sin \phi) \\ & + \sin \alpha \cos \beta(\cos \Psi \sin \theta \cos \phi + \sin \Psi \sin \phi)] + V_N \\ & - l_x(\dot{\Psi} \sin \Psi \cos \theta - \dot{\theta} \cos \Psi \sin \theta) \\ & + l_y[\dot{\theta} \sin \phi \cos \theta \cos \Psi + \dot{\phi}(\sin \phi \sin \Psi + \cos \phi \sin \theta \cos \Psi) \\ & - \dot{\Psi}(\cos \phi \cos \Psi + \sin \theta \sin \phi \sin \Psi)] \\ & + l_z[\dot{\theta} \cos \phi \cos \theta \cos \Psi + \dot{\phi}(\cos \phi \sin \Psi - \sin \phi \sin \theta \cos \Psi) \\ & + \dot{\Psi}(\sin \phi \cos \Psi - \sin \theta \cos \theta \sin \Psi)] \end{aligned} \quad (2.2)$$

$$\begin{aligned}
W_E = & -\bar{V}[\cos \alpha \cos \beta \sin \Psi \cos \theta + \sin \beta(\cos \Psi \cos \phi + \sin \Psi \sin \theta \sin \phi) \\
& + \sin \alpha \cos \beta(\sin \Psi \sin \theta \cos \phi - \cos \Psi \sin \phi)] + V_E \\
& - l_x(\dot{\theta} \sin \theta \sin \Psi - \ddot{\Psi} \cos \phi \cos \theta) \\
& + l_y[\dot{\theta} \sin \phi \cos \theta \sin \Psi + \dot{\phi}(-\sin \phi \cos \Psi + \cos \phi \sin \theta \sin \Psi) \\
& - \ddot{\Psi}(\cos \phi \sin \Psi - \sin \theta \sin \phi \cos \Psi)] \\
& + l_z[\dot{\theta} \cos \phi \cos \theta \sin \Psi - \dot{\phi}(\cos \phi \cos \Psi + \sin \phi \sin \theta \sin \Psi) \\
& + \ddot{\Psi}(\sin \phi \sin \Psi + \sin \theta \cos \phi \cos \Psi)]
\end{aligned} \tag{2.3}$$

$$\begin{aligned}
W_Z = & -\bar{V}[-\cos \alpha \cos \beta \sin \theta + \sin \beta \cos \theta \sin \phi + \sin \alpha \cos \beta \cos \theta \cos \phi] \\
& + V_Z + l_x \dot{\theta} \cos \theta - l_y[\dot{\theta} \sin \phi \sin \theta - \dot{\phi} \cos \phi \cos \theta] \\
& - l_z[\dot{\theta} \cos \phi \sin \theta + \dot{\phi} \sin \phi \cos \theta]
\end{aligned} \tag{2.4}$$

where W_N , W_E , and W_Z represent the north, east, and vertical components, respectively, of the wind velocity vector. Inspection of these equations shows the variables required in computing wind velocity vector components are those listed and defined in Table 2.1.

Sections 2.1 and 2.2 describe the basic principles of the various sensors available for making the required measurements and the advantages and disadvantages of different types. However, a review of overall systems for measuring wind as applied to different aircraft as reported in the literature is given first. Brown, et al. (1974) describes a research gust probe system. The system was installed on a DC-6 aircraft. It was initially developed and used in the Barbados oceanographic and meteorological experiment (BOMEX). A digital instead of an analog recording system was subsequently added and the system was used in the International Field Year on the Great Lakes project (IFYGL). The system was essentially composed of a fixed vane sensor mounted on a noseboom. The fixed vane sensor is reported in Crooks, et al. (1976) and consists of a vertical sensor (α -vane) and a lateral sensor (β -vane) attached to a specially constructed strain gauge beam. Ambient pressure is sensed by a Conrac type 555 T-1 absolute pressure transducer/servo assembly. A thermistor temperature probe assembly and a microwave cavity instrument to

Table 2.1 Variables required for wind computations.

Symbol	Description
t	time(sec)
α	angle of attack (rad)
β	sideslip angle (rad)
ϕ	roll angle (rad)
θ	pitch angle (rad)
Ψ	heading angle (rad)
$\dot{\phi}$	roll rate (rad/sec)
$\dot{\theta}$	pitch rate (rad/sec)
$\dot{\Psi}$	yaw rate (rad/sec)
P	static pressure (Kp_a)
T	temperature (Kelvin)
LAT	latitude (deg)
LONG	longitude (deg)
V_N	north-south airplane inertial velocity (m/sec)
V_E	east- west airplane inertial velocity (m/sec)
V_Z	vertical airplane inertial velocity (m/sec)
\bar{V}	true airspeed (m/sec)

measure index of refractivity are also mounted on the noseboom. Two Statham strain gauge accelometers were mounted on the boom to sense normal and lateral boom accelerations. A third Statham strain gauge accelometer which was temperature controlled was used to sense longitudinal accelerations of the aircraft. A Litton LTN-51 inertial navigation system provided the basic information regarding aircraft motion with respect to the earth. Signals recorded from the INS were vertical acceleration, roll, and pitch. Aircraft angular motions rates of pitch, roll, and yaw were provided by gyros. Elevator position was also monitored. A model MC013 data acquisition system provided means of measuring up to 64 analog voltages at sample rates up to 3,200 samples per second (50 scans per second of 64 inputs); thus provided a recording of all digital forms along with the time, day of the year and manually entered header data. Recording was carried out on a 7-track gapped tape, IBM compatible.

Gamo, et al. (1975, 1976), Yamamoto, et al. (1977), and Yokoyama, et al. (1977a, 1977b) describe an airborne measurement system mounted on a Cessna 207 aircraft. The system consisted of a hotwire anemometer used for measuring longitudinal velocity fluctuations (observations are made with the aircraft flying parallel to the wind), sonic anemometer used to measure vertical fluctuations, horizontal vanes used to measure the lateral component of the wind, thermistor psychrometer used to measure mean temperature and humidity, sonic thermometer used to measure temperature fluctuations, thermocouple thermometer also used to measure temperature fluctuations, and a radiation thermometer used to measure surface temperature. The airplane's pitching, rolling, and yaw angles and vertical, lateral, and longitudinal accelerations were measured with an inertial platform system.

Scott, et al. (1989) describes the meteorological measurement system incorporated on the NASA ER-2 aircraft. The meteorological measurement system (MMS)

consists of a special inertial navigation system, a differential pressure system installed in the nose of the aircraft, a data acquisition system, and airdata instrumentation. The high resolution INS is especially configured with a data bus which is updated at 25 Hz. The differential pressure system provides sensitive measurements of the airflow angles (angle-of-attack and angle-of-sideslip). The data acquisition system meets the requirements to sample, control, and process 45 parameters at a sampling rate up to 40 Hz. per parameter and store the data in a tape recorder (20 MB.) and a hermetically sealed Winchester hard disk (10 MB.). Special and redundant instrumentation for aircraft and pressure measurements are also installed on the aircraft.

Poellet (1990) describes the University of North Dakota, Cessna Citation II, airborne weather research system. Parameters of temperature, dewpoint and pressure are measured by relatively standard methods using state-of-the-art instrumentation. The position measurements are based on a Litton LTN-76 inertial navigation system. Air motion measurements are derived from measurements of acceleration pitch, roll and yaw combined with angles-of-attack and sideslip and indicated airspeed. The instrumentation pallet also includes radiation instrumentation, cloud microphysics measurement equipment, and a forward or side looking video camera to provide a visual record of flight conditions. Data are sampled at various rates from 1-24 times per second. The sampling is controlled by the onboard computer system which also displays the data in real time.

A number of other reports discuss evaluation of different instrumentation for use in atmospheric measurement programs. Murrow and Rhyne (1975) describe flight instrumentation for atmospheric measurements; Lenschow and Kelley (1975) discuss atmospheric mesoscale measurements from aircraft including instrumentation and measurement techniques; Bjarke and Ehernberger (1989) discuss inflight

techniques for wind measurements in support of the space shuttle program, and Lenschow (1986) discusses aircraft measurements in the boundary layer.

The following section describes the physical principles of some of these instruments used in the aforementioned systems.

2.1 Relative Airspeed

The relative airspeed vector requires a magnitude and direction measurement. Magnitude is generally calculated with pitot measurements and direction with either flow vanes or differential pressure transducers.

Relative airspeed magnitude is computed from the equation

$$V_a = \left(\frac{p_o}{p}\right)^{-\frac{k-1}{2k}} \sqrt{kRT_o} \sqrt{\left[\left(\frac{p_o}{p}\right)^{\frac{k-1}{k}} - 1\right] \left[\frac{2}{k-1}\right]} \quad (2.5)$$

where the measured parameters are total pressure, p_o , static pressure, p , and total temperature, T_o . Figure 2.1 illustrates schematically the measurements required to determine airspeed magnitude, and a detailed derivation of Equation 2.5 is given in Appendix A.

The direction of the air relative to a probe is fixed by the angle-of-attack, α , and sideslip angle, β . These angles are generally determined with either a differential pressures flow angle probe or vanes. A comparison of the flow angle differential pressure probe versus vane measurements is given in Appendix A. The pressure differential flow angle probe is illustrated in Figure 2.2(a) and the vane system in Figure 2.2(b).

A variety of types of flow angle measurement techniques are reported in the literature. Gracey (1958) reviews and summarizes methods of measuring angle-of-attack on aircraft. Three types of angle-of-attack sensing devices – the pivoted vane, the differential pressure tube, and the null seeking pressure tube – are presented. Flight data on the position errors for three sensors locations (ahead of the

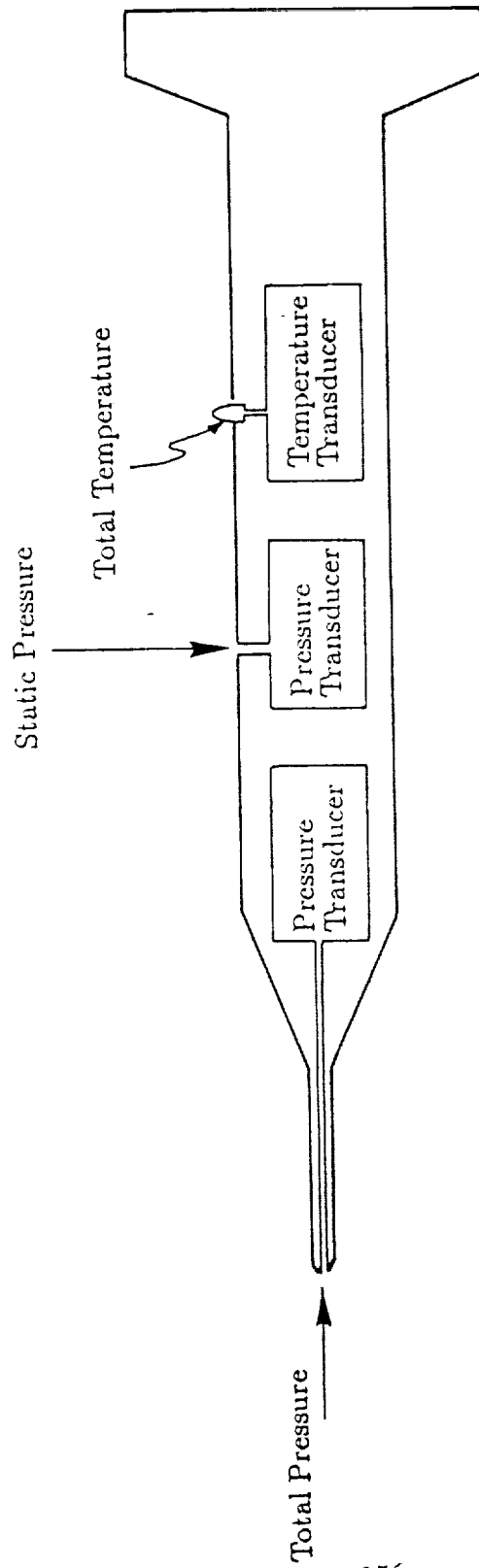
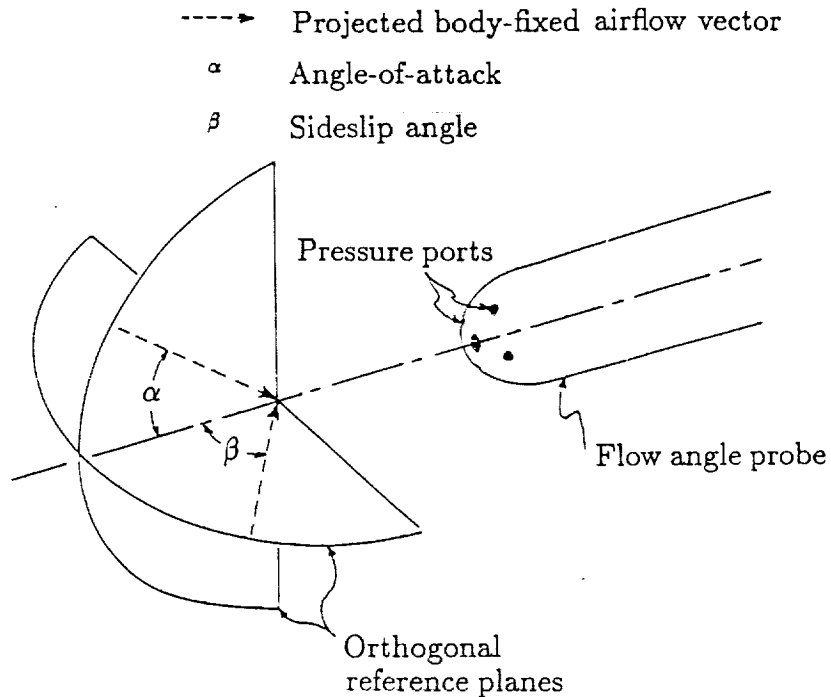
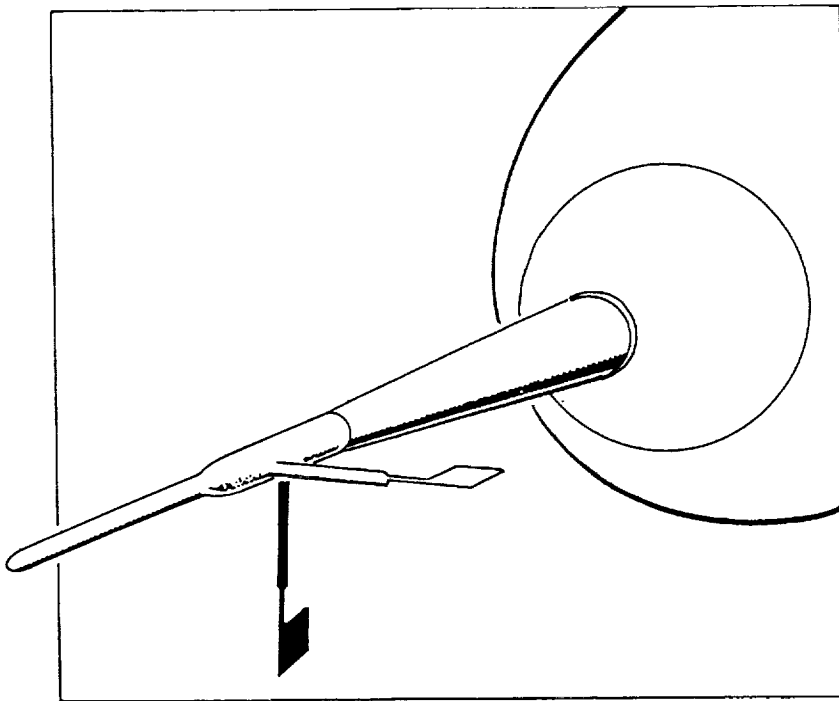


Figure 2.1 Physical quantities required for airspeed measurement.

15



a) Differential pressure probe



b) Vanes

Figure 2.2 Angle-of-attack and sideslip angle type sensors.

fuselage-nose, ahead of the wing- tip, and on the forebody of the fuselage) are also presented. Gracey reports that for operations throughout the subsonic, transonic, and supersonic speed ranges, a position ahead of the fuselage-nose will provide the best installation. Moreover, if the shape of the fuselage-nose is not too blunt, the position error will be essentially zero when the sensor is located 1.5 or more fuselage diameters ahead of the fuselage. The report concludes with various methods of calibrating angle-of-attack installations in flight.

Lenschow (1971) describes two types of vanes that were used to measure the angle of airstream with respect to an aircraft. One type is a rotating vane that is free to align itself with the airstream and the angle is sensed by the angle transducer. The other type is constrained from rotating and the angle is obtained by measuring the force exerted on the vane by the airstream and dividing by the pitot-static pressure. It is reported that the free vane measures the angle directly and is not sensitive to acceleration while the constrained vane has a faster response time and has no bearing friction. With an aircraft speed of 70 m/s, both vanes are able to resolve changes in angles of less than 0.02 degrees, which corresponds to a gust velocity of about 2 cm/s, and to respond to within 5% of a step function change in angle in a distance of less than 5 meters.

Barna and Crossman (1976) carried out experimental studies of the aerodynamic performance and dynamic response of flow direction sensing vanes. Systematic investigations of a variety of aerodynamic surfaces were carried out. Single vanes consisting of flat plates of various plan forms having aspect ratios between 0.5 and 5; bi-vanes with aspect ratio of 2.5; various cones and box vanes; and various cruciform configurations were all studied. Lift and drag force measurements and damping and frequency tests were all performed under a variety of flow conditions in a wind tunnel.

AT

Lenschow, et al. (1978a) reports the status of air motion measurements on a NCAR aircraft for three types of gusts probe sensors. Measurement of airflow angles were studied for: a fixed "constained" vane which measures the force of the airstream on the vane surface at varying flow angles, a rotating vane which aligns itself with the airstream, and a differential pressure probe which senses the pressure difference across a symmetric set of ports at various flow angles. They conclude that although the frequency response of most of the gust probe sensors is sufficient for turbulence flux measurements, it is not sufficient for measuring high frequency characteristics of turbulence such as direct measurements of viscous dissipation or the variation in turbulence intensity on very small scales. Lenschow, et al. (1978b) therefore studied a hot-wire anemometer system capable of measuring two frequencies of several kilohertz. The sensing elements of the hot-wire anemometer were typically fine tungsten wires $4 \mu m$ in diameter and 1.25 mm long. These were mounted transverse to the airflow on a probe attached to the aircraft nose-boom. The nose-boom mount permitted velocity measurements within a few tens of centimeters of the standard gust probe sensors at a location that is relatively free of upwash effects induced by flow around the aircraft. Lenschow, et al. concluded that the hot-wire anemometer system is an effective means of extending aircraft velocity measurements to high frequencies and small space scales and that the commercial tungsten wire probes were found to be sufficiently strong so that breakage was not a severe problem in clear air. Further applications of the hot-wire system were reported to consist of measurements of the vertical and transverse velocity components with multiple wires placed at angles to the flow. Jacobsen (1977) reports use of a three-wire array mounted on a trailing aircraft to measure vorticities generated by a large aircraft.

The NASA ER-2 aircraft uses the nose of the aircraft as a differential pressure

transducer system. This concept has been studied by others. Hillje and Tymms (1980) investigated the use of a biconic spike probe on the nose of the space shuttle external tanks to evaluate ascent airdata. Pressure measurements were calibrated to obtain vehicle speed, attitude (relative to the local air mass) and dynamic pressure during launch. They describe the geometry of the ascent airdata system and results of wind tunnel tests carried out for calibration. They concluded that from wind tunnel calibrations, a 30 degree/10 degree spike measured pressure could be converted to the desired airdata parameters for post flight analysis. A typical value for the angle-of-attack error for a Mach range between 0.6 and 1.0 and an $\alpha = 3$ degrees was estimated at ± 0.32 . Other accuracies of the system are presented in the paper. Hillje and Nelson (1981) provide additional data on the space shuttle ascent airdata system.

Brown, Friehe, and Lenschow (1983) describe the use of pressure fluctuations on the nose of an aircraft for measuring the air motion. Measurements of angle-of-attack and sideslip angles and dynamic pressure are described. The sensing probe consisted of an array of five pressure holes in the standard radome of a twin jet research aircraft. Comparisons with air motion measurements (angle-of-attack and dynamic pressure) obtained from conventional differential pressure flow angle sensors at the tip of a nose-boom 1.5 fuselage diameters ahead of the aircraft body are reported. The results indicate that the radome system works well down to scale sizes slightly larger than the fuselage diameter. Finer scale measurements were found to be limited by pressure transducer response. It was learned from comparison of the power spectra determined from the conventional and from the radome angles-of-attack that the response of the radome system was superior to the conventional system due to the shorter pressure lines that were used.

Other types of pressure differential probes have been reported. For example,

19

Hermann, et al. (1984) describes an airfoil probe for angle-of-attack measurements. The results of the study showed that a small airfoil probe consisting of a small canard wing mounted appropriately on an airframe and properly tapped can serve as a viable probe for sensing angle-of-attack. An NACA 0012 airfoil section was used in wind tunnel tests. The study reported that differential pressure coefficients greater than 3 at high angles-of-attack were achieved. These coefficients are reported to be an improvement of a factor of 2-3 over comparable coefficients obtained from hemispheric probes.

In addition to the direction of the relative air velocity, the magnitude must also be measured. Computation of the magnitude of relative airspeed requires a measurement of total temperature. Total temperature is typically measured with a thermocouple or resistance temperature device (RTD). Typically, a total temperature probe is designed with the temperature sensing device situated in a volume where the air is partially stagnated, vented, and shielded to minimize radiation heat losses. For example, the NASA F-104 and the NASA ER-2 instrumented aircraft obtain total temperature measurements from a strut-mounted transducer positioned on their respective fuselages.

The quality of the total temperature measurement, however, is less important than the quality of the total and static pressure measurements, and the uncertainty in the final wind calculation is virtually independent of small errors in the total temperature measurement. Therefore, an inexpensive thermocouple generally gives sufficient performance. Insulation of the thermocouple from the fuselages is necessary to prevent the thermocouple from measuring the temperature of the aircraft instead of the air with each instrument calibration is required. Each type of instrument, however, has its own calibration problems. The following briefly summarizes the literature associated with calibration of airborne wind measurement instruments.

Gracey and Scheithauer (1951) present results of a flight investigation of the variation of static pressure error on a static pressure tube with distance ahead of a wing and a fuselage. A discussion of the effect of distance in front of the aircraft on the error of static pressure measurement is presented for both a wing tip installation and a fuselage-nose installation.

It is reported by Haering (1990) that the airdata calibration required for measuring winds with an instrumented aircraft must be more accurate than that needed for other aircraft research programs. He reports tower fly-bys with the NASA F-104 aircraft and the use of radar acceleration-decelerations to calibrate Mach number and total temperature. The F-104 aircraft and instrumentation configuration, flight test maneuvers, data corrections, calibration techniques and resulting calibration and data repeatability are discussed. The paper concludes that the Mach number indicator could be calibrated repeatedly at ± 0.003 subsonically and ± 0.005 supersonically. Total temperature was calibrated and found to have a recovery factor of 0.986 with a ± 0.009 scatter in the data. The author recommends, from his investigation, a number of design and operation procedures for future airdata systems for aircraft used to measure winds aloft. These include (1) using a nose-boom with dual angle-of-attack and flank angle-of-attack vanes to reduce the sensitivity of upwash and sidewash on Mach number; (2) rigidly attaching the nose-boom and IRU to the same structure to minimize geometric alignment variability.

Geenen and Moulton (1991) describe a system to calibrate airdata probes at angles-of-attack between 0 and 90 degrees. The system uses a test fixture mounted to the roof of a ground vehicle which includes an onboard instrumentation and data acquisition system for measuring pressures and flow angles. The system was designed to provide convenient and inexpensive airdata probe calibrations for projects which require airdata at high angles-of-attack. The authors note that previous sub-

sonic data for the NACA standard pitot-static tube with vane type flow direction indicators was limited to 20 degrees angle-of-attack. The new type of probe introduced was tested to 90 degrees angle-of-attack in a wind tunnel and with the ground vehicle system. They also report an airdata probe with a swiveling pitot-static tube and the calibration of it with the ground vehicle system. They conclude that the swiveling-head airdata probe's larger region of total and static pressure insensitivity to angle-of-attack and angle-sideslip make it more suitable for high angle-of-attack flight than the standard NACA airdata probe.

Moes and Whitmore (1991) present preliminary results from an airdata enhancement algorithm with application to high angle-of-attack flight. The technique is developed to improve the fidelity of airdata measurements during dynamic maneuvers. The technique is reported to be particularly useful for airdata measured during flight at high angular rates and high angles-of-attack. A Kalman filter was used to combine information from research airdata, linear accelerometers, angular rate gyros, and altitude gyros to determine better estimates of airdata quantities such as angle-of-attack, angle-of-sideslip, airspeed and altitude. The paper develops the state and observational equations used by the Kalman filter and shows how the state and measurement coherence matrix was determined from flight data. Flight data is used to demonstrate the results of the technique and the results are compared to an independent measurement source. Flight test data from the F-18 HARV were used to show that the Kalman filter-estimated airdata is more realistic than measured airdata during high angle-of-attack and high angular maneuvering. This has been verified using information from radar and meteorological data.

Larson and Ehernberger (1985) describe a flight test technique for controlled survey runs to determine horizontal atmospheric pressure variations and systematic altitude errors that result from space positioning measurements. The survey

data can be used not only for improved airdata calibration but also for atmospheric structure and space positioning accuracy performance. The authors report that data from the survey technique developed indicate that increased accuracy and improved static pressure position error calibration using radar and rawinsonde pressure measurements was achieved. In addition, the survey technique can be useful in studies of pressure gradients, atmospheric refraction and radar tracking performance.

Larson, et al. (1987) carried out flight tests with an F-14 aircraft to evaluate the use of flush pressure orifice on the nose section for obtaining airdata at transonic speeds over a large range of flow angles. The flight tests provided data to validate algorithms developed for the shuttle entry airdata system design at NASA Langley Research Center. Data were obtained for Mach numbers between 0.6-1.6 for angles-of-attack up to 26 degrees and sideslip angles up to 11 degrees. The authors conclude that with careful calibration of airdata systems with all flush orifices can provide accurate airdata information over a large range of flow angles. Several orifices on the nose cap were found to be suitable for determination of stagnation pressure. Other orifices on the nose section aft of the nose cap were shown to be suitable for determining static pressure. Pairs of orifices on the nose cap provided the most sensitive measurement for determining angles-of-attack and sideslip, although orifices located further aft on the nose section could also be used.

2.2 Inertial Measurements

Vehicle inertial attitude and velocity are typically provided by inertial navigation systems (INS) for wind measurements from aircraft borne sensors.

Ground speeds and angles, as well as Euler angles and rates, are determined from the INS. Two types of INS have been used: stable platform systems and strapped down systems. The NASA B57 Camberra and the NASA ER-2 aircraft use a stable platform system Carousel IV and Litton LTN-72RH, respectively, while

the NASA F-104 employed a strapped down, ring laser gyro. A brief description of an INS system is that the INS utilize inertial elements (i.e., accelerometers and gyros) to sense vehicle acceleration from which velocity and position can be determined. In the stable platform system these sensors are mounted on gimballed platforms, containing at least three gimbals, which isolate them from vehicle motion and physically locate them in the desired coordinate reference frame. In local level north pointing systems, this reference frame is the local geodetic frame, and the gyro and accelerometer input axes are forced to remain as closely coincident as possible to the north, east, and vertical directions when the vehicle is in motion.

If the sensors are "strapped down" on the carriers directly, no gimbals and servo-motors are necessary. This type of INS mechanism is called a strapdown system (SDS). The accelerometer signals are measured in a body-fixed coordinate frame and transformed to a navigational reference frame by means of the gyro signals. This results in the following advantages in comparison with the stable platform systems (Lechner (1980)):

- simple mechanical construction
 - the provision of accelerations and angular rates in body-fixed axes
 - easy maintenance due to the modular construction
- and the economical provision of redundancy by means of skewed sensitivity axes.

However, against these advantages must be weighed certain drawbacks:

- increased demands on the efficiency of the navigation computer
- and extreme demands on the accuracy of the sensors, which have to measure the full dynamic environment of the SDS.

Regardless of which type of INS is used, it can introduce significant dynamic error into the wind vector computed from the measured ground speeds. These errors

are discussed in detail in the section on error analysis.

Considerable literature is available on INS systems. General descriptions are given in Puckett and Ramo (1959); O'Donnell (1964); and Pitman (1962).

Gorenshteyn and Shul'man (1970) describe the theoretical principles underlining inertial navigation and the basic functional elements of inertial navigation systems. General and specific representations of the algorithms for determining the running coordinates of an object are examined as applied to certain practically important methods of constructing an INS. The classification, analysis of error, preparation for operation, and also problems of protecting INS from external sources is also discussed.

Lechner, Hotop, and Zenz (1983) provide a description of the instruments and the data evaluation techniques for testing of inertial navigation systems both hardware and software. They discuss the inertial navigation system (platform systems) installed in an aircraft and how it provides signals for course and altitude, ground speed, and position determination. They note that the systems can be flight tested for various criteria: checking the system accuracy, determining its reliability, checking the aiding method for increasing the system's accuracy, obtaining knowledge as to the air behavior of an inertial systems in flight by means of the use of air models and optimal filters. They also point out that external measurement aids are available which include radar tracking systems, cinetheodolites and TACAN for exact positioning of the aircraft.

A complete description of the Carousel IV inertial navigation system used in the NASA B-57 aircraft is provided in the System Technical Description Manual, provided by the manufacturer (AC Electronics, Division of General Motors Corporation). Weber (1975) also reports on statistical studies of the accuracy of the Carousel IV inertial navigation system. Three Carousel IV inertial navigation sys-

tems were studied by Weber for accuracy during flights over the north Atlantic. Errors associated with inertial platform are also discussed by Geller (1968). Geller describes the differential equations for navigation errors of a local level and undamped inertial platform that continuously rotates in azimuth. From these, the time response equations for the vector position error produced by a constant level gyro drift error, as a function of platform rotation rate, are computed and evaluated. The paper shows that platform rotation attenuates the systems position error due to gyro bias and that this attenuation is a nonlinear function of rotation rate.

McConnell (1966) reports on the kinematics of a three axis gimballed system. The equations of constraint which must be satisfied during gimballed motion are studied. The phenomena of gimbal lock and gimbal flipping are considered and demonstrated for one type of vehicle motion. Curves indicating angular displacement, velocities and accelerations are computed and presented showing the need of a redundant four axis gimbal system to avoid gimbal lock.

Rhynne (1980) reports an experimental assessment made of two commercially available inertial navigation systems with regard to their inertial velocity measurement capability. This study was particularly designed for use in wind, windshear, and long wavelength atmospheric turbulence measurements. The assessment was based on 52 sets of postflight measurements of velocity (error) during a Schuler cycle (84 minutes) while the inertial navigation system was still operating but the aircraft was motionless. A maximum postflight error for the 52 cases was found to have a root mean square value of 2.82 m/s with little or no correlation of error magnitude with flight duration in the 1-6 hour range. As discussed in Section 3.2, this Schuler drift effect in the INS system has a particularly significant influence on the accuracy of the wind measurements.

Strapdown inertial navigation systems as contrasted to the platform systems

are becoming more prevalent. Studies associated with error analysis in the strap-down inertial navigation systems have been reported. Shibata (1986) describes the strapdown inertial navigation error equations based on a quaternion relationship between fixed body frame and navigation (local vertical) frame for terrestrial hybrid navigation systems. Potter (1982) proposes steady-state Kalman filters used as estimators for a strapdown INS. The report describes investigations as to the sensitivity of the steady-state Kalman filters to inaccuracy in the filter parameters such as the dimensional stability derivatives.

Hotop (1985) describes the measuring and data analysis technique used for flight testing two Litton LTN-90 laser gyro strapdown type navigation systems. Reference data was produced by the Carousel IV. In the mean, accuracies of 1.4 km per hour maximum for position, of 1.2 m/s for velocity and of less than 0.1 degrees for angular position and azimuth were reported for the LTN-90 navigation systems.

Miller (1980) presents a description of an algorithm for attitude and navigation computations for strapdown inertial navigation systems. Also, Friedland (1978) presents a brief review of the theory of strapdown and inertial navigation systems. He shows that the error in the quaternion vector causes a scale factor error and an equivalent tilt vector error that propagates the same way as the platform tilt vector in a gimbaled system. A set of equations for error analysis are derived and interpreted in this paper.

Error equations for the Psi-angle in strapdown inertial navigation systems are provided by Weinreb and Bar-Itzhack (1978). It is proven in this paper that apart from a sign change the side angle differential equation in the error analysis of strapdown inertial navigation systems is identical to the one used in conventional gimbaled inertial navigation systems.

3.0 UNCERTAINTY ANALYSIS

The design of an instrument system requires an uncertainty analysis to quantify the affect of individual instrument uncertainties on the final wind velocity determined by combining the measured values through the reduction equations. Appendix B contains a detailed uncertainty analysis procedure. Typical magnitudes of potential uncertainties are presented graphically in Section 3.1. Other uncertainties resulting during operations and calibration problems also must be considered in a measurement of wind from an aircraft. The propagation of error from measurements inaccuracy of pressure, temperature, flow angle, angular displacement, and inertial velocity and discussed in Section 3.1. Error encountered during flight operations are described in Section 3.2.

3.1 Design Uncertainties

Figure 3.1 shows the effect of pressure and temperature measurement uncertainties on calculated airspeed. The airspeed uncertainty, which is calculated from the combination of Equations (A.2) through (A.7), is based on the assumptions that the static and total pressure measurement uncertainties are equal and that supersonic free stream flow is compressed by a normal shock wave before coming into contact with the ports used for pressure measurements.

Figure 3.1 also indicates that the minimal airspeed uncertainty is calculated from measurements made near unity Mach number. However, because pitot probes used for total and static pressure measurements are known to induce localized regions of supersonic flow, the simple one-dimensional theory used here may not be adequate for uncertainty predictions near unity Mach number. The uncertainty in the transonic airspeed calculation requires testing and indepth analysis.

Figure 3.2 shows the uncertainty in the square of the magnitude of the relative

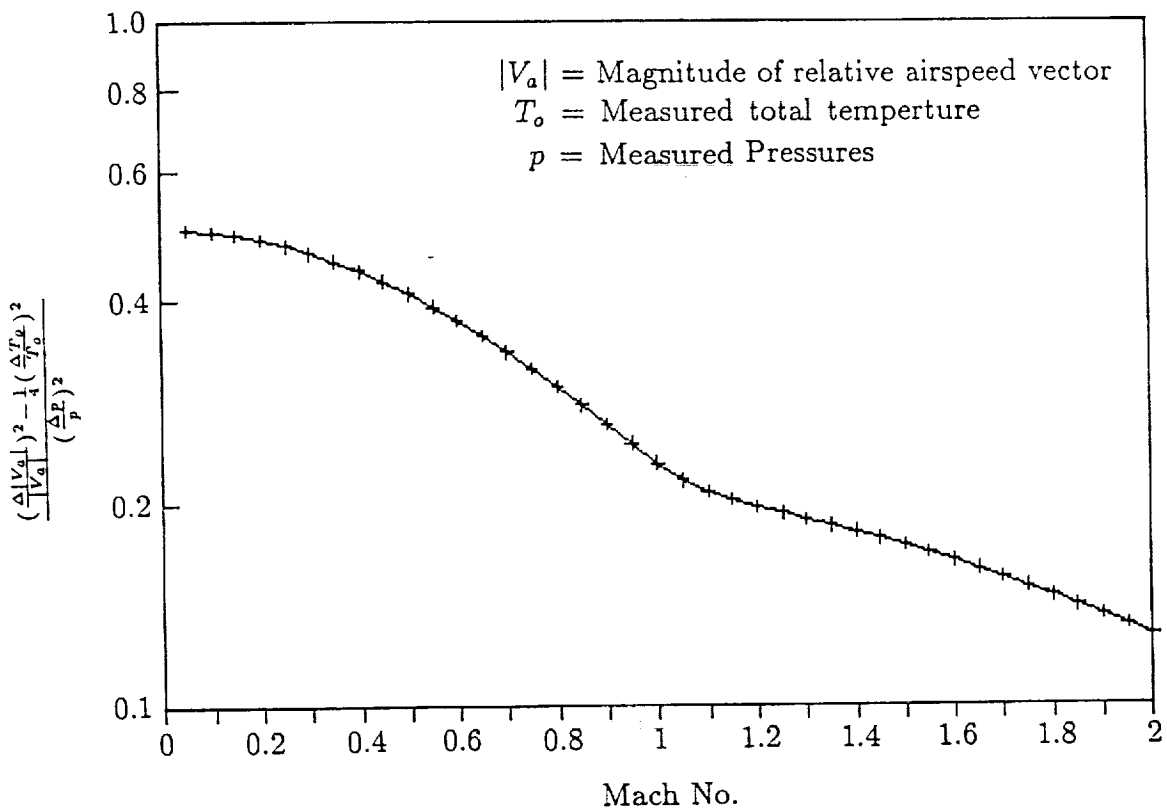


Figure 3.1 Calculated airspeed uncertainty as a function of pressure and temperature measurement uncertainties.

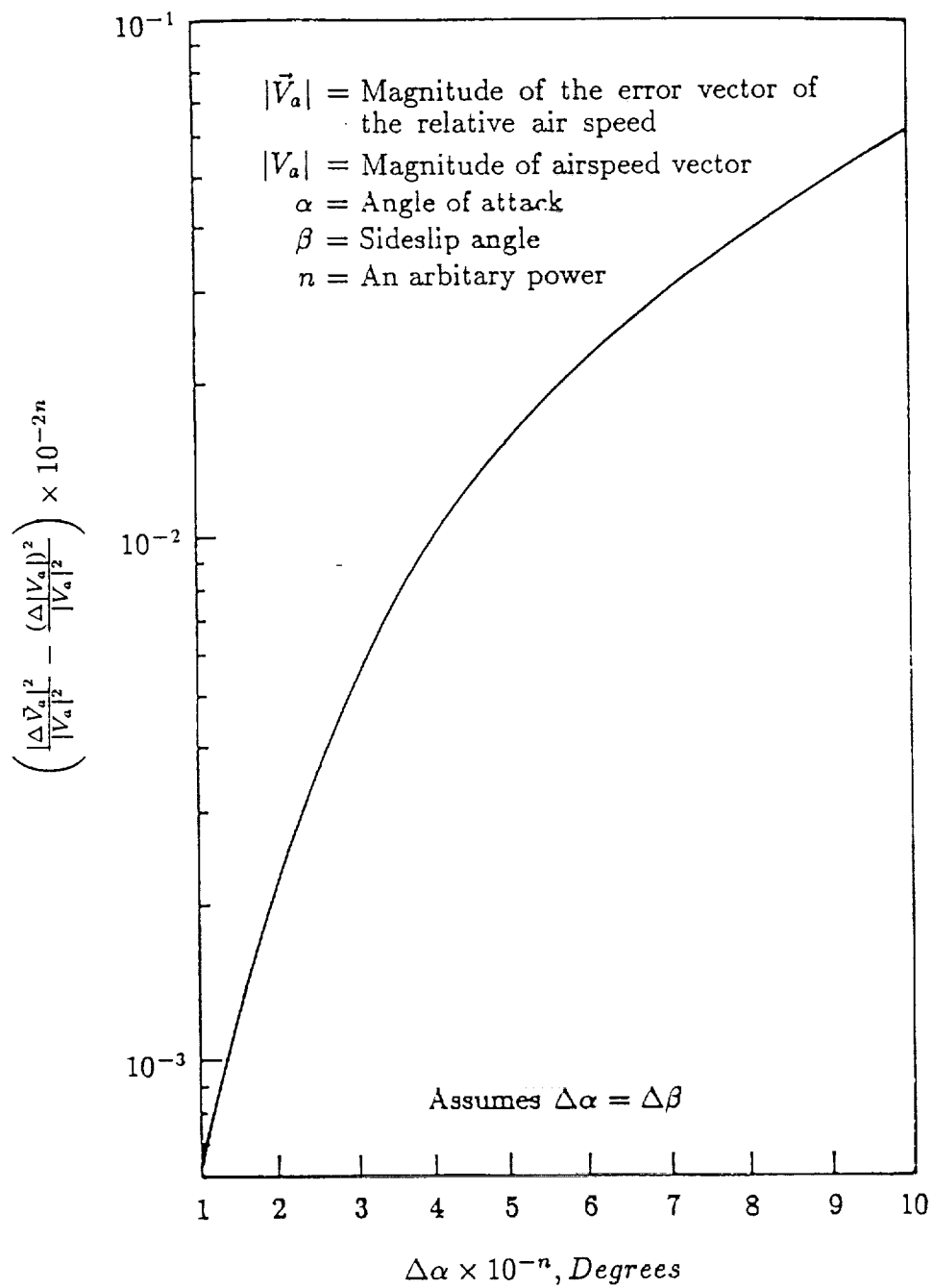


Figure 3.2 Relative airspeed velocity uncertainty as a function of airspeed and flow angle uncertainties.

velocity of the air vector, $|\Delta \vec{V}_a|^2$, resulting from the airspeed uncertainty and the measured flow angle uncertainty. The uncertainty in $|\Delta \vec{V}_a|$ (see Equation (A.9)) is based on the assumption that the flow angles, α and β , are small ($< 5^\circ$) and the flow angle uncertainties, $\Delta\alpha$ and $\Delta\beta$, are equal.

Figure 3.3 shows the uncertainty in the square of the magnitude of the wind velocity error vector $|\Delta \vec{W}|^2$. The uncertainty is plotted as a function of the uncertainty in the Euler angles where it is assumed $\Delta\phi = \Delta\theta = \Delta\psi$.

Figures 3.1, 3.2, and 3.3 are tools developed for a “back-of-the-envelope” determination of the wind velocity uncertainty from the uncertainties in airborne measurements. The use of these relations is illustrated by an example.

Assume that the parameters measured on an airplane have the uncertainties listed in Table 3.1.

Table 3.1 Example Measurement Uncertainties.

$\frac{\Delta p}{p}$	0.5 %
$\frac{\Delta T_o}{T_o}$	0.5 %
$\Delta\alpha, \Delta\beta$	0.1 deg.
$\Delta\phi, \Delta\theta, \Delta\Psi$	0.1 deg
$ \Delta V_e $	1 m/s

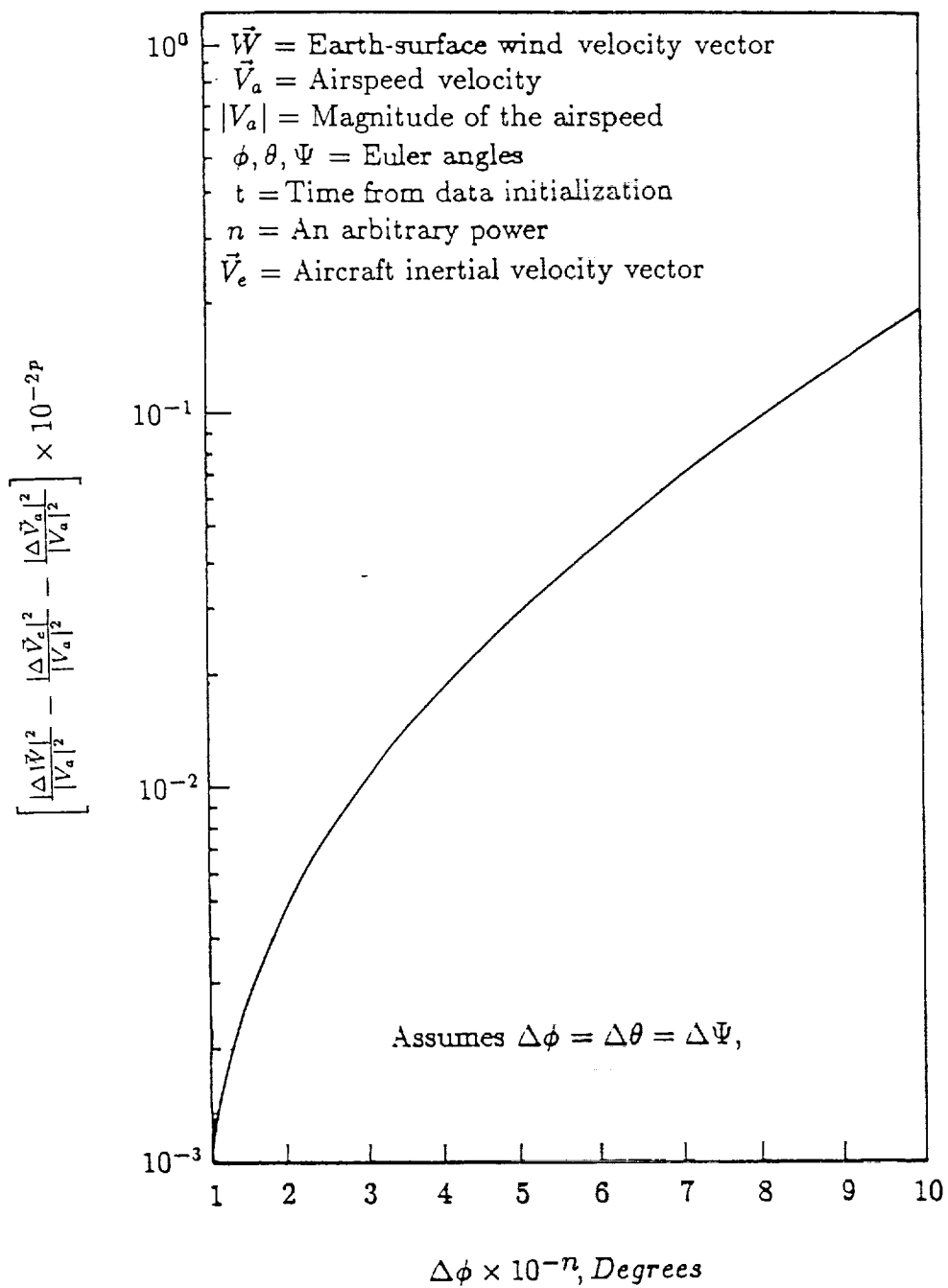


Figure 3.3 Wind velocity uncertainty as a function of relative airspeed velocity uncertainty, inertial velocity uncertainty, euler angle uncertainty, and airspeed.

If the airplane is flying at Mach 0.5 at sea level ($V_a \approx 345\text{m/s}$), the pressure and temperature measurement uncertainties can be used with Figure 3.1 to determine the relative airspeed uncertainty of 0.4%.

Figure 3.2 is then used to determine the effect of the angle-of-attack and sideslip angle uncertainties. For the given flow angle uncertainty of 0.1 deg., the power n on the abscissa of Figure 3.2 is set equal to -1 and the relative magnitude of the uncertainty of the relative airspeed velocity is 0.5%. Figure 3.3 is used in a similar manner, with the uncertainty in the measured Euler angles and in the inertial velocity, a relative wind velocity uncertainty of $\pm 2.3\text{ m/s}$ can be calculated. Note that no information about the direction uncertainty is contained in the figures.

3.2 Operational and Dynamic Uncertainties

Extensive investigation reported by Chang and Frost (1985); Frost, et al. (1985); Ringnes and Frost (1985); and Hill (1990) using data gathered with the Cambera B-57 aircraft has been carried out. The following draws heavily from these reports.

3.2.1 Sources of Inaccuracy in Data Reduction

Instrumentation errors influence the quantities appearing on the right-hand side of Equations 2.2, 2.3, and 2.4 and thus the accuracy of the computed wind velocities. Of these sources of instrumentation errors, the most difficult to correct is the dynamic error in the velocity inherent in the INS, termed the Schuler error to which aircraft motions contribute. All other errors can be removed by careful calibration. The effects on the magnitude of the measured wind and also turbulence calculations due to the sources of error in the instrumentation are presented next.

3.2.2 Inertial Velocity and Position Errors

The accuracy of the calculations of horizontal winds depends upon the performance of the INS and its capability to provide correct measurements of the inertial

(ground) speed of the aircraft. In recent years mechanical and electronic advances have greatly improved INS accuracy. However, a cumulative oscillation in the INS stable platform element called the Schuler drift effect, first pointed out in the famous paper by Schuler (1923), can be quite significant. Inertial navigation theory including derivation of the Schuler pendulum effects is explained in many textbooks (see for example, Boxmeyer (1964)). The Schuler error is essentially periodic with a period near that of an earth radius pendulum, 84.4 minutes. Huber and Bogers (1983) point out that a platform used in an airplane cannot strictly be kept tuned to $T_o = 84.4$ minutes after takeoff since R (distance between the airplane and center of the earth) and g (gravitational acceleration) change with altitude. They propose to define $T_o = 84.4$ minutes as the Schuler constant (for the earth). The actual period of oscillation proposed by these authors for a specific Schuler-adjusted system takes into account the gravity gradient, the mass distribution in the system, and the centrifugal forces due to the velocity of the carrying vehicle. This is called the actual oscillation period. The actual oscillation period of a specific Schuler-adjusted system (acceleration insensitive system) under specific circumstances is given by them as:

$$T = k \cdot 2\pi \sqrt{R/g}$$

where k will always have a value between 0.5 and ∞ . The Schuler error behaves sinusoidally and will thus change polarity. The error caused by a slow oscillation of the INS stable platform causes the two horizontal accelerometers to detect a part of the gravity vector. This false indication of acceleration is carried through the integration for velocity and produces errors in the W_E and W_N values. Distance traveled or geographical position is obtained from a second integration of the measured accelerations. Thus the Schuler oscillations will create errors in acceleration, velocity, and position. The following procedures can be used to estimate the velocity

errors associated with Schuler drift.

Position error can be computed from aircraft data during overflight of landmarks where exact geographical locations are known. Since acceleration, velocity, and position errors are all interrelated, the Schuler error can experimentally be investigated by obtaining data on either one of the three parameters having a Schuler oscillation induced error. The velocity error is generally small but increases with time, e.g., after several hours of operation it can be on the order of 3 to 5 m/s (Rhyne (1980) and Lenschow (1983)). The magnitude of the position errors for the Carousel IV INS used in B-747 aircraft reported by Weber (1975) normally are on the order of 10 nautical miles or less even after transatlantic flights. These errors are not critical for pure navigation purposes. But, when the objective is to calculate wind velocity, the Schuler error can be quite important.

To illustrate the magnitude of in-flight Schuler error, data from a Flight with the NASA Cambera B-57 aircraft are presented (Frost, et al. (1987)). A box pattern flight plan as shown in Figure 3.4 was flown sequentially at 1000 ft levels over Boulder, Colorado, in February 1984. Details of the flight and results are given in Chang and Frost (1985). Each time the B-57 flew the leg heading east, an event marker on the ground was activated to record the moment a north-south running road lined up perpendicular to the flight path (see Figure 3.4). INS recorded longitude at the time of the event marker can thus be compared with the known longitude of the road to construct the Schuler position error (see Figure 3.5a). The exact latitude of the aircraft at the time of the event markers is less certain. In fact, it depends upon the ability of the pilot to fly the intended flight path. But, since the flight paths were flown toward a fixed landmark, only small deviations in the latitude position of the east-west runs would occur. A similar indication of position errors has also been plotted for the latitude, Figure 3.5b. In both cases, the error

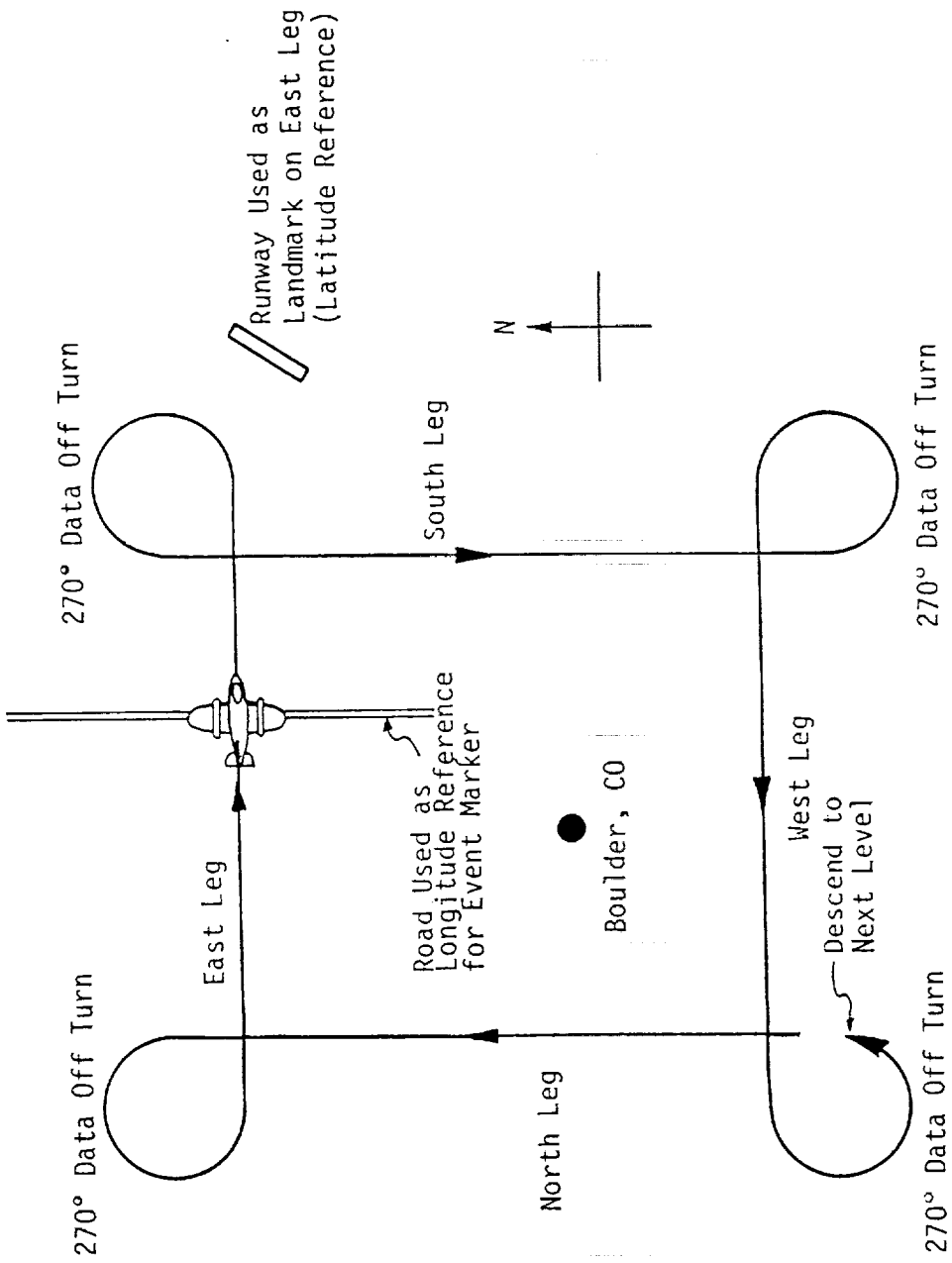
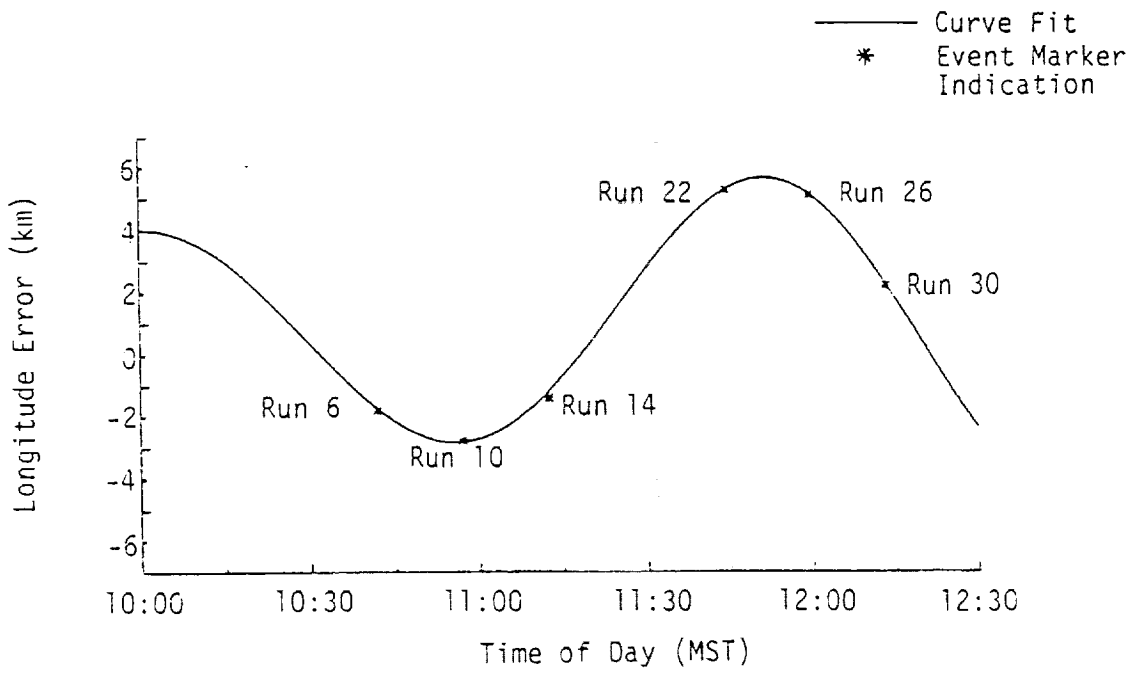
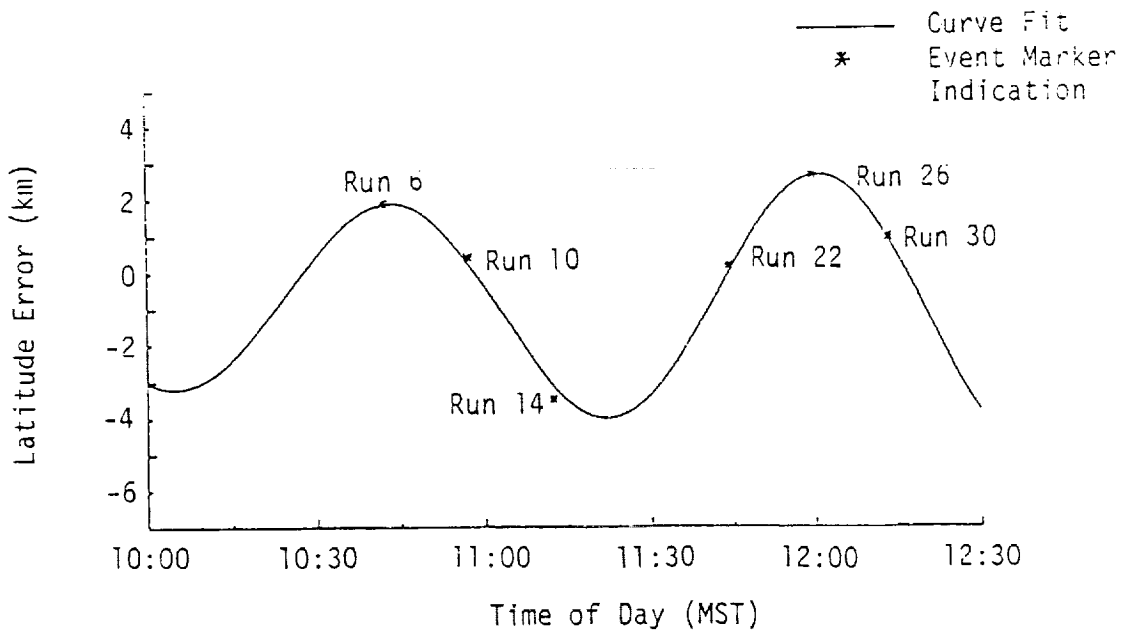


Figure 3.4 Event marker location of B-57 on box pattern flights.



(a) Error in INS longitude indication



(b) Error in INS latitude indication

Figure 3.5 In-flight Schuler position error.

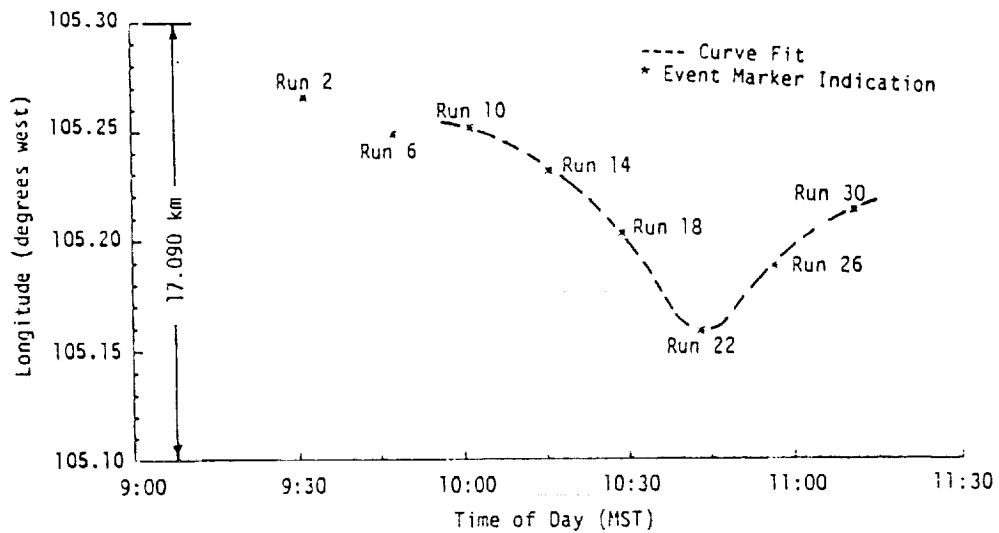
appears to have a sinusoidal behavior. A curve fit of the data suggest the latitude error has a 77-minute period of oscillation, and the longitude has an 111-minute period. The latitudinal period is reasonably close to the Schuler constant of 84 minutes, but the longitudinal period does not conform to that for the latitude.

Another flight following the same flight pattern and the same technique for marking geographical position by event markers is shown in Figure 3.6. The dashed lines outline sinusoidal trends but are not represented by mathematical equations. The latitude oscillation compares with a period of approximately 110 minutes which is similar to the previously reported longitude oscillation. The longitude error contains more scatter in the data, although the period seems to be of roughly the same length as the latitude oscillation on this flight.

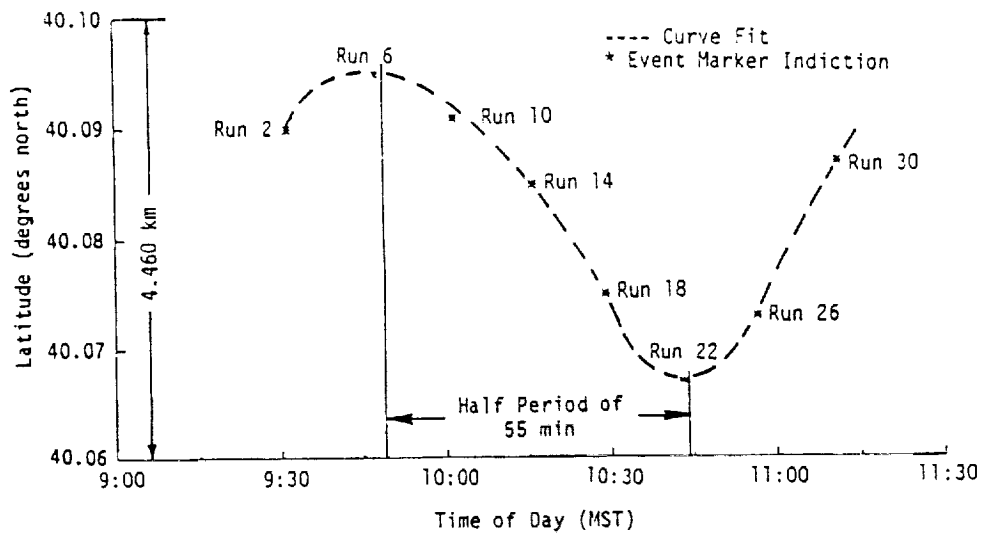
The magnitude INS position errors identified are within a range of less than 15 km or 10 nautical miles. From a commercial aircraft operation standpoint, these errors are not a large problem, particularly in the proximity of an airport where other means of navigation are available. However, Schuler position errors are of significance for wind measurements. Exact ground tracks are needed to determine terrain effects on turbulence such as wake regions behind mountains, etc. An error on the order of several kilometers can drastically distort the picture.

The INS velocity errors which are related to position error can be of the same order of magnitude as the wind speed being measured. An estimate of the velocity errors are presented in Figure 3.7. The velocity error curves are calculated by taking the derivative of the position error curve fits illustrated in Figure 3.5. The influence of these errors is discussed later.

The Schuler error was further investigated with other flights. The aircraft was tracked by the NASA EPS-16 # 34 tracking radar. The radar track provided the location and the ground speed of the aircraft throughout the flight. The post-flight

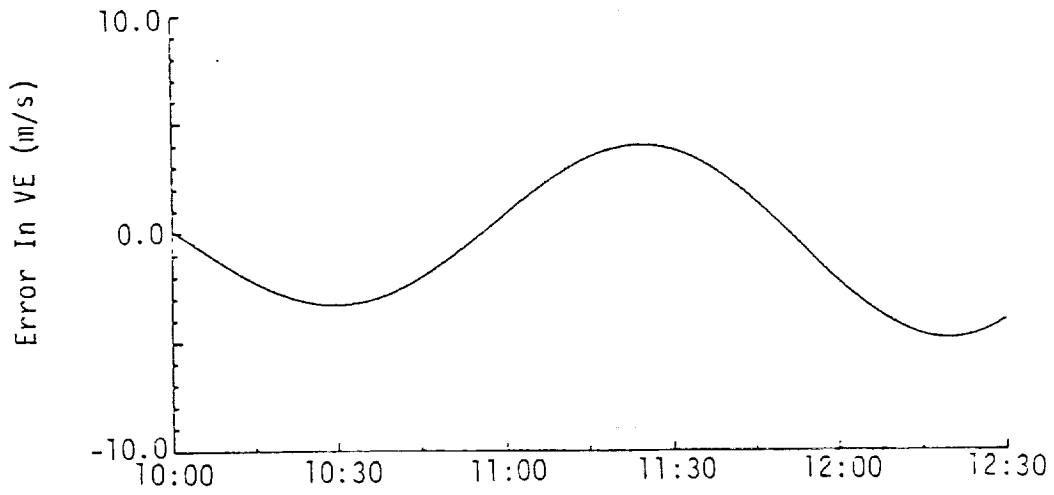


(a) Drift in INS longitude indication

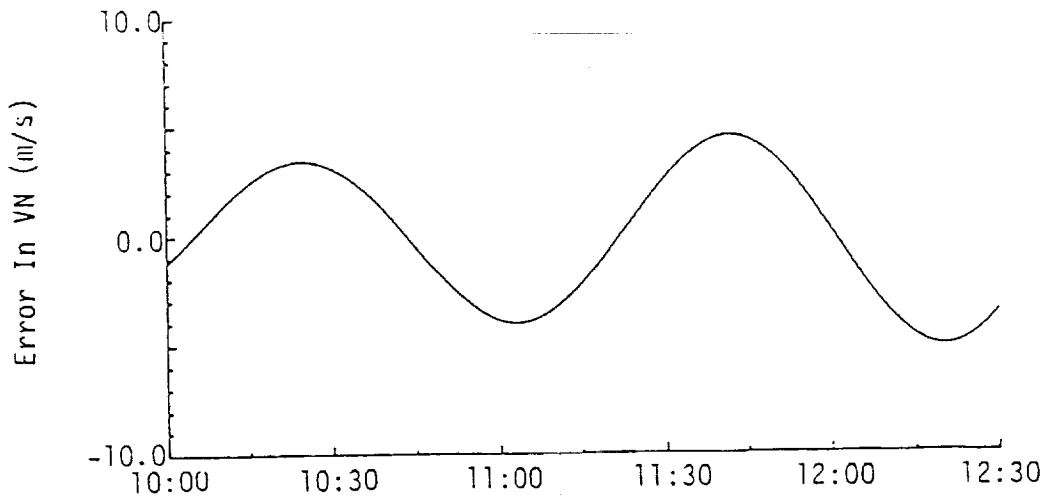


(b) Drift in INS latitude indication

Figure 3.6 In-flight Schuler position error.



(a) East inertial speed error



(b) North inertial speed error

Figure 3.7 In-flight Schuler inertial speed error.

Schuler velocity errors were investigated. The north-south and east-west velocity errors of the flight and the ensuing post-flight velocity measurements are plotted in Figures 3.8 and 3.9. The in-flight velocity errors are obtained by comparing aircraft and radar data assuming the radar indications are free of error. The data recorded on the ground is a direct measure of the indicated velocity from the INS while the aircraft was parked and hence not moving. This velocity fluctuation is attributed to the Schuler error. The INS was left on during the entire time span covered in the plots. Both figures show one complete cycle of a near perfect 84-minute Schuler oscillation in the post-flight data while the vehicle was parked. This is in keeping with Huber and Bogers (1983) who noted that near the ground without accelerations involved the Schuler oscillations will have an 84.4-minute period. In the first half of the flight the errors are more random in their behavior and the oscillation is irregular. This complicates attempts to model or predict the error in advance. Lenschow (1972) suggests that post-flight data recorded with a stationary aircraft be used to back out the error. He proposed to simply trace back a recorded post-flight error oscillation with an 84-minute period constant amplitude sinusoidal curve. The Frost, et al. (1987) study shows, however, that both the period and the amplitude of the velocity error are altered substantially during flight and thus the Lenschow (1972) approach would not be successful in their case. It should be noted that while the inertial velocity measurement errors strongly influence the horizontal wind vector calculations, they generally have little effect on the gust velocity computations because the effect of the slow variations in velocity is greatly diminished or eliminated when the average velocity is removed.

3.2.3 Flow Vane Errors

Ringnes and Frost (1985) observed in analyzing the B-57 data that constant differences existed between the angles of attack measured at the three different

41

152

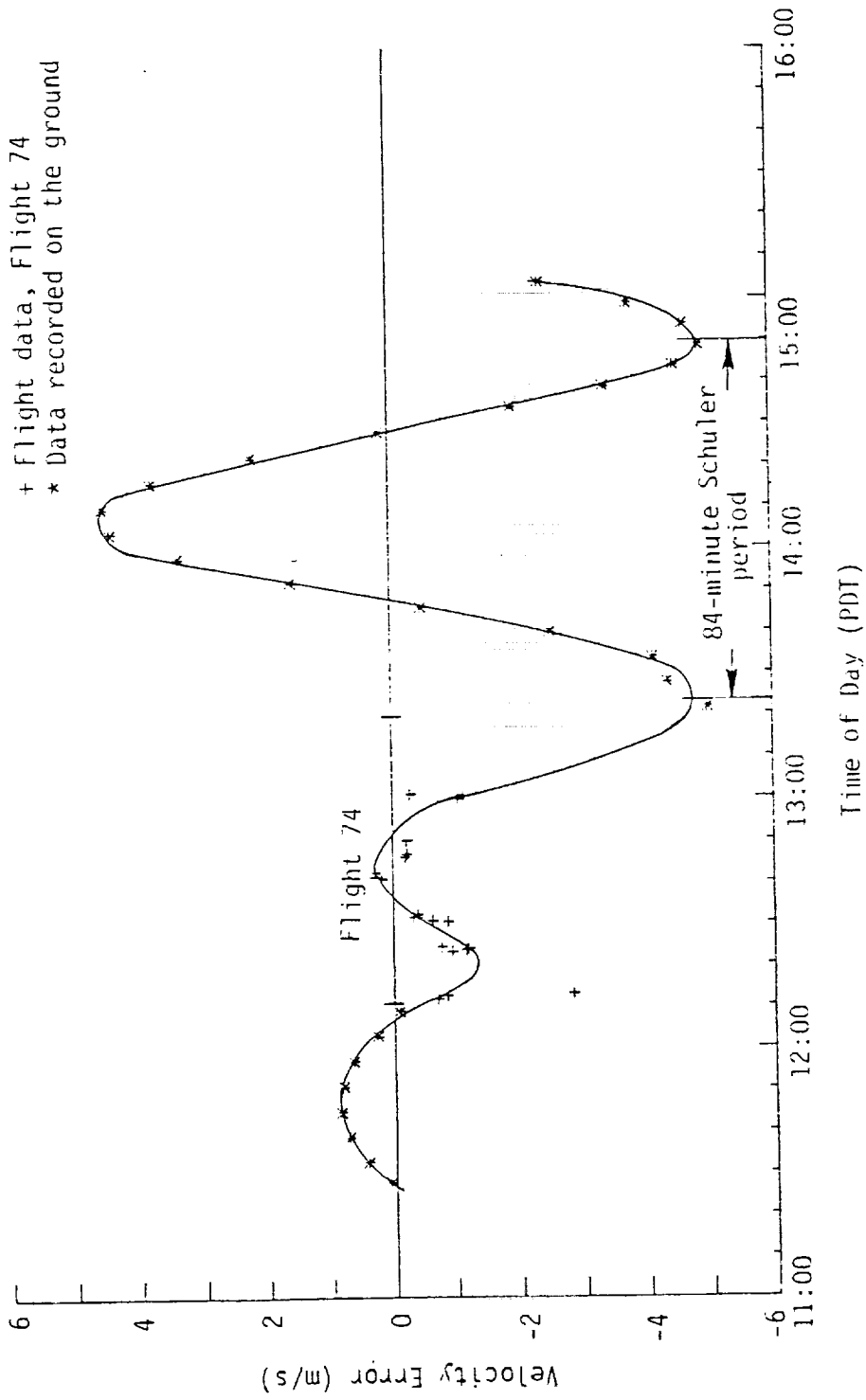


Figure 3.8 Error in east inertial speed.

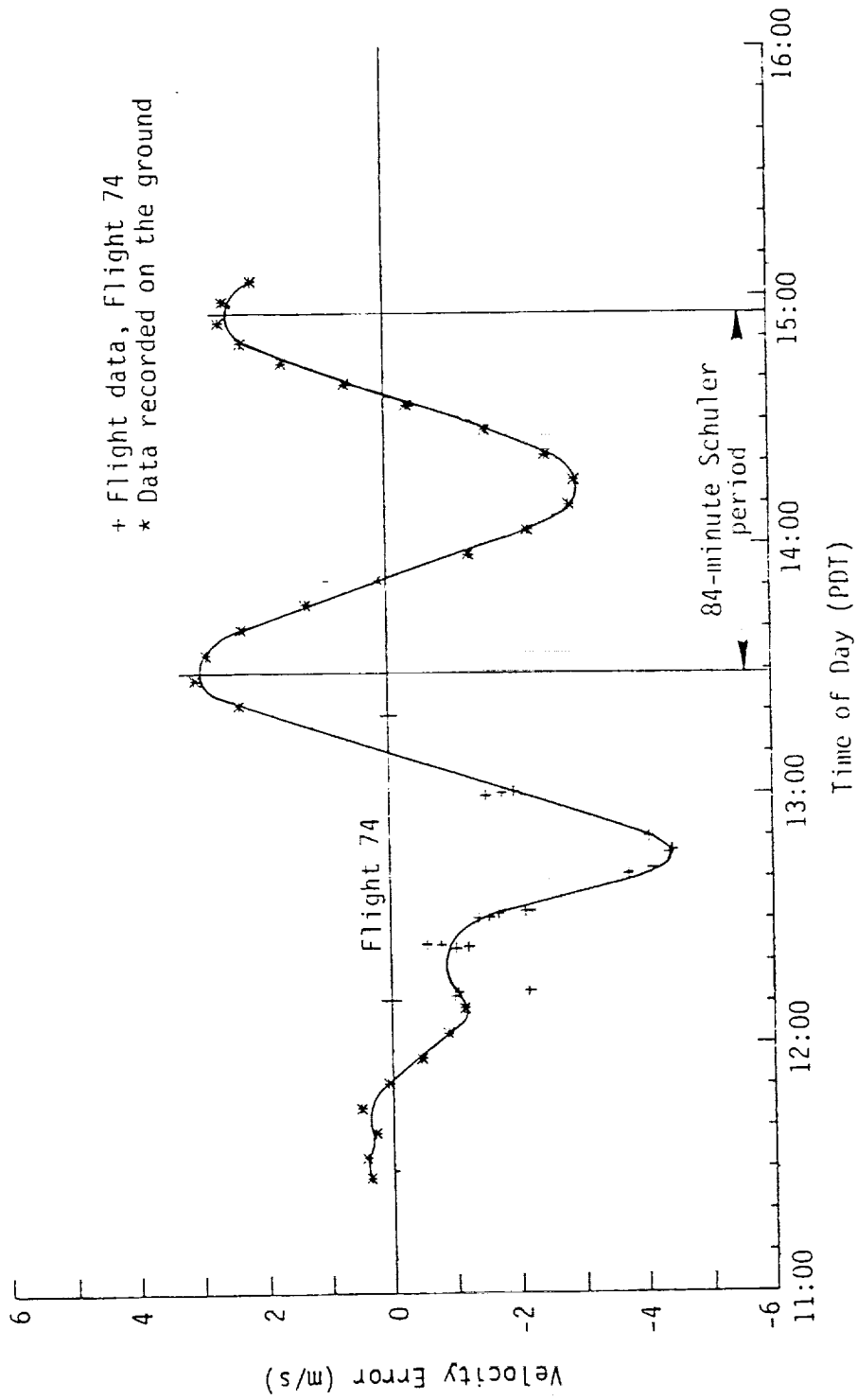


Figure 3.9 Error in north inertial speed.

stations along the wing. The constant offset from the true value again has little influence on the computed turbulence since the mean value is removed during the computation. The angle of attack terms have negligible effect on the computed values and therefore the inaccuracies cause no problems in the total horizontal wind vector computation. The cause of the angle-of-attack difference, however, were attributed to misalignment of the wing tip booms.

The average sideslip angles were also found to be different from the expected value. All aircraft are designed directionally stable and will fly with zero average sideslip angle unless forcefully kept in a sideslip flight condition. During one flight an average sideslip angle of 2.23 degrees was recorded. The source of the error is not clear but boom misalignment or problems with the data acquisition system were suspected causes.

3.2.4 Influence of Error Corrections

The influence the INS velocity and position, sideslip angle, and airspeed errors have on the calculation of horizontal winds is discussed next. A series of wind vectors are plotted before and after corrections have been made along the flight path recorded by the INS during given flights of the NASA Cambera B-57. Each vector represents a one-second average from the 40 samples per second data tapes.

In Figure 3.10 one of the box patterns flown on a particular flight is plotted. In this figure, no corrections have been made. There are some obvious inconsistencies in the wind vectors, particularly, at the corners where it is expected that the wind should agree closer between the two runs. The aircraft made 270-degree turns between runs which take less than two minutes. The wind direction is not expected to change significantly during that short of an interval. Instrumentation errors are, therefore, the probable cause for the discontinuities in wind direction. Figure 3.11 differs from Figure 3.10 only by removal of the 2.23-degree sideslip error in

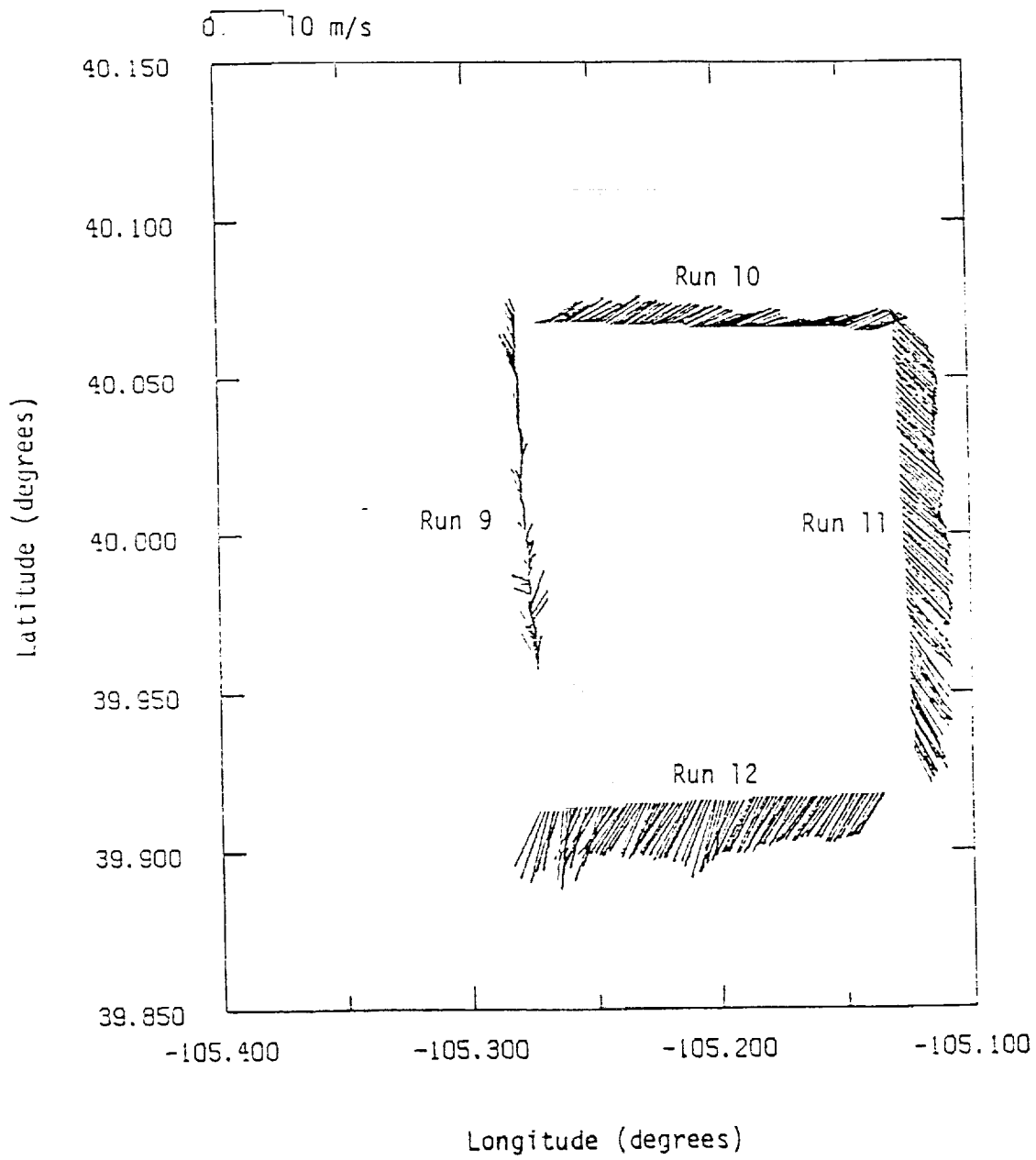


Figure 3.10 Horizontal wind vectors without corrections.

45
156

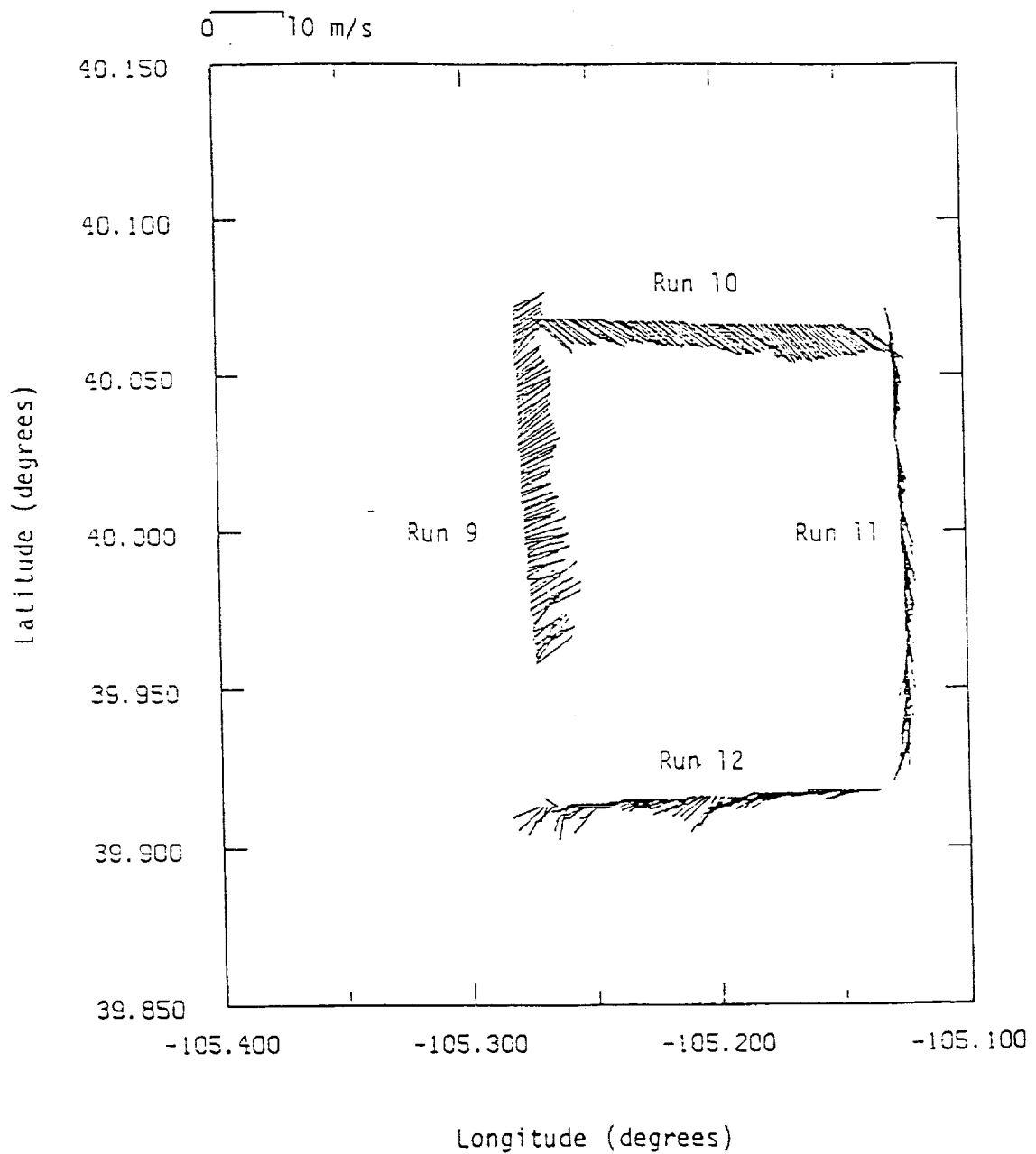


Figure 3.11 Horizontal wind vectors with sideslip-angle corrections

the calculation of the wind vectors. It is debatable whether this correction alone has improved the wind vectors but it clearly demonstrates that seemingly small errors have significant effect on the wind vectors. In Figure 3.12 corrections have been made for all known errors. The discontinuities in the wind vectors at the corners have all but vanished except for the bottom left-hand corner. However, as the numerical order of the runs indicates the box pattern was flown in a clockwise direction; thus, the beginning of the first leg of the run and the last are separated in time by approximately 15 minutes. Therefore, it is conceivable that the wind could have changed in that time span.

Discussion of other sources of errors and their magnitudes is given in the aforementioned references. These are less significant in calculating wind velocities and the interested reader should consult the references directly for more information.

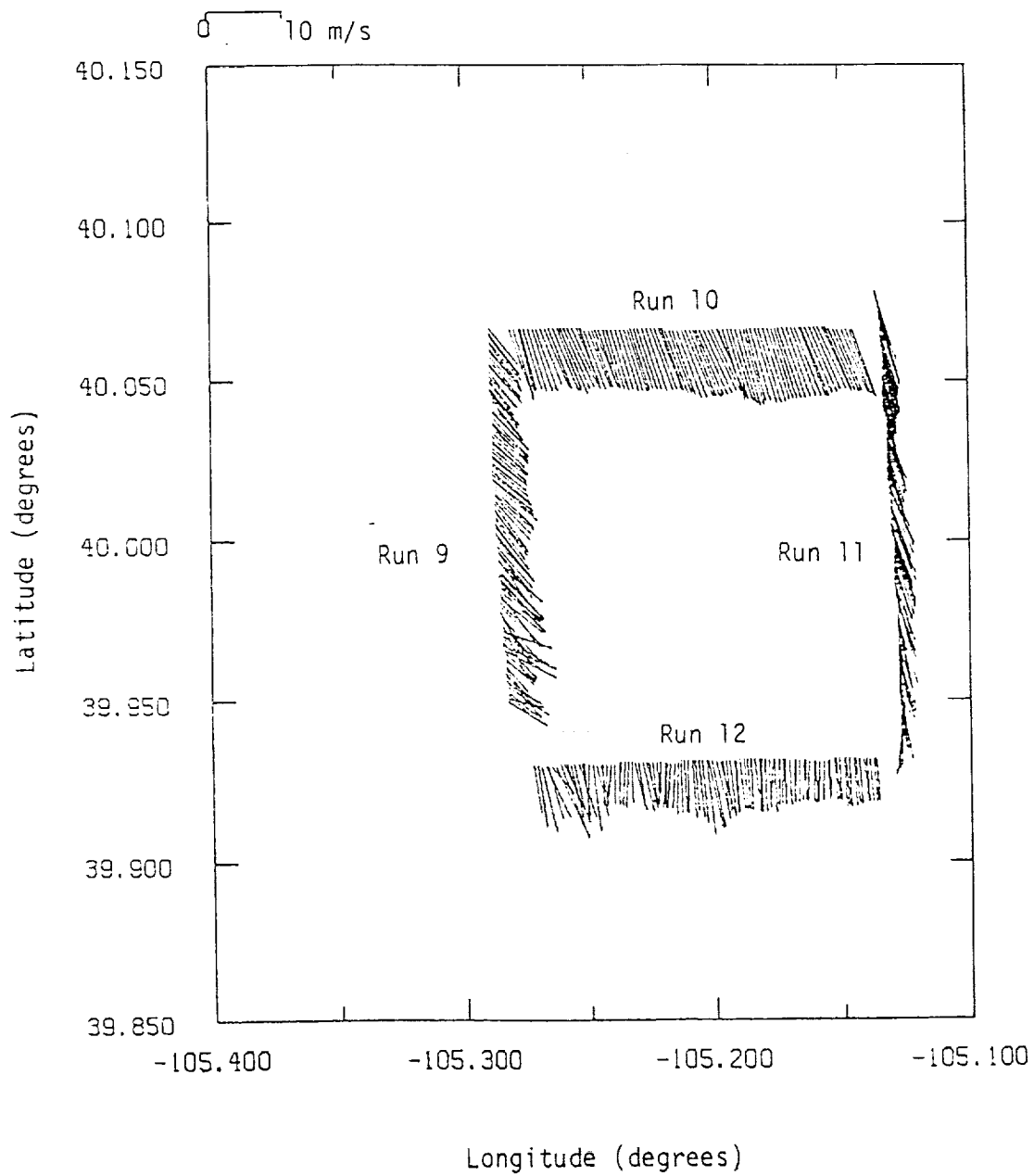


Figure 3.12 Horizontal wind vectors after airspeed, sideslip-angle and inertial velocity and position corrections.

4.0 DATA COMMUNICATION

4.1 Data Transmission

Communication of transducer data to a ground based data acquisition system is generally required for an instrumented aircraft measurement program. Therefore, telemetry techniques capable of transmitting instrumentation data to the ground-based data acquisition system are required. Although several methods are available, specifically, three telemetry methods are most promising: pulse-amplitude modulation (PAM), frequency modulation (FM-FM), and pulse-code modulation (PCM). The PCM telemetry technique is potentially the best for aircraft measurements based on cost and performance factors, which are discussed in detail in this section.

Several factors influence the choice of telemetry techniques for a specific application, including noise, filtering, and sample rate. Signals are especially susceptible to noise contamination along data transmission lines between the transducer and amplifier. Standard practices involving the use of twisted-pair wires, shielded cables, and differential-input amplifiers, can be used to minimize noise picked up by transmission wires. Since several of the specified transducers have maximum signal levels in the millivolt range, their signals must be amplified to a level compatible to the data acquisition system. If the transducer signal is amplified before the noise is introduced, the problem is greatly reduced early in the transmission path. For this reason, only transducers with integral amplifiers should be used. Integral-transducer amplifiers reduce the parts count significantly in addition to reducing noise.

Additional signal conditioning, such as filtering, is not generally required aboard the aircraft, but must be performed by the ground-based data acquisition system. The data acquisition system includes an appropriate mass storage device for later

retrieval and conditioning of the wind data. Figure 4.1 illustrates the data path aboard the aircraft.

Although the telemetry data link must introduce a minimal amount of noise, other constraints on the design are equally important with the telemetry data link. Specifically, sample rate (when applicable) and cost must be considered. The minimum tolerable sample rate of the aircraft's telemetry system is dependent on the data layer thickness and the speed of the aircraft. For a detectable layer, d , and an aircraft speed, V , the minimum sample frequency per channel is:

$$f_s = \frac{2V}{d} \quad (4.1)$$

since a minimum of two samples must be taken for a layer to be detected where V = speed of the rocket, d = minimum shear layer resolution, and f_s = sample frequency. Figure 4.2 is an example plot of required sampling frequency for an 11-channel system as a function of vertical ascent rate. This takes into account neither oversampling, which would be required with a digital filter nor the use of multiple data channels, which could be used on the aircraft. Oversampling n channels s times results in a sample frequency

$$f_s = \frac{2Vns}{d} \quad (4.2)$$

The minimum sample frequency is not a factor if an FM-FM system is used. FM-FM systems transmit a continuous signal of summed subcarrier oscillator signals which correspond to individual transducer voltage signals. The minimum detectable data layer thicknesses depend on the center frequency and modulation index of the individual subcarrier oscillators. Therefore, provided that the center frequencies are sufficiently higher than the cutoff frequencies of the corresponding transducers, no data will be lost due to frequency limitations of the telemetry system.

PAM and PCM are not continuous telemetry schemes and thus must sample no slower than the minimum sample frequency as described above. PAM is the

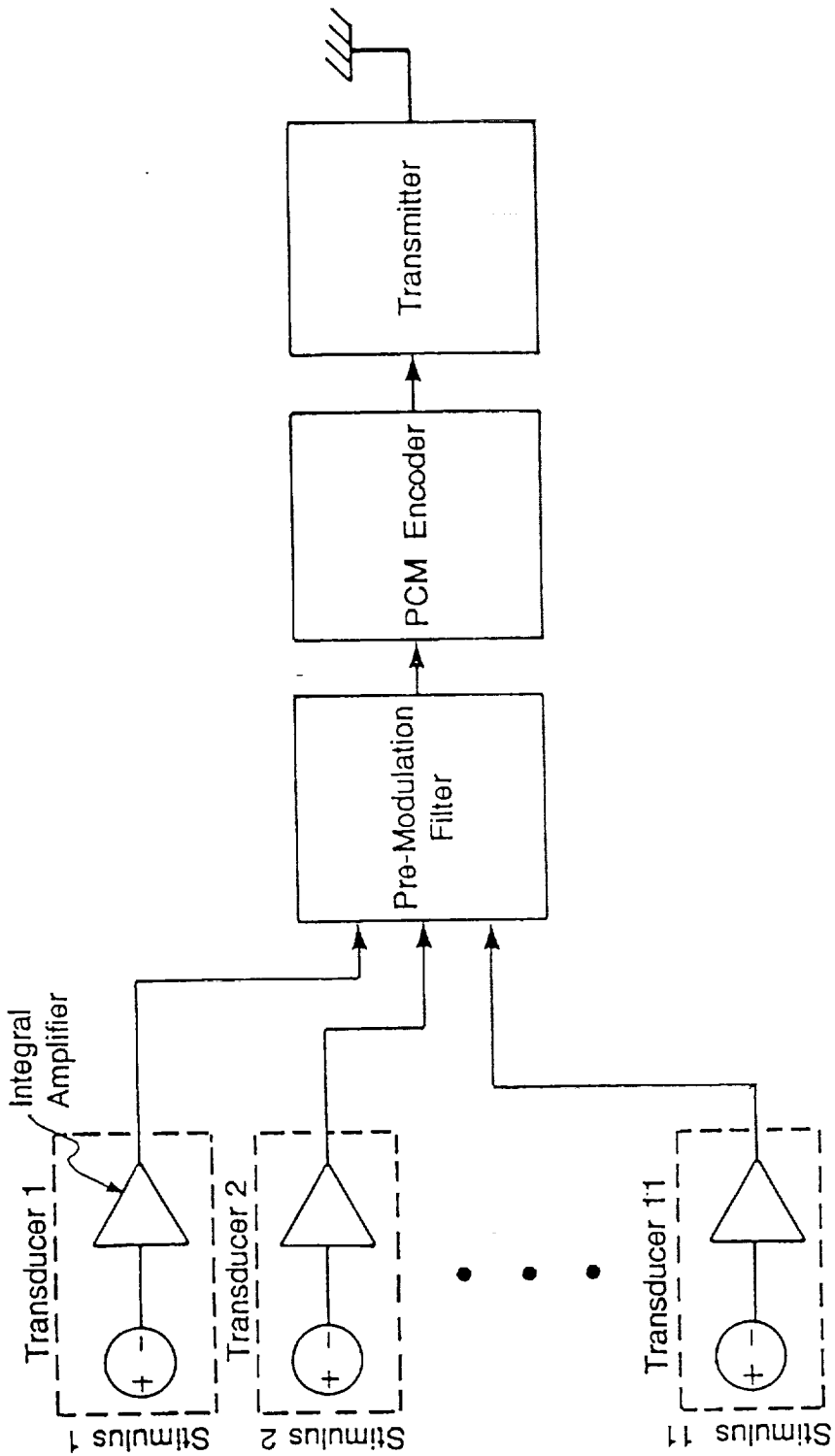


Figure 4.1 Data path aboard aircraft.

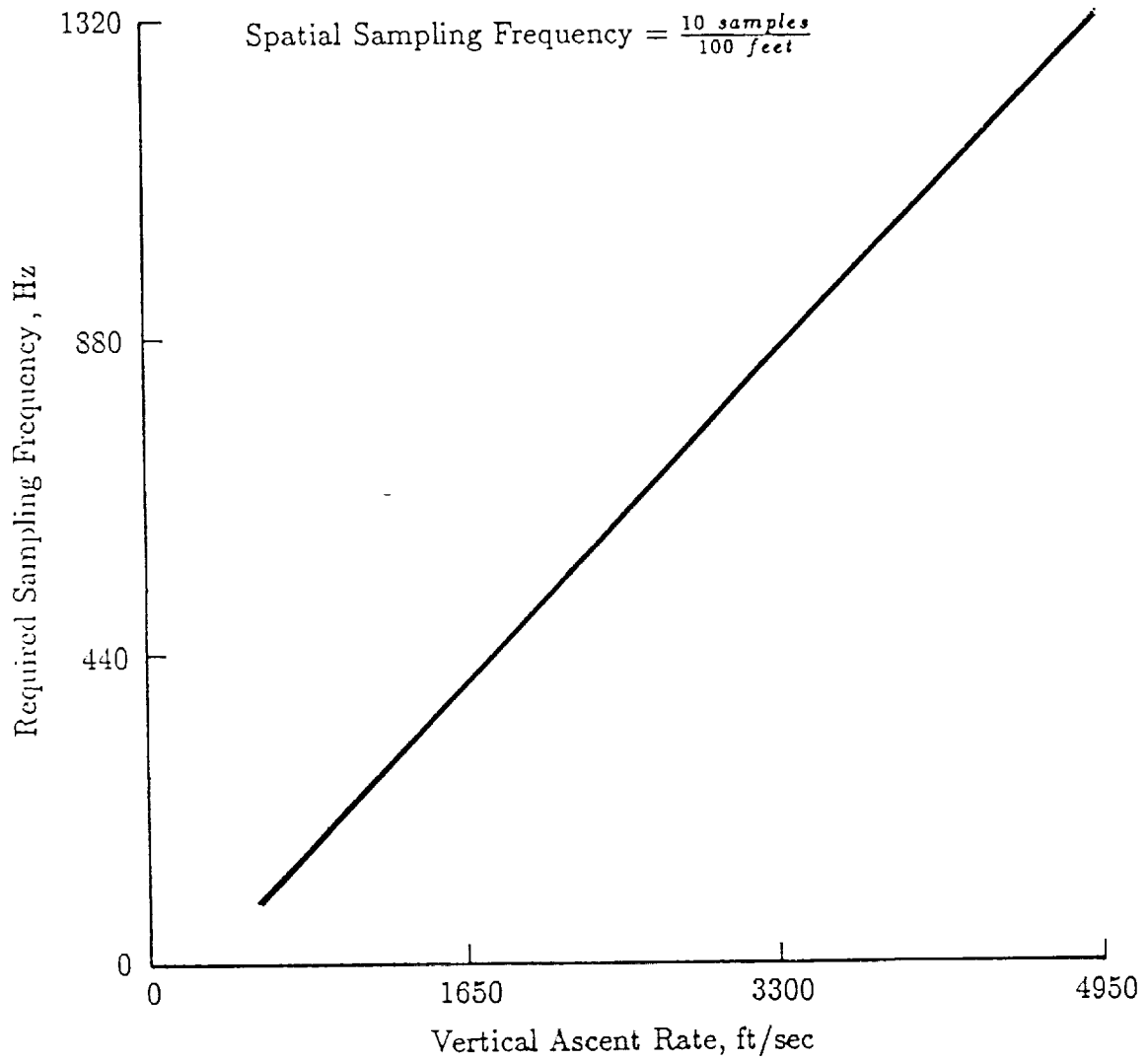


Figure 4.2 Minimum sampling frequency for 11-channel system.

simplest method of time-division multiplexing: the separate transducer outputs are sequentially switched to a common output which forms a composite waveform of the individual channels' outputs. The period of the waveform is equal to the sample interval of one channel times the total number of channels in the system. PCM operates similarly, with the exception that data is converted from analog signals to digital signals. Current sample rates of PAM and PCM encoders are up to 200,000 samples/sec and 3.2 megabits/sec respectively.

Crosstalk, gain and offset errors, and incidental frequency modulation are sources of error in data transmission. Of the three telemetry methods considered, PAM has the poorest absolute accuracy specification: typical errors between 2% and 5% of full scale can be expected. FM-FM system accuracy, as well as that of the other two methods, is highly dependent upon proper setup of the transducer output gain and offset. Depending on how close to launch time the transducer calibration is made, errors of 1% to 4% can be expected from an FM-FM telemetry system. If proper setup is obtained with a PCM system, the error induced by this system will be one least-significant bit (LSB) since the data is converted to a digital form. For an 8-bit telemetry system, one LSB equals one part in 2^8 ; or about 0.4%.

The recommended telemetry technique is the PCM system, based on reasonable cost, sufficient sample rate, and superior accuracy to the other methods of telemetry. This type of system allows more flexibility with the number of data channels transmitted than the FM-FM system since the latter will require additional capital expenditures for each additional channel transmitted. Additionally, the worst-case error of the final data will be due primarily to the transducers instead of the telemetry system as would be the case with PAM. Table 4.1 summarizes the characteristics of the three telemetry methods.

Table 4.1 Telemetry comparison.

Telemetry Method	Data Channel Capacity	Availability	Accuracy	Cost
PAM	Low	Low	Low	Low
FM-FM	Low	Moderate	Moderate	High
PCM	High	High	High	Moderate

Other necessary components of an onboard telemetry data link are the transmission antennas and the transmitter. Three blade antennas mounted on the rocket will transmit the telemetry signal adequately in all directions. The transmitter can be adjusted to broadcast a selected frequency which must correspond to the frequency of the receiver on the ground. This flexibility in transmission frequency could prove to be beneficial in regard to the frequency allocation and certification by the National Telecommunications and Information Administration (NTIA) upon review by the Spectrum Planning Subcommittee (SPS). The transmission frequency will typically be in the L or S band in the radio frequency spectrum.

4.2 Data Acquisition

A ground based data acquisition system is required for storing and processing the telemetered wind parameter data. An appropriate system is described next. A ground station consisting of a telemetry reception, data acquisition, and data processing system will produce all desired atmospheric profile data, store historical atmospheric profiles for future profile predictions, and permit portability to various sites.

The choice of data acquisition system is dependent on the type of telemetry system aboard the aircraft. Even though the transmitter and receiver remain the same for all types of telemetry considered, the way in which the signal is decoded to provide data from all channels is determined by the format used to transform the data signal to a telemetry signal. Since PCM is recommended as the optimum telemetry scheme for most applications, a data acquisition system compatible with PCM is discussed.

The fundamental components of a PCM data acquisition system consist of the following:

1. a PCM bit decoder to translate the frequency-modulated radio signal into a digital pulse stream,
2. a data decommutator to separate the digital signal into individual channel signals,
3. a digital-to-analog converter to transform the digital channel data into analog data, and
4. a serial time-code reader to provide time correlation with the acquired data.

In addition to these requirements, other features that will greatly benefit system quality will be incorporated. These include adaptability to a range of PCM codes, digital and analog mass storage capability, real-time display of multiple channel signals, and scaling and manipulation of these channels into desired engineering-unit parameters. These features will be incorporated into a user-friendly, stand-alone system, and will result in a highly versatile telemetry system.

Turn-key telemetry data acquisition systems are available which will accommodate all requirements for aircrafts data system. One particular system includes both the hardware and the software which obtains telemetry data. In addition to

fulfilling all of the cited requirements, the system provides data record archiving and editing capability, 16 channels of real-time analog output, user-programmable display formatting, and various scaling and look-up table capabilities. This system is available as a retrofit to a dedicated IBM PC/AT compatible or as a rackmountable 80386 system with a 100 megabyte hard disk drive. The latter option is viewed as being the more advantageous one since the data acquisition system may be installed in a single rack with the ground station receiver and a multi-channel analog tape machine used as a back-up data storage device.

5.0 SUMMARY

A review of salient features associated with measuring winds from aircraft has been given. Included is a discussion of the typical instruments and systems, the equations for reducing aircraft measurement to winds in the earth coordinates system, error analysis for assessing the accuracy of instrumentation, as well as, procedures for correcting and calibrating for errors associated with flight operations and an overview of methods for communicating measurements from the aircraft to ground station for data processing. Throughout the report a summary of the literature pertaining to various techniques available for measuring winds including some of the measurement programs for which instrumented aircraft have been developed and employed is provided. A discussion of the various types of instrumentation that have been used in previous programs, the reported potential errors and methods of correcting and calibrating the instruments and the problems associated with obtaining accurate ground speed values from INS systems is given.

The report provides a guide to researchers in the process of developing instrumented aircraft for measurement of atmospheric phenomena.

6.0 REFERENCES

- An Introduction to Inertial Navigation, Litton Guidance & Control Systems brochure, Woodland Hills, CA.
- Axford, D.N. (1968): "On the Accuracy of the Wind Measurements Using an Inertial Platform in an Aircraft, and an Example of a Measurement of the Vertical Mesostructure of the Atmosphere.", Journal of Applied Meteorology, Vol. 7:645-666.
- Barna, P.S., and G.R. Crossman (1976): "Experimental Studies on the Aerodynamic Performance and Dynamic Response of Flow Direction Sensing Vanes", NASA CR-2683, May.
- Benjamin, S.G. (1989): "An Isentropic Meso α -Scale Analysis System and Its Sensitivity to Aircraft and Surface Observations", Monthly Weather Review, Vol. 117, pp. 1586- 1603.
- Bjarke, L.J., and L.J. Ehernberger (1989): "An In-Flight Technique for Wind Measurement in Support of the Space Shuttle Program". NASA TM-4154, November.
- Boxmeyer, C. (1964): Inertial Navigation Systems, McGraw- Hill Book Co., New York, NY.
- Brown, E.N., C.A. Friehe, and D.H. Lenschow (1983): "The Use of Pressure Fluctuations on the Nose of an Aircraft for Measuring Air Motion", Journal of Climate and Applied Meteorology, Vol. 22, pp. 171-180, January.
- Brown, W.J., Jr., J.D. McFadden, H.J. Mason, Jr., and C.W. Travis (1974): "Analysis of the Research Flight Facility Gust Probe System", Journal of Applied Meteorology, Vol. 13, No. 1, pp. 156-167, February.
- Bryer, D.W., and R.C. Pankhurst (1971): Pressure-probe Methods for Determining Wind Speed and Flow Direction, Her Majesty's Stationary Office, London.
- Chang, H.P., and W. Frost (1985): "NASA B-57B Orographic Data Reduction and Analysis Relative to PBL Parameterization Models." Final report for NASA Goddard Space Flight Center under Contract NAS5-28558.
- Crooks, W.M., F.M. Hoblit, D.T. Prophet, et al. (1967): "Project HICAT An Investigation of High Altitude Clear Air Turbulence", Air Force Flight Dynamics Laboratory, Wright-Patterson ARB, OH, Volume 1, Report AFFDL-TR-67-123.

- Davis, R.E., R.A. Champine, and L.J. Ehernberger (1979): "Meteorological and Operational Aspects of 46 Clear Air Turbulence Sampling Missions with an Instrumented B-57B Aircraft, Volume I - Program Study", prepared for NASA Langley Research Center, NASA TM-80044.
- Dutton, J.A., and D.H. Lenschow (1962): "An Airborne Measuring System for Micrometeorological Studies", Studies of the Three-Dimensional Structure of the Planetary Boundary Layer, Sec. 5, Dept. of Meteor, Univ. of Wisconsin, Final Report Contract DA-36-039-SC-80282, USAEPG, Ft. Huachuca, AZ.
- Etkin, B. (1972): Dynamics of Atmospheric Flight, John Wiley & Sons, New York.
- Fisher, B.D., G.L. Keyser, Jr., P.L. Deal, M.E. Thomas, and F.L. Pitts (1980): "Storm Hazards '79 - F-106B Operations Summary", NASA TM-81779.
- Fisher, B.D., G.L. Keyser, Jr., and P.L. Deal (1982): "Lightning Attachment Patterns and Flight Conditions for Storm Hazards '80", NASA TP-2087.
- Friedland, B. (1978): "Analysis Strapdown Navigation Using Quaternions", IEEE Transactions on Aerospace and Electronic Systems, Vol. AES-14, No. 5, pp. 764-768, September.
- Frost, W., M.C. Lin, H.P. Chang, and E.A. Ringnes (1985): "Analysis of Data from NASA B-57B Gust Gradient Program." Final report for NASA Marshall Space Flight Center under Contracts NAS8-36177 and NASS-35347.
- Frost, W. to C.K. Hill. "Action Item from NASA Dryden Meeting, May 14, 1987." FWG Associates Memorandum, dated 20-May-87, with revision 21-Aug-87.
- Frost, W., H.P. Chang, and E.A. Ringnes (1987): "Analyses and Assessments of Spanwise Gust Gradient Data from NASA B-57B Aircraft", NASA Langley Research Center, Final Report Contract NAS1-17989.
- Gage, K.S., and G.D. Nastrom (1986): "Theoretical Interpretation of Atmospheric Wavenumber Spectra of Wind and Temperature Observed by Commercial Aircraft During GASP", Journal of the Atmospheric Sciences, Vol. 43, No. 7, pp. 729-740.
- Gamo, M., et al., (1975): "Observed Characteristics of the Standard Deviation of the Vertical Wind Velocity in Upper Part of the Atmospheric Boundary Layer", J. Meteor. Soc., Japan, 53.
- Gamo, M., et al., (1976): "Structure of the Atmospheric Boundary Layer Derived from Airborne Measurements of the Energy Dissipation Rate ϵ ", J. Meteor. Soc., Japan, 54.

- Ganzer, V.M., R.G. Joppa, and G. van der Wees (1977): "Analysis of Low Altitude Atmospheric Turbulence Data Measured in Flight", prepared by the University of Washington for NASA Ames Research Center, NASA CR-2886.
- Geenen, R.J., and B.J. Moulton (1991): "A System for Testing Airdata Probes at High Angles of Attack Using a Ground Vehicle", AIAA-91-0088, 29th Aerospace Sciences Meeting, Reno, NV, January 7-10.
- Geller, E.S. (1968): "Inertial System Platform Rotation", IEEE Transactions on Aerospace and Electronic Systems, Vol. AES-4, No. 4, pp. 557-568, July.
- Gorenshteyn, I.A., and I.A. Shul'man (1970): "Inertial Navigation Systems", DTIC Technical Report FTD-HC-23-327-71, January.
- Gosink, J. (1982): "Measurements of Katabatic Winds Between Dome C and Dumont d'Urville", Pure Appl. Geophys., Vol. 120, pp. 503-526.
- Gracey, W., and E.F. Scheithauer (1951): "Flight Investigation of the Variation of Static-Pressure Error of a Static-Pressure Tube with Distance Ahead of a Wing and a Fuselage", National Advisory Committee for Aeronautics TN-2311, March.
- Gracey, W. (1958): "Summary of Methods of Measuring Angle of Attack on Aircraft", National Advisory Committee for Aeronautics TN-4351, August.
- Gracey, W. (1981): Measurement of Aircraft Speed and Altitude, John Wiley & Sons.
- Hacker, J.M., and P. Schwerdtfeger (1988): "The FIAMS Research Aircraft", System Description FIAMS Technical Report 8, Flinders Institute for Atmospheric and Marine Sciences, Flinders University of South Australia, Bedford Park, S.A., 5042.
- Haering, E.A., Jr. (1990): "Airdata Calibration of a High-Performance Aircraft for Measuring Atmospheric Wind Profiles", NASA TM-101714, January.
- Hatley, C.M. (1989): "Prelaunch Wind Monitoring Via Aircraft." CR S33450D, SIR Presentation at Johnson Space Center, Houston, Texas, November 14.
- Hermann, P.J., D.B. Finley, S.C. Rehfeldt, and L.C. Benishek (1984): "Airfoil Probe for Angle-of-Attack Measurement", Journal of Aircraft, Vol. 21, No. 1, pp. 87, January.
- Hill, C.K. (1990): "Feasibility of Measuring Prelaunch Wind Profiles in Support of STS Operations with an Instrumented Aircraft", PhD. Dissertation, The University of Tennessee, Knoxville, TN, May.
- Hillje, E.R. and D.E. Tymms (1980): "The Ascent Air Data System for the Space Shuttle", AIAA Paper 80-0422, March.

- Hillje, E.R. and R.L. Nelson (1981): "Post Flight Analysis of the Space Shuttle Ascent Air Data System", AIAA Paper 81-2457, November.
- Hillje, E.R., and R.L. Nelson (1990): "Ascent Air Data System Results From the Space Shuttle Flight Test Program", NASA-Lyndon B. Johnson Space Center, Houston, TX. Personal communications.
- Hotop, H.J. (1985): "Flight Testing the Litton LTN 90 Laser Gyro Strapdown System for Civil Aviation", European Space Agency, ESA- TT-904, March.
- Huber, C., and W.J. Bogers (1983): "The Schuler Principle: A Discussion of Some Facts and Misconceptions", EUT Research Report 83-E-136 (ISBN 90-6144-136-6), Eindhoven University of Technology, Dept. of Electrical Engineering, Eindhoven, The Netherlands, May.
- Jacobsen, R.A. (1977): "Hot-Wire Anemometry for In-Flight Measurement of Aircraft Wake Vortices", DISA Information, 21, pp. 21-27.
- Karakashev, V.A. (1972): "Use of External Information on the Linear Velocity of a Vehicle for Correcting Inertial Navigation Systems", NTIS, Springfield, VA, Report No. JPRS 57282, October 17.
- Kraus, H., J.M. Hacker, and J. Hartmann (1990): "An Observational Aircraft-Based Study of Sea-Breeze Frontogenesis", Boundary-Layer Meteorology, Vol. 53, pp. 223-265.
- Larson, T.J., and L.J. Ehernberger (1985): "A Constant Altitude Flight Survey Method for Mapping Atmospheric Ambient Pressures and Systematic Radar Errors", NASA TM-86733, June.
- Larson, T.J., S.A. Whitmore, L.J. Ehernberger, J.B. Johnson, and P.M. Siemers, III (1987): "Qualitative Evaluation of a Flush Air Data System at Transonic Speeds and High Angles of Attack", NASA Technical Paper 2716, April.
- Lechner, W., H.J. Hotop, and H.P. Zenz (1983): "Flight Testing of Inertial Navigation Systems - Hardware and Software Description", European Space Agency, ESA-TT-772, March.
- Lenschow, D.H. (1965): "Airborne Measurements of Atmospheric Boundary Layer Structure", Studies of the Effects of Variations in Boundary Conditions on the Atmospheric Boundary Layer, Sec. 4, Dept. of Meteor, Univ. of Wisconsin, Final Report Contract DA-36-039-AMC-00878(E), USAERDA, Ft. Huachuca, AZ.
- Lenschow, D.H., and W.B. Johnson, Jr. (1968): "Concurrent Airplane and Balloon Measurements of Atmospheric Boundary-Layer Structure over a Forest", Journal of Applied Meteorology, Vol. 7, No. 1, pp. 79-89.

- Lenschow, D.H. (1971): "Vanes for Sensing Incidence Angles of the Air from an Aircraft", Journal of Applied Meteorology, Vol. 10, pp. 1339-1343, December.
- Lenschow, D.H. (1972): "The Measurement of Air Velocity and Temperature Using the NCAR Buffalo Aircraft Measuring System." NCAR-TN/EDD-74.
- Lenschow, D.H., and N.D. Kelley (1975): "Atmospheric Mesoscale Measurements from Aircraft", 3rd Symposium on Meteorological Observations and Instrumentation, The National Center for Atmospheric Research, Boulder, CO.
- Lenschow, D.H., C.A. Cullian, R.B. Friesen, and E.N. Brown (1978): "The Status of Air Motion Measurements on NCAR Aircraft", 4th Symposium on Meteorological Observations and Instrumentation, April 10-14, American Meteorological Society, Boston, MA.
- Lenschow, D.H., C.A. Friehe, and J.C. LaRue (1978): "The Development of an Airborne Hot-Wire Anemometer System", 4th Symposium on Meteorological Observations and Instrumentation, American Meteorological Society, Boston, MA.
- Lenschow, D.H. (1983): "Aircraft Measurements in the Boundary Layer", A Chapter in Probing the Atmospheric Boundary Layer, originally prepared for the AMS Short Course on Instruments and Techniques for Probing the Atmospheric Boundary Layer, August 8-12, Boulder, CO.
- Lenschow, D.H., X.S. Li, C.J. Zhu, and B.B. Stankov (1987): "The Stably Stratified Boundary Layer Over The Great Plains", Boundary-Layer Meteorology, Vol. 42, pp. 95-121.
- Leshner, C. (1990): Personal communication with T.S. Paige. Orbital Science Corporation, Chandler, AZ.
- Luers, J.K., and C.D. MacArthur (1972): "Ultimate Wind Sensing Capabilities of the Jimsphere and Other Rising Balloon Systems." NASA CR-2048, June.
- MacPherson, J.I. (1973): "A description of the NAE T-33 Turbulence Research Aircraft, Instrumentation, and Data Analysis", DME/NAE Quarterly Bulletin No. 1972(4), Ottawa.
- McBean, G.A., and J.I. MacPherson (1976): "Velocity and Scalar Statistics", Boundary Layer Meteorology, Vol. 10, pp. 181-197.
- McConnell, K.G. (1966): "Kinematics of a Three-Axis Gimbal System", proceedings of the Third Southeastern Conference on Theoretical and Applied Mechanics, University of South Carolina, Vol. 3, March 31-April 1.

- McFadden, J.D., C.W. Travis, R.E. Gilmer, and R.E. McGavin (1970): "Water Vapor Flux Measurements from ESSA Aircraft", Preprints Symp. Tropical Meteorology, Honolulu, Amer. Meteor. Soc., BIII, 1-6.
- Meissner, C.W., Jr. (1976): "A Flight Instrumentation System for Acquisition of Atmospheric Turbulence Data", prepared for NASA Langley Research Center, NASA TN D-8314.
- Miller, R.B. (1982): "Strapdown Inertial Navigation Systems: An Algorithm for Attitude and Navigation Computations", Department of Defence, Melbourne, Victoria, Australia.
- Moes, T.R., and S.A. Whitmore (1991): "Preliminary Results From an Airdata Enhancement Algorithm with Application to High Angle-of-Attack Flight", AIAA-91-0672, 29th Aerospace Sciences Meeting, Reno, NV, January 7-10.
- Murrow, H.N., and R.H. Rhyne (19xxx): "Flight Instrumentation for Turbulence Measurements in the Atmosphere", Personal correspondence, NASA Langley Research Center, Hampton, VA.
- NSTS 08211 (1988): "Launch Systems Evaluation Advisory Team (LSEAT) Integrated Support Plan", Lyndon B. Johnson Space Center, Houston, TX, July 25.
- O'Donnell, C.F., eds. (1964): Inertial Navigation - Analysis and Design, McGraw-Hill Book Company, Inc., New York, NY.
- Parish, T.R., and D.H. Bromwich (1989): "Instrumented Aircraft Observations of the Katabatic Wind Regime Near Terra Nova Bay", Monthly Weather Review, Vol. 117, pp. 1570-1585.
- Pitman, G.R., Jr., eds. (1962): Inertial Guidance, John Wiley & Sons, Inc., New York, NY.
- Poellet, M. (1990): "University of North Dakota Cessna Citation II", Personal correspondence, August.
- Potter, G.G. (1982): "A Sensitivity Analysis of the Kalman Filter as Applied to an Inertial Navigation System", Naval Postgraduate School Thesis, Monterey, CA, June.
- Puckett, A.E., and S. Ramo (1959): Guided Missile Engineering, McGraw-Hill Book Company, Inc., New York, NY.
- Renard, R.J., and M.S. Foster (1978): "The Airborne Research Data System (ARDS): Description and Evaluation of Meteorological Data Recorded During Selected 1977 Antarctic Flight", Rep. No. NPS 63-78-002, Naval Postgraduate School, Monterey, pp. 90.

- Rhyne, R.H. (1980): "Accuracy of Aircraft Velocities Obtained From Inertial Navigation Systems for Application to Airborne Wind Measurements", NASA TM-81826, July.
- Rider, C.K., M.R. Thomson, and F.E. Verinder (1971): "Measurement of Extreme Mechanical Turbulence During Low Level Flights by Mirage A3-76", Department of Supply, Australian Defense Scientific Service, Structures and Materials Report 333.
- Ringnes, E.A., and W. Frost (1985): "Analysis of Aerodynamic Coefficients Using Gust Gradient Data: Spanwise Turbulence Effects on Airplane Response." NASA CR-3961.
- Sakamoto, G.M. (1976): "Aerodynamic Characteristics of a Vane Flow Angularity Sensor System Capable of Measuring Flightpath Accelerations for the Mach Number Range from 0.40 to 2.54", NASA TN D-8242, May.
- Scott, S.G., T.P. Bui, K.R. Chan, and S.W. Bowen (1988): "The Meteorological Measurement System on the NASA ER-2 Aircraft", submitted to the Journal of Geophysical Research.
- Scott, S.G., T.P. Bui, R. Chan, and S.W. Bowen (1989): "The Meteorological Measurement System on the NASA ER-2 Aircraft." NASA Ames Research Center, Moffet Field, CA, June.
- Shaw, W.A. (1966): "Developments in Theoretical and Applied Mechanics", Vol. 3, proceedings of the Third Southeastern Conference on Theoretical and Applied Mechanics, University of South Carolina, March 31-April 1.
- Shibata, M. (1986): "Error Analysis Strapdown Inertial Navigation Using Quaternions", Journal of Guidance, Control, and Dynamics, Vol. 9, No. 3, pp. 379, May-June.
- Schuler, M. (1923): "Die Störung von Pendel und Kreiselapparaten durch die Beschleunigung des Fahrzeuges, Physik Z., Vol. 24, July. A translation appears in Inertial Guidance (G.R. Pittman, Jr., ed.). John Wiley & Sons, Inc., New York, NY.
- Stromberg, I.M., C.S. Mill, T.W. Choularton, and M.W. Gallagher (1989): "A Case Study of Stably Stratified Airflow Over the Pennines Using An Instrumented Glider", Boundary-Layer Meteorology, Vol. 46, pp. 153-168.
- System Technical Description - Carousel IV Inertial Navigation System, A.C. Electronics, Division of General Motors Corp.
- Telford, J.W., and P.B. Wagner (1974): "The Measurement of Horizontal Air Motion near Clouds from Aircraft", Journal of the Atmospheric Sciences, Vol. 31, No. 8, pp. 2066-2080.

- Telford, J.W., P.B. Wagner, and A. Vaziri (1977): "The Measurement of Air Motion from Aircraft", Journal of Applied Meteorology, Vol. 16, pp. 156-166.
- Waco, D.E., (1979): "Meteorological and Operational Aspects of 46 Clear Air Turbulence Sampling Missions with an Instrumented B-57B Aircraft, Volume II (Appendix C) - Turbulence Missions", prepared for NASA Langley Research Center, NASA TM-80045.
- Weber, O. (1975): "Statistical Studies on the Accuracy of Carousel IV Inertial Navigation Systems After Flights Over the North Atlantic", ERSO TT-136, West Germany.
- Weinreb, A., and I.Y. Bar-Itzhack (1978): "The Psi-Angle Error Equation in Strap-down Inertial Navigation Systems", IEEE Transactions on Aerospace and Electronic Systems, Vol. AES-14, No. 3, pp. 539-544, May.
- Winebarger, R.M. (1986): "Loads and Motions of an F-106B Flying Through Thunderstorms", NASA TM-87671, May.
- Woodfield, A.A., and J.M. Vaughn (1983): "Airspeed and Wind Shear Measurements with an Airborne CO₂ Continuous Wave Laser", Royal Aircraft Establishment, TR-83061, July.
- Yamamoto, S., et al. (1977): "Airborne Measurements of Turbulence heat Fluxes", J. Meteor. Soc., Japan, 55.
- Yokoyama, O., et al. (1977): "On the Turbulent Quantities in the Atmospheric Mixing Layer", J. Meteor. Soc., Japan, 55.
- Yokoyama, O., et al. (1977): "On the Turbulent Quantities in the Neutral Atmospheric Boundary Layer", J. Meteor. Soc., Japan, 55.

APPENDIX A

Wind Vector Calculations from an Airborne Platform

Windspeed and direction, based on measurements made from an airborne platform, are calculated from the vector addition

$$\vec{W} = \vec{V}_e - \vec{V}_a \quad (A.1)$$

where \vec{W} is the wind velocity with respect to an observer on earth, \vec{V}_a is the air velocity according to an observer on the airborne platform, and \vec{V}_e is the platform velocity in the frame of the earth. Measurements from the platform provide the information for airspeed and direction in a coordinate system that rolls, pitches, and yaws with the platform. An inertial measurement system on board the aircraft measures the angles, angular velocity, and linear velocity which describe the platform motion and orientation with respect to the earth. With the airflow vector known in the moving coordinate system and the orientation of the moving coordinate system with respect to the earth known, the wind vector in the earthbound coordinate system can be calculated.

A.1 Body-Fixed Frame

Airspeed in the coordinate system fixed to an aircraft (the true airspeed of the aircraft), is calculated from total pressure, ambient pressure, and total temperature measurements. Etkin (1973) calls this coordinate system the body-fixed coordinates, which is defined as having the x-axis pointing forward through the aircraft nose along the aircraft centerline, the y-axis pointing out the starboard wing, and the z-axis pointing out the aircraft underside. The origin of the coordinate system is located at the aircraft center of gravity.

The magnitude of the relative speed of the air to the aircraft, $|V_a|$, is determined

from the Mach number, Ma , and the sonic speed, c , by:

$$V_a = cMa \quad (A.2)$$

The Mach number of the airplane is calculated from the total and ambient pressures according to the expression

$$Ma = \sqrt{\left[\left(\frac{p_0}{p} \right)^{\frac{k-1}{k}} - 1 \right] \left[\frac{2}{k-1} \right]} \quad (A.3)$$

where p_0 is the total pressure, p is the ambient pressure, k is the ratio of specific heats for air (1.4), and Ma represents the Mach number.

The total pressure and static pressure measurements, or pitot measurements, are taken, respectively, where the airflow is brought adiabatically and isentropically to rest and where the flow speed is undisturbed from the free stream flow. When the vehicle is traveling supersonically, a shock wave in front of the rocket or attached to the rocket will reduce the total pressure and increase the static pressure, compared to the total pressure and static pressure on the supersonic side of the shock wave. The subsonic Mach number calculated from Equation (A.3) is subsequently less than the free stream Mach number. The shock wave in front of the total and static pressure transducers, mounted on the rocket nose cone or at the end of a boom, is assumed to be a normal shock wave. For the airspeed calculation, the free stream Mach number (on the supersonic side of the shock wave) is calculated from the measured total pressure and measured static pressure from

$$Ma_2^2 = \left[\left(\frac{p_0}{p} \right)^{\frac{k-1}{k}} - 1 \right] \left[\frac{2}{k-1} \right] \quad (A.4)$$

and

$$Ma_1^2 = \frac{(k-1)Ma_2^2 + 2}{2kMa_2^2 - (k-1)} \quad (A.5)$$

where Ma_2^2 = subsonic Mach number squared at the sensor, and Ma_1^2 = supersonic free stream Mach number squared.

The sonic speed is defined by

$$c = \sqrt{kRT} \quad (A.6)$$

where R is the ideal gas constant for air, and T is the static temperature of the air.

Since only total temperature can be measured, the static temperature of the air is calculated from the relationship between the known Mach number, the total temperature, and the static temperature:

$$T = T_o \left[1 + \frac{k-1}{2} Ma^2 \right]^{-1} \quad (A.7)$$

where T_o is the airstream total temperature.

With static temperature calculated, the sonic speed can be calculated from Equation (A.5) and airspeed is calculated from Equation (A.4). The airstream speed is then calculated from total pressure, static pressure, and total temperature from the expression

$$V_a = \left(\frac{p_o}{p} \right)^{-\frac{k-1}{2k}} \sqrt{kRT_o} \sqrt{\left[\left(\frac{p_o}{p} \right)^{\frac{k-1}{k}} - 1 \right] \left[\frac{2}{k-1} \right]} \quad (A.8)$$

The direction of the air relative to a probe is fixed by the angle-of-attack, α , and sideslip angle, β . In the body-fixed coordinate system the components of the relative airspeed vector are:

$$V_{BF} = |V_a| \begin{pmatrix} \cos \alpha \cos \beta \\ \cos \alpha \sin \beta \\ \sin \alpha \end{pmatrix} \quad (A.9)$$

The Dryden F-104 and the Ames ER-2 use different methods for measuring α and β . The Dryden F-104 uses flow vanes such as shown in Figure A.1, and the Ames ER-2 uses differential pressure measurements on the radome (Figure A.2) which are correlated to particular flow angles.

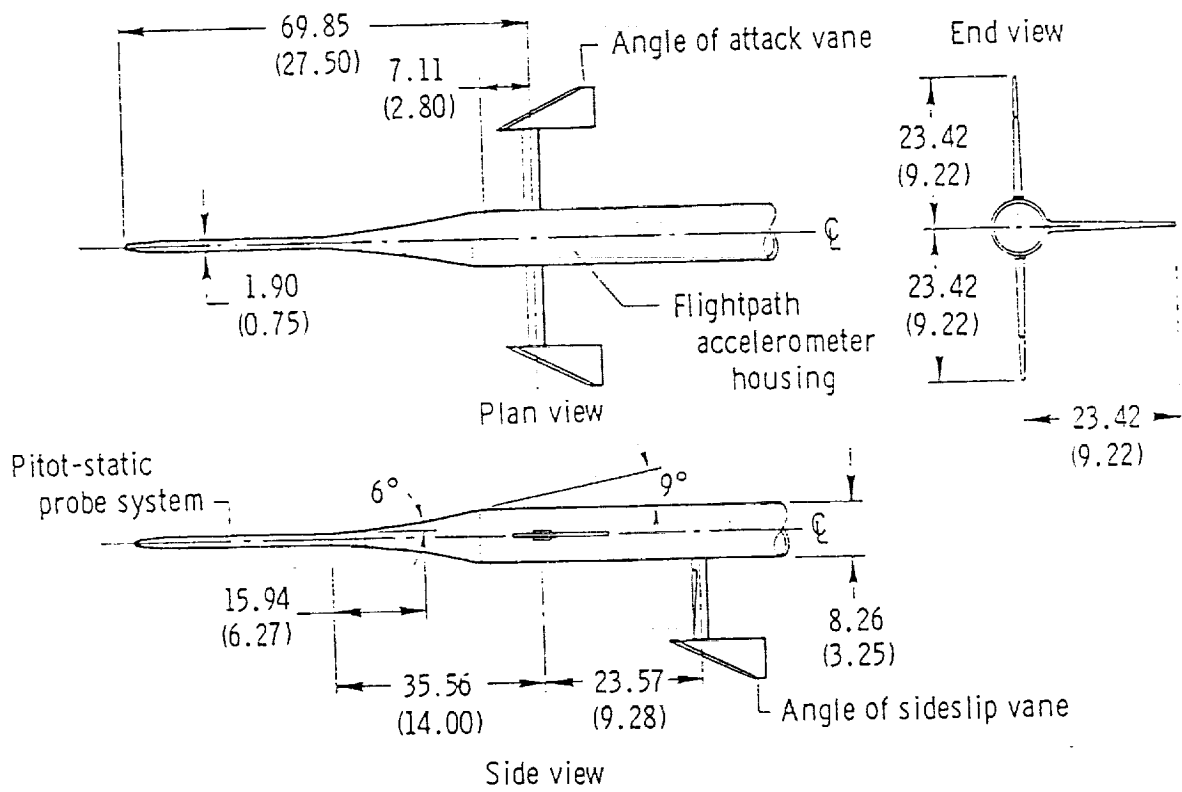


Figure A.1 Free vanes on an air data probe for flow angle measurements (Sakamoto, 1976).

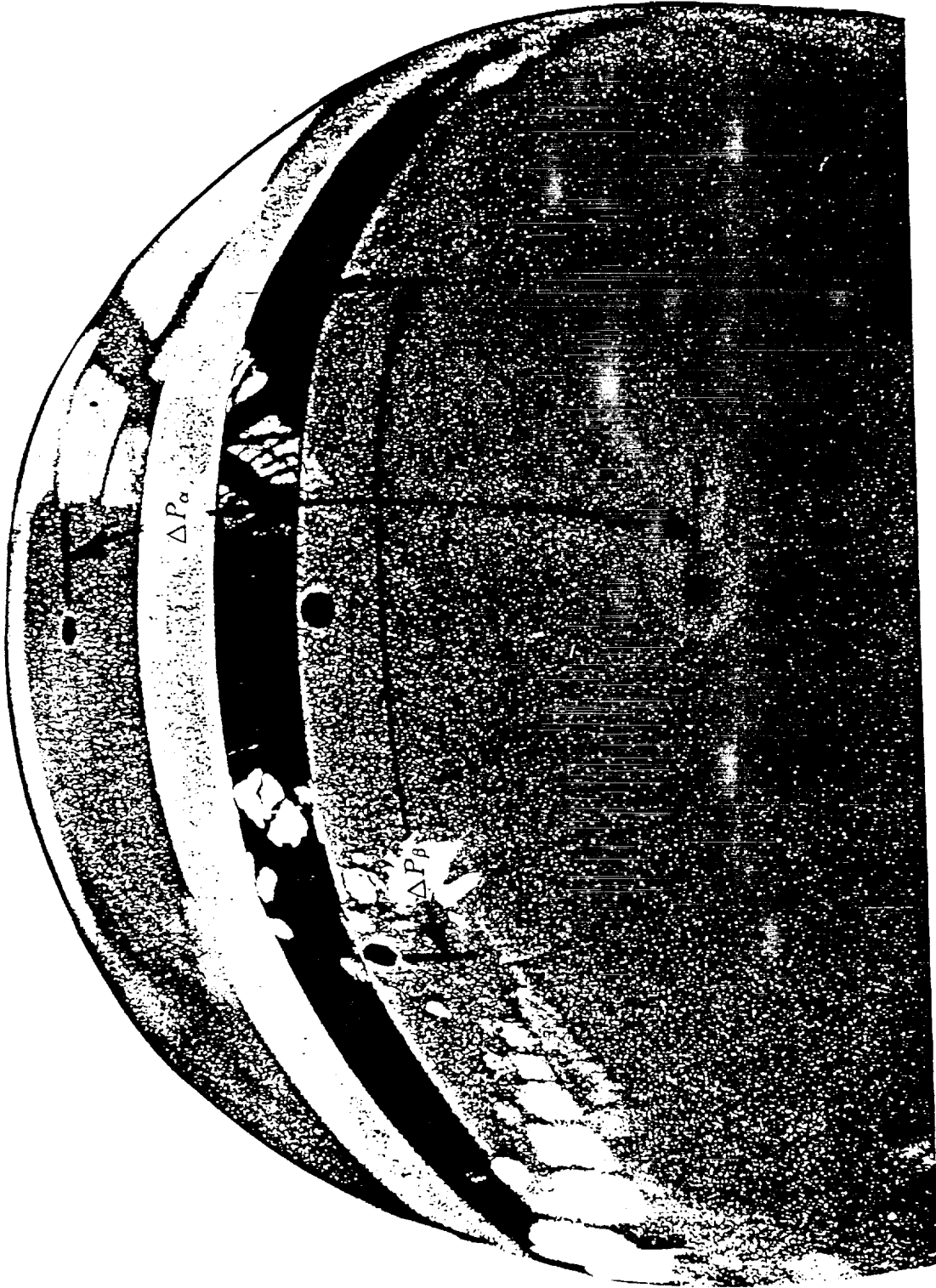


Figure A.2 ER-2 radome with angle-of-attack and sideslip angle pressure ports (Scott, et al., 1989).

The standard NACA airdata probe, which is used by the Dryden F-104, is equipped with vanes which measure airflow direction by vane displacement. The actual flow angle is found by correcting the displacement angle according to wind tunnel calibrations for varying Mach number, angle-of-attack and sideslip. Figure A.3 shows typical flow angle errors and indicated flow angles (Sakamoto, 1976).

Similarly to the differential pressure measurement system on the ER-2, probes are designed to measure flow angles and flight Mach number for aircraft and wind tunnels from differential pressure measurements. Such a probe, with a hemispherical head, is illustrated in Figure 2.2. A flow angle in a given plane would be calculated from (see Scott, et al. (1989))

$$\alpha = \frac{\Delta p}{kq} \quad (A.10)$$

where α is the flow angle, Δp is the differential pressure, k is the airflow angle sensitivity factor, and q is the dynamic pressure, $p_o - p$. The airflow angle sensitivity factor would be found from wind tunnel calibrations and is roughly constant within small Mach number domains. Bryer and Pankhurst (1971) recommended that for high subsonic, transonic, and low supersonic measurements, a hemispherical probe be used (Figure 2.2).

Before the air velocity is transformed into the earth-surface coordinates, with the x-axis pointed north, the y-axis pointed east, the z-axis pointed down, and the origin fixed to an observer on earth, the vehicle rotation rate must be accounted for in the body-fixed frame. The instruments that measure the pressures and angles necessary for the wind vector calculation rotate around the vehicle center of gravity. The linear velocity of the instruments due to the vehicle rotation is

$$\vec{V}_r = \vec{\omega} \times \vec{r} = \begin{pmatrix} p \\ q \\ r \end{pmatrix} \times \vec{r} \quad (A.11)$$

11

182

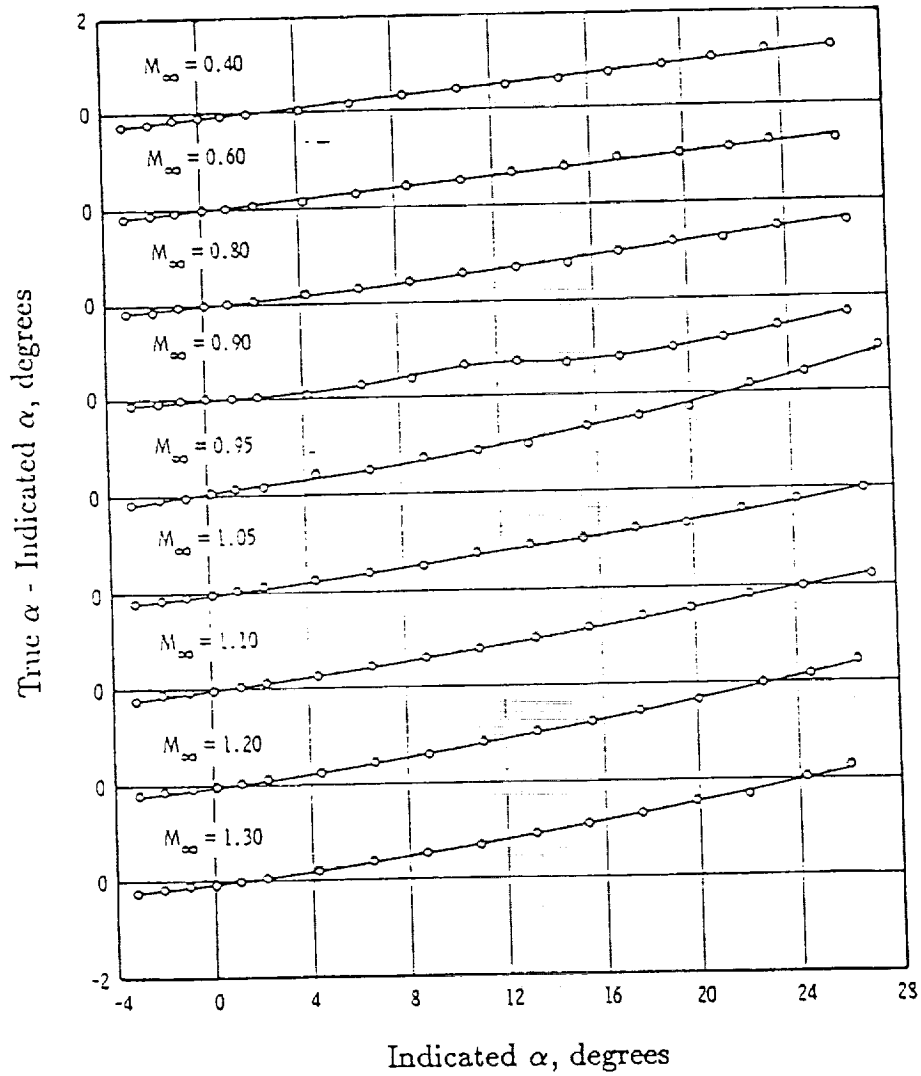


Figure A.3 Typical flow angle error from free vanes (Sakamoto, 1976).

where p is the vehicle rate of roll, q is the vehicle rate of pitch, r is the vehicle rate of yaw, and \vec{r} is the position vector of the instruments. The instrument velocity vector must be added to the relative airspeed velocity vector. The air velocity to be transformed from the body-fixed to an intermediate frame (the vehicle-centered vertical frame) is then

$$\vec{V} = |V_a| \begin{pmatrix} \cos \alpha \cos \beta \\ \cos \alpha \sin \beta \\ \sin \alpha \end{pmatrix} + \vec{\omega} \times \vec{r} \quad (A.12)$$

A.2 Vehicle-Centered Vertical Frame

The vehicle-centered vertical frame, as defined by Etkin (1972), has its origin fixed at the aircraft center of gravity, with the x-axis pointed north, the y-axis pointed east, and the z-axis pointed in the direction of the local gravity vector. Etkin (1972) gives the transformation of vector components from a body-fixed to a vehicle-centered vertical coordinates as

$$V_{VC} = \begin{pmatrix} \cos \theta & \sin \phi \sin \theta \cos \Psi & \cos \phi \sin \theta \cos \Psi \\ \cos \theta \sin \Psi & -\cos \phi \sin \Psi & +\sin \phi \sin \Psi \\ -\sin \theta & \sin \phi \sin \theta \sin \Psi & \cos \phi \sin \theta \sin \Psi \\ & +\cos \phi \cos \Psi & -\sin \phi \cos \Psi \\ & \sin \phi \cos \theta & \cos \phi \cos \theta \end{pmatrix} V_{BF} \quad (A.13)$$

where ϕ = aircraft roll angle, θ = pitch angle, and Ψ = yaw angle. The angles ϕ , θ , and Ψ , called the Euler angles.

These angles are typically provided by gyroscopic measurements from an inertial navigation system (INS).

A.3 Earth-Surface Frame

The vehicle-centered vertical frame and the earth-surface frame differ only in the relative velocity between their respective origins. Thus the transformation of a vector from the former to the latter involves only the addition of the velocity of the vehicle-centered vertical frame relative to earth-surface. This relative velocity is simply the ground speed of the vehicle:

$$\vec{W} = \vec{V}_e - \vec{V}_a \quad (A.14)$$

The vehicle ground speed is determined by integration of acceleration measurements on the aircraft. Typically, an INS provides velocity information in the earth-surface frame. If acceleration measurements only are used they are transformed from the frame of the vehicle to the earth-surface frame by the same vector transformation used with the calculated air velocity.

APPENDIX B

Error Analysis for Instrumentation Requirements for Wind Velocity Calculation from Measurements Made from an Airborne Platform

The uncertainty in the calculation of a wind vector from measurements made on an airborne platform is determined herein with the Taylor series error propagation approximation

$$(\Delta F)^2 = \sum_{i=1}^n \left(\frac{\partial F}{\partial \xi_i} \right)^2 (\Delta \xi_i)^2 \quad (B.1)$$

where F is the parameter of interest and the set of ξ_i are the independent variables governing F .

In the case of wind calculations from an airborne platform, the platform being an airplane or a rocket, Equation (B.1) becomes:

$$|\Delta \vec{W}|^2 = |\Delta \vec{V}_e - \Delta \vec{V}_a|^2 \quad (B.2)$$

where \vec{W} is the wind vector, \vec{V}_e is the inertial velocity vector of the vehicle (or ground speed) in the earth-surface frame, and \vec{V}_a is the relative airspeed vector. The inertial velocity, which is determined by an INS, radar, radio navigation, or other means, and is treated in this analysis as a given function of the instrumentation.

The earth-surface frame is defined as a Cartesian coordinate system with the x -axis pointed north, the y -axis pointed east, and the z -axis pointed down. The origin of the earth-surface frame is arbitrary since the wind vector is a velocity rather than a position. The earth-surface frame is not considered curvilinear here, since the earth can be approximated as flat for the spatial scale of interest.

The error in the vehicle ground speed vector, $\Delta \vec{V}_e$, which is dependent on the instrumentation used for that measurement, is an independent variable in the error analysis. The relative air velocity vector is also an independent variable in the error analysis and is a function of the inaccuracies of the relative airspeed

instrumentation. The error analysis is best carried out in terms of components in the particular reference frames of interest. Toward this goal the relative airspeed vector components typically measured in the body-fixed frame are transformed into the earth fixed frame. The matrix equation is:

$$V_{a_{EF}} = L_{VB} V_{a_{BF}} \quad (B.3)$$

where $V_{a_{BF}}$ is the relative airspeed column matrix of components measured in the body-fixed frame, and L_{VB} is the transformation matrix which rotates a vector in the body-fixed frame to the earth fixed frame.

The body-fixed frame is defined, in terms of an aircraft, as having the x -axis projected from the aircraft nose along the fuselage centerline, the y -axis projected from the starboard wing, the z -axis projected from the aircraft underside. The origin of the coordinate system is at the aircraft center of gravity. Etkin (1973) derives the transformation matrix L_{VB} as:

$$L_{VB} = \begin{pmatrix} \cos \Psi & \sin \phi \sin \theta \cos \Psi & \cos \phi \sin \theta \cos \Psi \\ & -\cos \phi \sin \Psi & +\sin \phi \sin \Psi \\ \cos \theta \sin \Psi & \sin \phi \sin \theta \sin \Psi & \cos \phi \sin \theta \sin \Psi \\ & +\cos \phi \cos \Psi & -\sin \phi \cos \Psi \\ -\sin \theta & \sin \phi \cos \theta & \cos \phi \cos \theta \end{pmatrix} \quad (B.4)$$

where ϕ is aircraft bank, θ is aircraft elevation, and Ψ is aircraft heading.

The components of \vec{V}_a , in the body fixed coordinates, are defined for convenience as

$$V_{a_{BF}} = (V_x, V_y, V_z) \quad (B.5)$$

and the error as

$$\Delta V_{a_{BF}} = (\Delta V_x, \Delta V_y, \Delta V_z) \quad (B.6)$$

The components of \vec{V}_a , in the earth fixed coordinates or vehicle centered coordinates, are defined as

$$V_{a_{VC}} = (V'_x, V'_y, V'_z) \quad (B.7)$$

and

$$\Delta V_{avc} = (\Delta V'_x, \Delta V'_y, \Delta V'_z) \quad (B.8)$$

Three equations result from the expansion of Equation (B.3) with substitution into Equation (B.1). Using index notation, these equations are

$$(\Delta V'_j)^2 = \left(\frac{\partial V'_j}{\partial V'_i} \right)^2 (\Delta V'_i)^2 + \left(\frac{\partial V'_j}{\partial X_i} \right)^2 (\Delta X_i)^2 \quad (B.9)$$

where $X_1 = \phi$, $X_2 = \theta$, and $X_3 = \Psi$.

The derivatives on the R.H.S. of Equation (B.9) for $\Delta V'_x$ are

$$\frac{\partial V'_x}{\partial V_x} = \cos \theta \cos \Psi \quad (B.10)$$

$$\frac{\partial V'_x}{\partial V_y} = \sin \phi \sin \theta \cos \Psi - \cos \theta \sin \Psi, \quad (B.11)$$

$$\frac{\partial V'_x}{\partial V_z} = \cos \phi \sin \theta \cos \Psi + \sin \phi \sin \Psi, \quad (B.12)$$

$$\begin{aligned} \frac{\partial V'_x}{\partial \phi} &= V_y (\cos \phi \sin \theta \cos \Psi + \sin \phi \sin \Psi) \\ &\quad - V_z (\sin \phi \sin \theta \cos \Psi + \cos \phi \sin \Psi), \end{aligned} \quad (B.13)$$

$$\begin{aligned} \frac{\partial V'_x}{\partial \theta} &= -V_x (\sin \theta \cos \Psi) + V_y \sin \phi \cos \theta \cos \Psi \\ &\quad + V_z \cos \phi \cos \theta \cos \Psi, \end{aligned} \quad (B.14)$$

and

$$\begin{aligned} \frac{\partial V'_x}{\partial \Psi} &= -V_x \cos \theta \sin \Psi - V_y (\sin \phi \sin \theta \sin \Psi + \cos \phi \cos \Psi) \\ &\quad + V_z (-\cos \phi \sin \theta \sin \Psi + \sin \phi \cos \Psi) \end{aligned} \quad (B.15)$$

The derivatives on the R.H.S. of Equation (B.9) for $\Delta V'_y$ are

$$\frac{\partial V'_y}{\partial V_x} = \cos \theta \sin \Psi, \quad (B.16)$$

$$\frac{\partial V'_y}{\partial V_y} = \sin \phi \sin \theta \sin \Psi + \cos \phi \cos \Psi, \quad (B.17)$$

$$\frac{\partial V'_y}{\partial V_z} = \cos \phi \sin \theta \sin \Psi - \sin \phi \cos \Psi, \quad (B.18)$$

$$\begin{aligned}\frac{\partial V'_y}{\partial \phi} &= V_y(\cos \phi \sin \theta \sin \Psi - \sin \phi \cos \Psi) \\ &+ V_z(-\sin \phi \sin \theta \sin \Psi - \cos \phi \cos \Psi),\end{aligned}\quad (B.19)$$

$$\begin{aligned}\frac{\partial V'_y}{\partial \theta} &= -V_x \sin \theta \sin \Psi + V_y \sin \phi \cos \theta \sin \Psi \\ &+ V_z \cos \phi \cos \theta \sin \Psi,\end{aligned}\quad (B.20)$$

and

$$\begin{aligned}\frac{\partial V'_y}{\partial \Psi} &= V_x \cos \theta \cos \Psi + V_y(\sin \phi \sin \theta \cos \Psi - \cos \phi \sin \Psi) \\ &+ V_z(\cos \phi \sin \theta \cos \Psi + \sin \phi \sin \Psi)\end{aligned}\quad (B.21)$$

The derivatives on the R.H.S. of Equation (B.9) for $\Delta V'_z$ are

$$\frac{\partial V'_z}{\partial V_x} = -\sin \theta, \quad (B.22)$$

$$\frac{\partial V'_z}{\partial V_y} = \sin \phi \cos \theta, \quad (B.23)$$

$$\frac{\partial V'_z}{\partial V_z} = \cos \phi \cos \theta, \quad (B.24)$$

$$\frac{\partial V'_z}{\partial \phi} = V_y \cos \phi \cos \theta - V_z \sin \phi \cos \theta, \quad (B.25)$$

$$\frac{\partial V'_z}{\partial \theta} = -V_x \cos \theta - V_y \sin \phi \sin \theta - V_z \cos \phi \sin \theta, \quad (B.26)$$

and

$$\frac{\partial V'_z}{\partial \Psi} = 0 \quad (B.27)$$

With the assumption that the uncertainties in the Euler angles are approximately equal, Equations (B.10) - (B.27) can be simplified by inspection after substituting the small angle assumption for the bank, ϕ , elevation, θ , and heading, ψ , angles to:

$$|\Delta V_{a_{VC}}|^2 = |\Delta V_{a_{BF}}|^2 + 2(\Delta \phi)^2$$

The error in the angle measurements are considered equal, i.e., $\Delta \phi = \Delta \psi = \Delta \theta$. The uncertainty in the angles ϕ , θ , and Ψ is dependent on the instruments, usually

gyroscopes, which are used to measure those angles and thus, $\Delta\phi$, $\Delta\theta$, and $\Delta\Psi$ are independent variables in the error analysis.

At this point, the rotation rate of the vehicle should be considered in the error analysis. As the vehicle rotates, a wind vector is induced at the windspeed instrumentation proportional to the rotation rate and the distance between the aircraft center of gravity (c.g.) and the windspeed instrumentation. However, the product of the rotation rate and length between the c.g. and instrumentation is normally small and the contribution to the measured windspeed is not significant. Thus, the error contributed by the measured rate of the vehicle rotation will be neglected here.

The three components of the relative airspeed vector in the body-fixed frame, V_x , V_y , and V_z , are derived from the magnitude of the airspeed $|V_a|$, the angle-of-attack, α , and sideslip angle, β :

$$\begin{pmatrix} V_x \\ V_y \\ V_z \end{pmatrix} = |V_a| \begin{pmatrix} \cos \alpha \cos \beta \\ \cos \alpha \sin \beta \\ \sin \alpha \end{pmatrix} \quad (B.28)$$

The resultant errors in the calculations of the body-fixed wind vector components are:

$$\begin{aligned} (\Delta V_x)^2 &= \cos^2 \alpha \cos^2 \beta (\Delta |V_a|)^2 + |V_a|^2 \sin^2 \alpha \cos^2 \beta (\Delta \alpha)^2 \\ &+ |V_a|^2 \cos^2 \alpha \sin^2 \beta (\Delta \beta)^2, \end{aligned} \quad (B.29)$$

$$\begin{aligned} (\Delta V_y)^2 &= \cos^2 \alpha \sin^2 \beta (\Delta |V_a|)^2 + |V_a|^2 \sin^2 \alpha \cos^2 \beta (\Delta \alpha)^2 \\ &+ |V_a|^2 \cos^2 \alpha \cos^2 \beta (\Delta \beta)^2, \end{aligned} \quad (B.30)$$

and

$$(\Delta V_z)^2 = \sin^2 \alpha (\Delta |V_a|)^2 + |V_a|^2 \cos^2 \alpha (\Delta \alpha)^2 \quad (B.31)$$

Defining $|\Delta \vec{V}_a|^2 = (\Delta V_x)^2 + (\Delta V_y)^2 + (\Delta V_z)^2$, incorporating Equations (B.29), (B.30), and (B.31) and normalizing by the vehicle airspeed then with the small angle approximations, we can write:

$$\frac{|\Delta \vec{V}_a|^2}{|V_a|^2} = \left(\frac{\Delta |V_a|}{|V_a|} \right)^2 + 2(\Delta \alpha)^2 \quad (B.32)$$

where it is assumed $\Delta \alpha = \Delta \beta$.

The errors in the measured angle-of-attack and sideslip angles are functions of the instruments used to make these measurements and are therefore independent variables.

The magnitude or absolute value of the airspeed of the vehicle, $|V_a|$, is calculated as the product of the local sonic velocity and the vehicle flight Mach number:

$$|V_a| = cMa \quad (B.35)$$

For convenience which will become apparent, the square of the Mach number will be used:

$$|V_a| = c\sqrt{Ma^2} \quad (B.36)$$

Then

$$(\Delta |V_a|)^2 = Ma^2(\Delta c)^2 + \frac{c^2}{4Ma^2}(\Delta Ma^2)^2 \quad (B.37)$$

or

$$\left(\frac{\Delta |V_a|}{c} \right)^2 = Ma^2 \left(\frac{\Delta c}{c} \right)^2 + \frac{(\Delta Ma^2)^2}{4Ma^2} \quad (B.38)$$

The sonic velocity, c , is calculated from the static temperature of the wind from

$$c = \sqrt{kRT} \quad (B.39)$$

and

$$(\Delta c)^2 = \frac{kR}{4T}(\Delta T)^2 \quad (B.40)$$

where $k = 1.4$ is the ratio of specific heats for air, and R is the perfect gas constant for air. Equation (B.40) can be rearranged from division by Equation (B.39) twice:

$$\left(\frac{\Delta c}{c} \right)^2 = \frac{1}{4} \left(\frac{\Delta T}{T} \right)^2 \quad (B.41)$$

The static temperature is calculated from the Mach number and the total temperature, T_o , of the air surrounding the vehicle from the relationship

$$\frac{T_o}{T} = 1 + \frac{k-1}{2} Ma^2 \quad (B.42)$$

Rearranging Equation (B.42) as

$$T = T_o \left(1 + \frac{k-1}{2} Ma^2 \right)^{-1} \quad (B.43)$$

and substituting into Equation (B.1)

$$(\Delta T)^2 = \frac{(\Delta T_o)^2}{\left(1 + \frac{k-1}{2} Ma^2\right)^2} + \frac{T_o^2 (\Delta Ma^2)^2}{\left(\frac{k-1}{2} \left(1 + \frac{k-1}{2} Ma^2\right)\right)^2} \quad (B.44)$$

Equation (B.42) can be substituted back into Equation (B.44) for

$$(\Delta T)^2 = \frac{(\Delta T_o)^2}{(T_o/T)^2} + \frac{T_o^2 (\Delta Ma^2)^2}{\left(\frac{k-1}{2} (T_o/T)^2\right)^2} \quad (B.45)$$

or

$$\left(\frac{\Delta T}{T}\right)^2 = \left(\frac{\Delta T_o}{T_o}\right)^2 + \frac{(\Delta Ma^2)^2}{\frac{(k-1)^2}{4} \left(1 + \frac{k-1}{2} Ma^2\right)^2} \quad (B.46)$$

Since T_o is measured, T_o is an independent variable in the wind velocity calculations and the value of ΔT_o is dependent on the accuracy of the total temperature probe used for that measurement.

The Mach number is calculated as a function of the ratio of the dynamic and static pressure measured at the aircraft for subsonic flight by:

$$Ma^2 = \frac{2}{k-1} \left(\left(\frac{q}{p} - 1 \right)^{\frac{k-1}{k}} - 1 \right) \quad (B.47)$$

If the system is flying supersonically, the free stream Mach number is calculated with the Rayleigh pitot-tube formula:

$$\frac{q}{p} + 1 = \left(\frac{k+1}{2} M_1^2 \right)^{\frac{k}{k-1}} / \left(\frac{2k}{k+1} M_1^2 - \frac{k-1}{k+1} \right)^{\frac{1}{k-1}} \quad (B.48)$$

where Ma_1 = the supersonic free stream Mach number.

The uncertainty in the subsonic Mach number is calculated from Equation (B.47):

$$\left(\frac{\Delta Ma^2}{Ma^2} \right) = \left(\frac{\frac{2}{k} \left(1 + \frac{k-1}{2} Ma^2 \right)^{\frac{k}{k-1}} - 1}{Ma^2} \right)^2 \left(\frac{\Delta \frac{q}{p}}{\frac{q}{p}} \right)^2 \quad (B.50)$$

The uncertainty in the pressure ratio $\frac{q}{p}$ is evaluated from the two remaining independent variables in the wind velocity calculation

$$\left(\frac{\Delta q}{p}\right)^2 / \left(\frac{q}{p}\right)^2 = \left(\frac{\Delta p}{p}\right)^2 + \left(\frac{\Delta q}{q}\right)^2 \quad (B.52)$$

Likewise, the uncertainty in the supersonic Mach number can be shown to be

$$\left(\frac{\Delta M^2}{M^2}\right)^2 = 2 \left[\frac{M^2 - \frac{k-1}{2k}}{M^2 - \frac{1}{2}} \right]^2 \left[\frac{\frac{q}{p}}{\frac{q}{p} + 1} \right]^2 \left(\frac{\Delta p}{p}\right)^2$$

Finally, the uncertainty in wind velocity calculations from measurements made from a airborne platform is determined by the measured parameters \vec{V}_e , ϕ , θ , Ψ , T_o , p , p_o , α , and β , and their measurement uncertainties. This neglects any contribution to the wind velocity made by the rotation rate of the system, which is generally small.

APPENDIX C

CAPABILITIES OF THE EGRETT II AIRCRAFT

~~190~~
194

This section covers some of the capabilities of the EGRETT II developed by E-Systems, Greenville Division. This aircraft is a high altitude, long endurance platform for engineering, scientific, and environmental applications and research. This vehicle provides a cost effective operational platform. The acquisition cost of this aircraft is in the \$10M range.

This aircraft has participated in ICE. This vehicle holds several international records for single engine turbo-propeller aircraft.

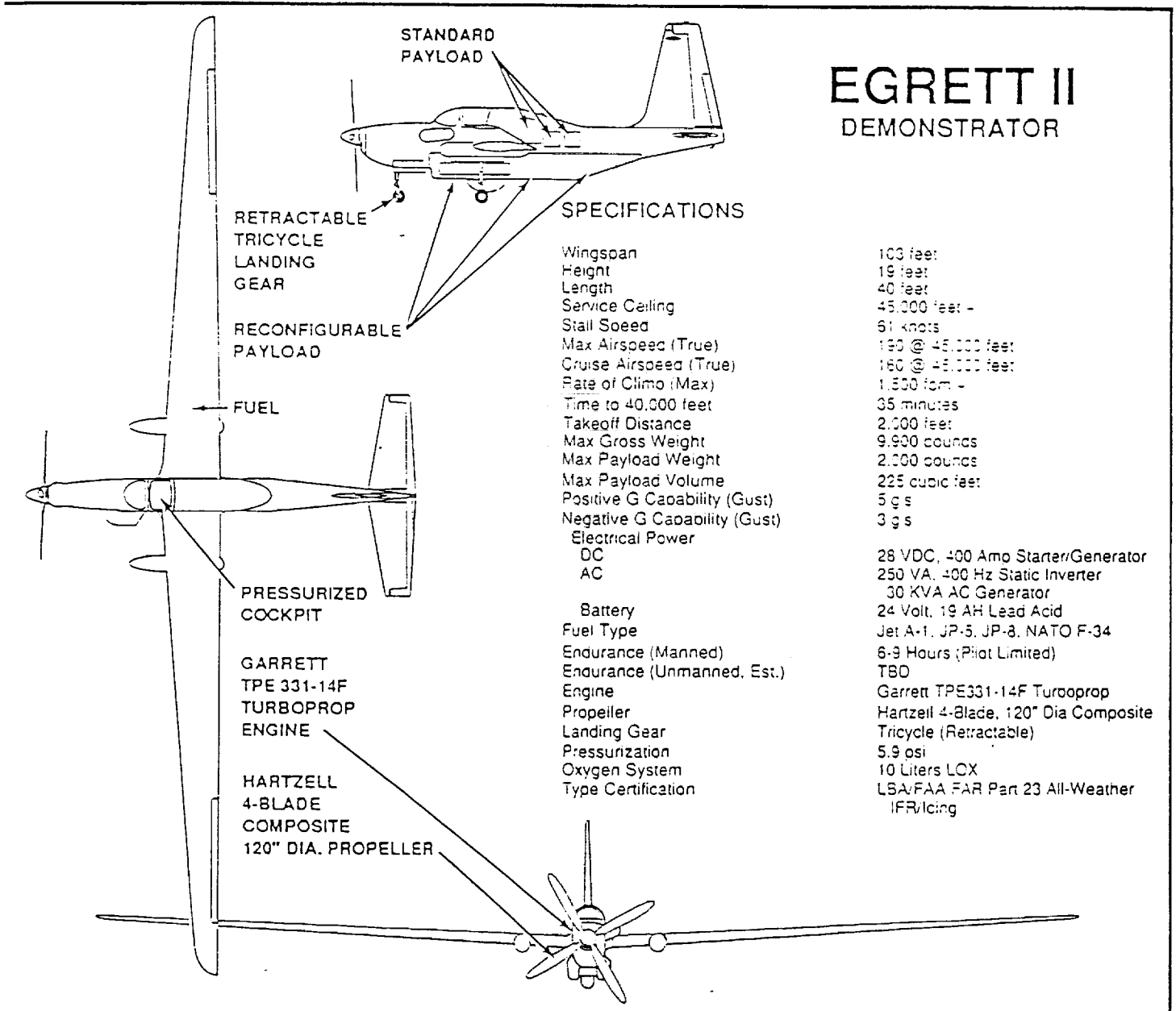


Figure C.1 EGRETT II characteristics (provided by E-Systems).

Table C.1 Payload, Weight, Altitude, Time, Range, and Cost of Certain Aircraft

AIRCRAFT	PAYLOAD Weight (lbs.)	ALTITUDE (Feet)	TIME (Hrs.)	MAX. RANGE (NM)	OPERATIONAL COST/HR. (EST)
<u>EGRETT II</u>	2000	50	10.0	2338	\$ 330
Super King Air 350	2438	35	7.5	1600	\$ 500
Learjet 55C	827	41	5.6	2500	\$ 700
Canadair Challenger 601-3A	2000	41	6.1	3700	\$ 1,200
Lockheed TR-1	3000	75	12.0	5400	\$10,000
Gulf Stream GIV	2000	45	10.5	3767	\$ 2,400
Cessna Citatise III	2620	47	3.5	2300	\$ 800

Table C.2 General Performance Capabilities, EGRETT II

Maximum Payload 2,200 lbs. (1000 Kg)

Endurance is in excess of 10 hrs

Range is in excess of 2000 NM

Certified operating altitude is 50,000 ft

Direct operating cost is approximately \$330/hr

Take-off distance is less than 2000 ft (610 m)

Landing distance is less than 3500 ft (1067 m)

50 feet obstacle, 5000 feet altitude, ISA

APPENDIX IV

**COVER SHEETS FROM SEPARATELY REPORTED
WORK FOR DEFENSE INTELLIGENCE AGENCY;
REDSTONE ARSENAL, AL**

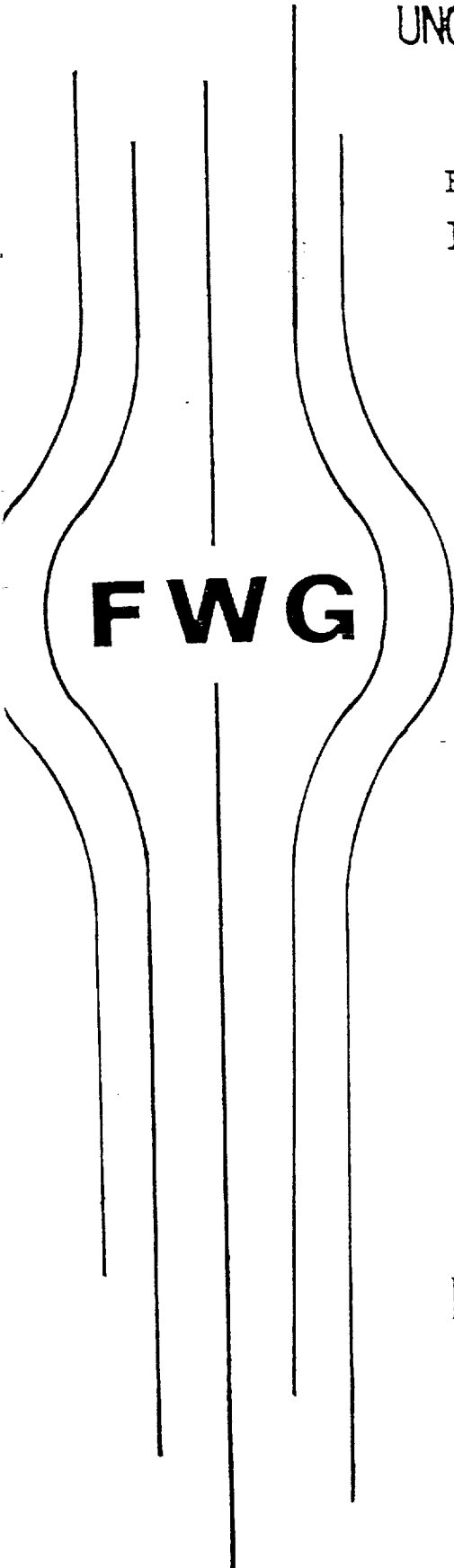
This appendix contains cover pages for the source code and user's manual for the digital simulation of the FD system. Also included is the cover sheet of the final report for the engineering analysis and technical studies involving specific radar tasks under Option 1. The manual, computer code and final report have been distributed to the U.S. Army Missile and Space Intelligence Center (AIAMS-X) at Redstone Arsenal, Alabama. Complete copies of the report are available if requested.

UNCLASSIFIED

FINAL REPORT

August 1991

FD Source Code (U)

A large graphic on the left side of the page, consisting of several vertical lines of varying lengths that converge at the top and bottom, forming a central, bulbous shape. Inside this shape, the letters "FWG" are printed in a bold, sans-serif font.

FWG

Prepared for:
U.S. Army Missile and Space Intelligence Center
ATTN: ALAMS-X
Redstone Arsenal, AL 35898-5500

Prepared By:
FWG Associates, Inc.
Huntsville Operation
P.O. Box 12056
Huntsville, AL 35815-2056

FWG ASSOCIATES, INC.
"Continuity with the Future"

UNCLASSIFIED WHEN SEPARATED FROM
PROJECT ZEST TICKER/TAPE
FINAL REPORT

UNCLASSIFIED

ENGINEERING ANALYSIS AND TECHNICAL STUDIES
INVOLVING SPECIFIC RADAR PROBLEMS

PREPARED BY: FWG Associates, Inc.
P.O. Box 1358
Tullahoma, TN 37388

PREPARED FOR: Defense Intelligence Agency
Attn: Chief
CROSSBOW-S Management Office
Redstone Arsenal, AL 35898-5500

DATE: May 1992



Report Documentation Page

1. Report No.	2. Government Accession No.	3. Recipient's Catalog No.	
4. Title and Subtitle Remote Sensing Technology Research and Instrumentation Platform Design		5. Report Date August 20, 1992	6. Performing Organization Code
		8. Performing Organization Report No.	
7. Author(s) FWG Associates, Inc. 217 Lakewood Drive Tullahoma, TN 37388		10. Work Unit No.	
		11. Contract or Grant No. NAS5-30936	
9. Performing Organization Name and Address FWG Associates, Inc. 217 Lakewood Drive Tullahoma, TN 37388		13. Type of Report and Period Covered Final Report	
		14. Sponsoring Agency Code	
2. Sponsoring Agency Name and Address NASA Goddard Space Flight Center Attn: Code 289/Marguerite Broadwell Greenbelt, MD 20771			
5. Supplementary Notes			
16. Abstract An instrumented pallet concept and definition of an aircraft with performance and payload capability to meet NASA's airborne turbulent flux measurement needs for advanced multiple global climate research and field experiments is presented. The report addresses airborne measurement requirements for general circulation model sub-scale parameterization research, specifies instrumentation capable of making these measurements, and describes a preliminary support pallet design. Also, a review of aircraft types and a recommendation of a manned and an unmanned aircraft capable of meeting flux parameterization research needs is given.			
17. Key Words (Suggested by Author(s)) Global Climate Modeling Flux Parameterization Airborne Measurements Atmospheric Research Aircraft Turbulent Flux		18. Distribution Statement Unclassified - Unlimited	
19. Security Classif. (of this report) Unclassified	20. Security Classif. (of this page) Unclassified	21. No. of pages 198	22. Price